Exploring the effect of osmotic pressure on creating load bearing regenerative cartilage implants

Exploring the effect of osmotic pressure on creating load bearing regenerative cartilage implants

Rienk Schuiringa

G.H. Schuiringa
Eindhoven University of Technology, The Netherlands

A catalogue record is available from the Eindhoven University of Technology Library
ISBN: 978-90-386-5830-8

Cover design by Studio Toussaint
Printed by ADC Dereumaux

Research presented in this thesis was performed under the framework of Chemelot InSciTe, supported by the partners of Regenerative Medicine Crossing Borders and powered by Health~Holland, Top Sector Life Sciences & Health.

Financial support by the Netherlands Society for Biomaterials and Tissue Engineering (NBTE), Anna Fonds te Leiden and the department of Biomedical Engineering of the Eindhoven University of Technology is gratefully acknowledged.

Exploring the effect of osmotic pressure on creating load bearing regenerative cartilage implants

PROEFSCHRIFT

ter verkrijging van de graad van doctor aan de Technische Universiteit Eindhoven, op gezag van de rector magnificus prof.dr. S.K. Lenaerts,
voor een commissie aangewezen door het College voor Promoties, in het openbaar te verdedigen op donderdag 21 september 2023 om 16:00 uur

door

Gerke Hendrik Schuiringa

geboren te Marum

Dit proefschrift is goedgekeurd door de promotoren en de samenstelling van de promotiecommissie is als volgt:

Voorzitter:	prof.dr. M. Merkx
Promotor:	prof.dr. K. Ito
Co-promotor:	dr. C.C. van Donkelaar
Promotiecommissieleden:	dr. S. Hofmann
	prof.dr. H.B.J. Karperien (Universiteit Twente)
	prof.dr.ir. J. Malda (UMC Utrecht)
	prof.dr. G.J.V.M. van Osch (Erasmus MC)
	prof. dr. T. Vermonden (Universiteit Utrecht)

Het onderzoek of ontwerp dat in dit proefschrift wordt beschreven is uitgevoerd in overeenstemming met de TU/e Gedragscode Wetenschapsbeoefening.

Table of Contents

1

General introduction

[Move•ment]
An act of moving: change of place or posture, by any means, from one situation to another; a change or development

To enable pain free and effortless movements, joints are necessary. In the human body, several synovial joints are presents, which allow certain degrees of freedom between articulating bones so that movement is enabled. In synovial joints, bones are joined by a fibrous capsule, which is filled with synovial fluid. The largest synovial joint in the human body is the knee, enabling mostly flexion and extension of the lower leg with regards to the upper leg, facilitating daily movements like walking, biking, and standing up from a sitting position.

1.1 Anatomy of the knee

The knee joint consists out of three bones, the femur, tibia, and patella, and has two major functions: enable movement, without losing stability, and to transmit loads (Fig. 1.1)[1]. Movement is enabled via the tibiofemoral joint, with a range of motion between the femur and the tibia reaching up to 160°, and the patellofemoral joint, in which the articulation of the patella over the femur minimizes the force needed by the quadriceps to extend the knee[1]. Tendons and ligaments provide stability externally and internally and enable movement of the joint by the connection to the quadriceps for extension and the hamstring for flexion[1]. On the end of the femur (condyles and trochlea), tibia plateau and patella, a thin layer of articular cartilage lines the bones[2].

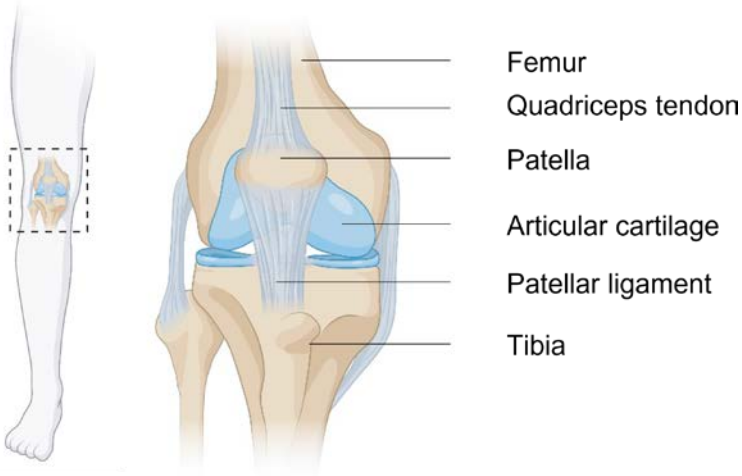

***Figure 1.1**: Anatomy of the knee joint, created by biorender.com.*

1.2 Articular cartilage

Articular cartilage is more or less the pearl of the human body, with the joint as the oyster: it possesses a blue/whitish appearance, a relatively simple, but sophisticated and highly specialized tissue, and can withstand high loads combined with a very low coefficient of friction. Within synovial joints, bones are lined with a thin layer (1-4 mm thickness) of articular cartilage, which does not contain blood vessels, nerves or lymphatics[2,3], thus leading to pain free movements. The smooth movement originates from the very low friction coefficient between articulating cartilage surfaces, reducing shear strains in the cartilage. This phenomenon arises by the binding of specific proteins and polysaccharides to the cartilage surface, the specific components in the synovial fluid, and the poroelastic mechanical properties of cartilage[4–8].

1.2.1 Cells

Chondrocytes account for 1-2% of the total volume of cartilage and are responsible for the synthesis and maintenance of the ECM, most importantly for the turnover of proteoglycans and repair of the collagen network. Due to this dense ECM, chondrocytes are trapped within the matrix, which restrains migration. Stimuli, among others hydrostatic pressure, growth factors mechanical loading, can activate chondrocytes to synthesize or degrade ECM. An important factor in mechanosensing is the pericullular matrix (PCM), surrounding chondrocytes or small groups of chondrocyte aggregates, together called chondrons. This PCM consists mainly of type VI collagen and perlecan, which provides integrity to the PCM and plays an important role in the cell signaling[9–11].

1.2.2 Articular cartilage structure and composition

Besides the previously mentioned features, articular cartilage enables transmission, absorption and redistribution of (high) loads within cartilage itself and to the underlying subchondral bone. This unique property originates from specific composition of cartilage and the Benninghoff arcades of collagen type II[12]. Articular cartilage consists mainly of water, approximately 80% of its wet weight, collagen and proteoglycans. The composition is zone dependent (Fig. 1.2). The collagen in healthy articular cartilage is almost a permanent structure, as no significant turnover has been observed[13].

Articular cartilage can be divided into 4 zones, which can be distinguished by cell morphology, ECM composition and structure[14,15]. The tangential or superficial zone consists mainly out of tightly packed parallel (to the surface) oriented type II collagen fibers[16], resulting in reduced shear stress and distribution of compressive

stress, therefore protecting the lower zones. The water content is high and the chondrocytes are flattened. On the articulating surface of the superficial layer, the glycoprotein lubricin / PRG4 can be found, which is produced by chondrocytes and synoviocytes and protects the cartilage surface[14].

The middle zone is a transition zone where type II collagen fibers bend from a parallel towards a perpendicular orientation in respect to the articulating surface[16]. Chondrocytes possess a rounded morphology and are lower in density[17]. The water content is lower than in the superficial zone. Hyaluronic acid polymer chains, with aggrecans bound to it are entangled in the collagen network. In the deep zone, type II collagen is oriented perpendicular to the surface. Moreover, a low water content, but a high proteoglycan content can be found and the cells are stacked in columns. The deep zone and calcified zone are delineated from each other by the tidemark. In the calcified zone, type X collagen is present, which provides anchoring to the subchondral bone. The low amount of chondrocytes present in the calcified zone exhibit a hypertrophic phenotype (Fig. 1.2)[3,14,18].

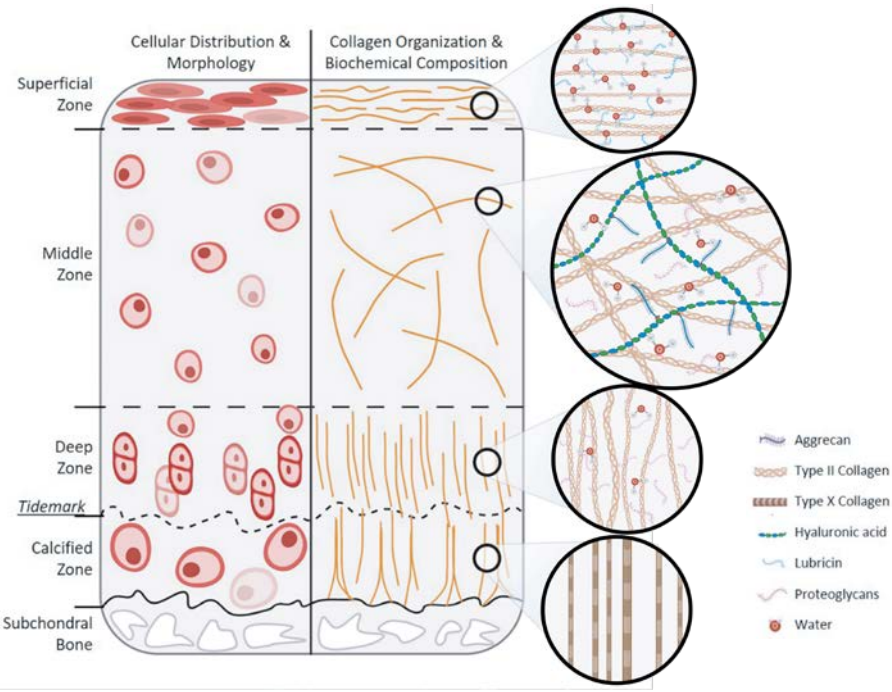

***Figure 1.2**: Depth dependent composition of articular cartilage. Adapted from Thorp et al.[19] under the terms of the Creative Commons Attribution 4.0 International License (https://creativecommons.org/licenses/by/4.0) and created with biorender.com*

1.2.3 Fixed charge density and osmotic pressure

As previously mentioned, the cartilage extracellular matrix consists mainly of water, collagens, and proteoglycans. Aggrecan is the most prevalent proteoglycan, which consists of a core protein with many chondroitin sulfate and keratan sulfate glycosaminoglycan chains attached to it. These aggrecan units can then form large aggregates by binding to a backbone of hyaluronic acid stabilized by link proteins (Fig. 1.3). These large aggregates are entrapped within the collagen structure, resulting in both a low hydraulic permeability (Table 1), meaning that it is harder for fluid to flow through the matrix, and a high negative fixed charge density (FCD) due to the sulfates groups of chondroitin sulfate and keratan sulfate[20]. The high FCD attracts free cations, and the excess concentration of ions attracts water through an osmotic pressure, which causes the tissue to swell. However, this swelling is restricted by the tension formed in the collagen network, a dense network of mainly type II collagen [12,20,21], and is directly linked to the unique load-bearing properties of articular cartilage[22].

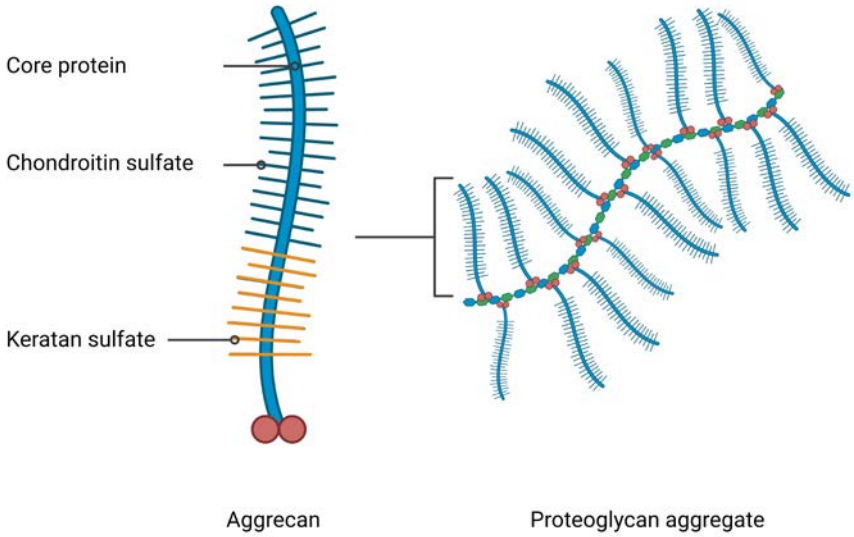

***Figure 1.3**: The structure of large proteoglycan aggregates, consisting of aggrecans (sulfates glycosaminoglycans attached to core protein) linked to backbone of hyaluronic acid. Created by biorender.com*

1.2.4 Mechanical properties of articular cartilage

With every movement of the knee under loading, articular cartilage is compressed. With imposing sustained compression, water will flow out of the tissue. The proteoglycan aggregates are not able to diffuse through the dense ECM as a result of their size and being bound to HA. This leads to a more compact aggrecan network and an even larger ion imbalance, resulting in an increased swelling potential while compressed. After removal of the load, water will flow back into the tissue be of high osmotic pressure, restoring the equilibrium[23] (Fig. 1.4). This is not only beneficial for the load-bearing properties, but also for the inflow of nutrients and the removal of waste products.

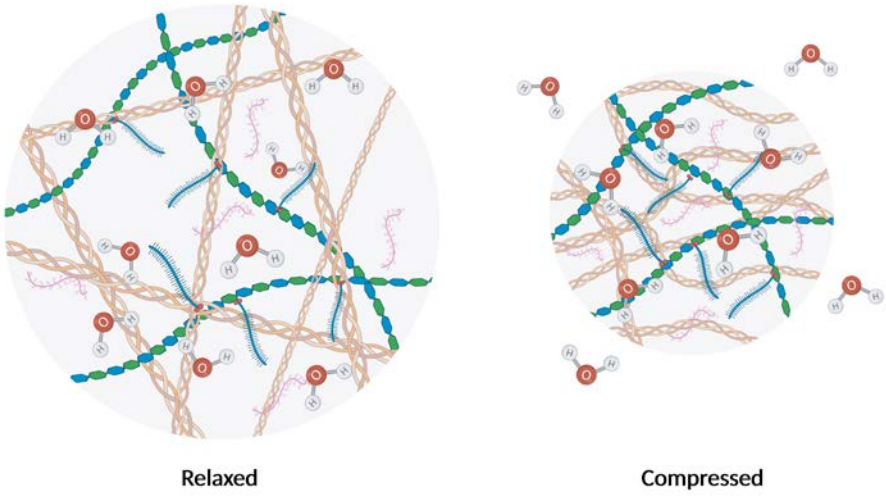

Figure 1.4: *Articular cartilage in equilibrium (left), where charged proteoglycan aggregates, attract water until the tensile forces of collagen restricts further swelling. When compressed (right), water is pressed out of the tissue, collagen is not under tension, and the charged density increases. This stimulates the tissue to swell to the original size after removal of the load. Adapted from Thorp et al.*[19] *under the terms of the Creative Commons Attribution 4.0 International License (https://creativecommons.org/licenses/by/4.0) and created with biorender.com*

Due to the dense structure, and thus the low hydraulic permeability, outflow of water is limited and the recovery is fast[20]. The osmotic pressure is dependent on the ion balance and thus on the FCD and the osmolarity of the bathing solution. This osmotic pressure dominates in the mechanical response, as 50% of the equilibrium modulus is taken up by the osmotic pressure[24–27]. When proteoglycans are removed from the tissue, the compressive modulus of articular cartilage drops to 2% of the original modulus[28]. Also the restriction of the collagen network plays an important

role, as degenerative changes in the collagen structure lead to less restriction of the swelling, resulting in decreased mechanical properties[29].

Upon normal loading conditions, the matrix is intrinsically incompressible due to the resistance of fluid flow, leading to fluid pressurization[30,31]. In time, fluid is pressed out of the cartilage until equilibrium is reached. Because of the structure and composition, articular cartilage is described as a poroviscoelastic material. The time-dependent and strain-rate dependent properties of articular cartilage originate from the previous described flow-dependent, combined with flow-independent properties. The latter comes from the intrinsic viscoelastic behavior of the collagen fibers[32–35]. These properties result in a creep or stress-relaxation behavior upon applying a force or displacement, respectively (Fig. 1.5)[25,36–39]. At equilibrium, the load is carried by the combination of the osmotic pressure and the deformed solid matrix[40,41]. These unique properties lead to the load bearing properties of articular cartilage, which differ between species, age and regions. In general, aggregate moduli range between 0.4-0.8 MPa, whereas Young's moduli range from 0.6 to 3 MPa (Table 1.1).

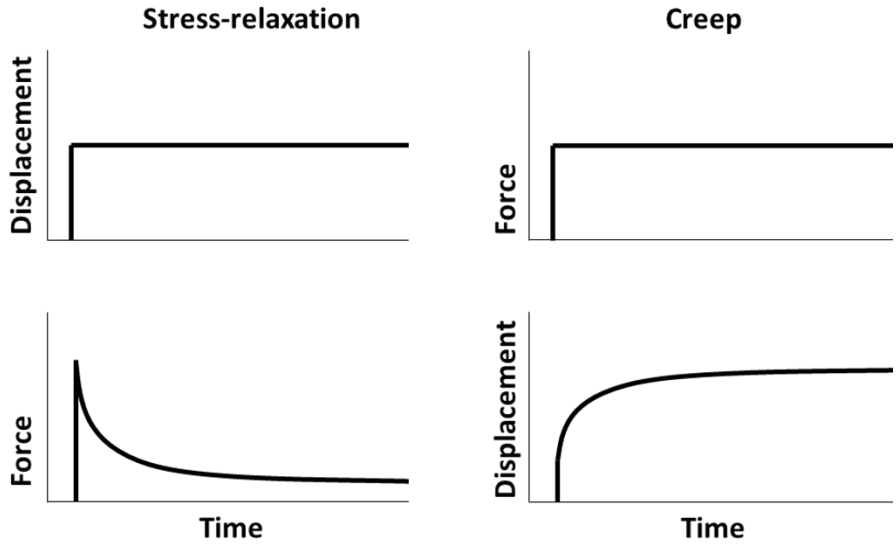

***Figure 1.5**: Stress-relaxation (left) and creep (right) behavior of articular cartilage.*

Table 1.1: *Mechanical properties of human and bovine articular cartilage in different regions.*

Sample Type	Tested region	Aggregate Modulus H_A (MPa)	Hydraulic permeability k (* 10^{-15} m4/Ns)	Compressive Young's Modulus E (MPa)
Human [42]	Lateral femoral condyle	0.701 ± 0.228	1.182 ± 0.207	-
	Medial femoral condyle	0.588 ± 0.114	1.137 ± 0.160	-
	Central patellar groove	0.530 ± 0.094	2.173 ± 0.730	-
Human [43]	Lateral tibial plateau	-	-	2.13 ± 0.74
	Medial tibial plateau			3.15 ± 1.42
Human [44]	Femoral trochlea	0.60	1.48	-
	Patella	0.42	2.46	-
Human [45]	patello-femoral groove	0.845 ± 0.383	-	0.581 ± 0.168
Human (elderly) [46]	Femoral head	2.40 ± 0.70	0.57 ± 0.34	1.57 ± 0.23
Bovine [46]	Humeral head	0.72 ± 0.33	1.3 ± 0.70	0.27 ± 0.15
Bovine[42]	Lateral femoral condyle	0.894 ± 0.293	0.426 ± 0.197	-
	Medial femoral condyle	0.899 ± 0.427	0.455 ± 0.332	-
	Central patellar groove	0.472 ± 0.147	1.422 ± 0.580	-
Bovine [47]	Humeral head	0.754 ± 0.198	-	0.677 ± 0.223
Bovine [48]	Distal femoral codyle	0.247 ± 0.018	-	-
Bovine[49]	Patella	0.66 ± 0.19	-	0.57 ± 0.17
	Medial femoral condyle	0.38 ± 0.19		0.31 ± 0.19
Bovine juvenile [50]	femoropatellar grooves	0.949 ± 0.021	2.72 ± 0.641	-

1.3 Cartilage articulation

Next to the load bearing properties, smooth articulation is the second most important property of articular cartilage. Due to a very low friction between the articulating surfaces, wear and tear of cartilage is prevented and shear stresses on chondrocytes are reduced. This very low friction arises by two types of lubrication modes. The first one is fluid-film lubrication, where friction is mainly dependent on the viscosity of the (synovial) fluid and the velocity between the two surfaces. In this lubrication regime, the fluid film is thicker than the roughness of the surface. The second boundary lubrication, where surfaces are in contact at the molecular level, and where contact pressures, surface roughness and the lubricant attaching to the boundary surfaces are the dominant factors for the resulting friction[51].

1.4 Focal cartilage defects & current treatments

Although cartilage is able withstand high loads for a human lifetime, sometimes

movement is impaired due to trauma or diseases. This can affect a smaller osteochondral region, in for example osteochondritis dissecans or osteochondral defects, or a whole joint, in for example osteoarthritis. The latter is a painful disease affecting joints and one of the main characteristics is the loss of cartilage, leading to bone-to-bone contact. In the Netherlands it is the most common disease, and eventually leading to impairment and a high burden for society[52]. Due to cartilage's avascular environment, regenerative capacity is limited, where articular cartilage tissue is unable to fully regenerate defects when the lesion diameter is larger than 6 mm[53]. For osteochondral defects, there is an increased risk of progression into osteoarthritis if left untreated[54], which stresses the importance of functional cartilage repair.

1.4.1 Current treatments

Treatments of knee pain often starts with conservative treatments using physiotherapy or medication. For focal cartilage lesions, some regenerative treatments are currently used in the clinic, for often younger patients (approximately until age of 60[55]) with some regenerative capacity using tissue or cell-based approaches, which might prevent or postpone the need of a total knee replacement at younger age, eventually leading to less replacement revisions[56,57]. A common technique used in the clinic is micro fracturing or drilling of focal defects, where the subchondral bone is drilled to release stem cells from the bone marrow to stimulate matrix deposition in the defect. Other examples are mosaicplasty, where little cylinders of combined cartilage and bone are implanted in the defect, mostly harvested from non-load bearing locations in the joint or obtained from donor material, autograft or allograft respectively. Another well accepted technique is autologous chondrocyte implantation (ACI), where chondrocytes are taken from the body, proliferated, and implanted back in the defect, with or without a cell carrier (matrix-induced autologous chondrocyte implantation, MACI). However, with all of these techniques, the newly synthesized tissue is often composed of or eventually becomes fibrocartilage, which is inferior to native articular cartilage because of the lower ratio of type I collagen to type II collagen, and lower aggrecan amounts, making it less durable in compression [58–60]. Alternatives are non-degradable implants, often metallic, but differences in stiffness between the implant and the surrounding tissue are known to cause load shielding of the adjacent cartilage and wear of the opposing cartilage[61,62].

1.4.2 Cartilage tissue engineering

To prevent these undesirable outcomes of current clinically used methods, the development of regenerative articular cartilage implants is envisioned to advance

the treatment of focal cartilage defects. Previous research has resulted in a broad range of new concepts and materials. By mimicking the native cell environment, hydrogels are generally considered one of the most promising material solutions [63–65]. Hydrogels are soft materials made of hydrophilic polymer networks that are able to absorb and retain water and are used as cell-carriers in articular cartilage tissue engineering. Polymers that are often used in cartilage tissue engineering are synthetic polymers, natural occurring polysaccharides or protein polymers, for example poly-ethylene glycol (PEG), agarose, hyaluronic acid, chondroitin sulfate and Gelatin methacrylate (GelMA), or combinations of these[66]. However, much more factors have influence on the success of tissue engineered cartilage, such as scaffolds architecture, cell source, chemical factors and physical factors[67] (Fig. 1.6).

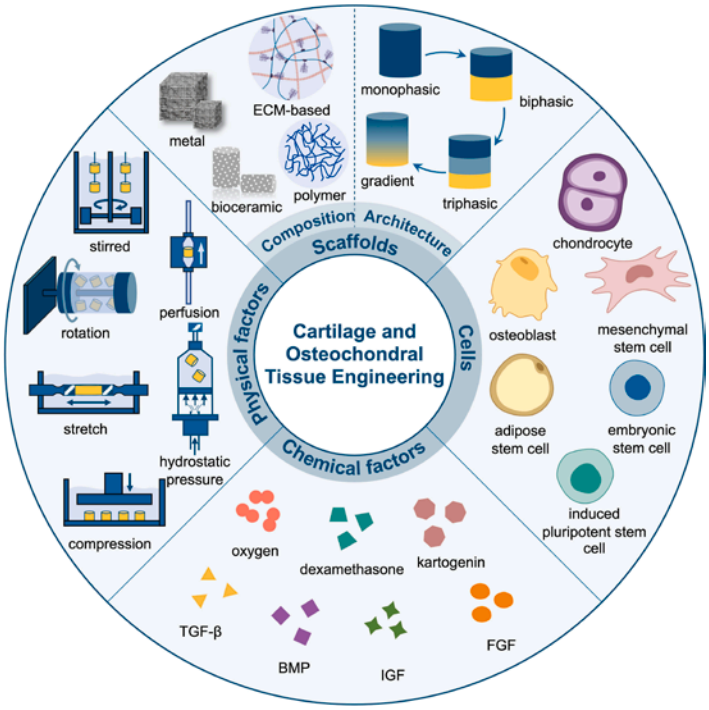

***Figure 1.6**: Factors involved in articular cartilage tissue engineering. Reprinted from Wei et al[67], under the terms of the Creative Commons Attribution 4.0 International License (https://creativecommons.org/licenses/by/4.0)*

1.5 Hypothesis

The main hurdle to overcome in tissue engineered cartilage is in general the low stiffness and strength, and therefore minimum load-bearing capacity of most hydrogels. Only a few hydrogel formulations reach the lower range of stiffnesses of native cartilage [68,69]. Therefore, several techniques have been developed to increase compressive stiffnesses of hydrogels, for example using fiber reinforcement by the introduction of 3D printed or woven scaffolds[70–72]. Using woven textile fabrics in cartilage tissue engineering, increased compressive stiffness is achieved with increased fiber content, tighter weave architecture and smaller pore sizes[73–76]. The addition of a water-rich hydrogel to these woven scaffolds did not alter the compressive stiffness[74,77]. This is in contrast to native cartilage, where collagen fibers themselves have limited effect on the compressive stiffness, except under extreme compression deformation[78]. Using an agarose hydrogel reinforced with a spacer fabric, consisting of a knitted top and bottom layer connected by pile yarns resulting in a 3D warp-knitted structure (Fig. 1.6), shows a threefold increase in stiffness in comparison to agarose alone[79]. However, the compressive stiffness of the resulting composite material is still inferior to native cartilage[79]. The introduction of a water-rich ECM with charged proteoglycans does have a large impact on the compressive stiffness, by the ability of the collagen fiber reinforcement to restrict the swelling of this ECM by tension of the collagen fibers[29]. As the pile yarns of the warp-knitted spacer fabric resemble the Benninghoff arcade-structure of collagen fibers in native cartilage, the overarching hypothesis in this thesis is that with the addition a of swelling hydrogel, restricted swelling can be achieved by the tension of these pile yarns. Using hydrogels incorporated with a FCD, water can be attracted in large amounts, mimicking the water-rich proteoglycan content of articular cartilage (Fig. 1.7). The restricted swelling of such hydrogels will result in an osmotic pressure, resembling healthy native cartilage's load-bearing principle.

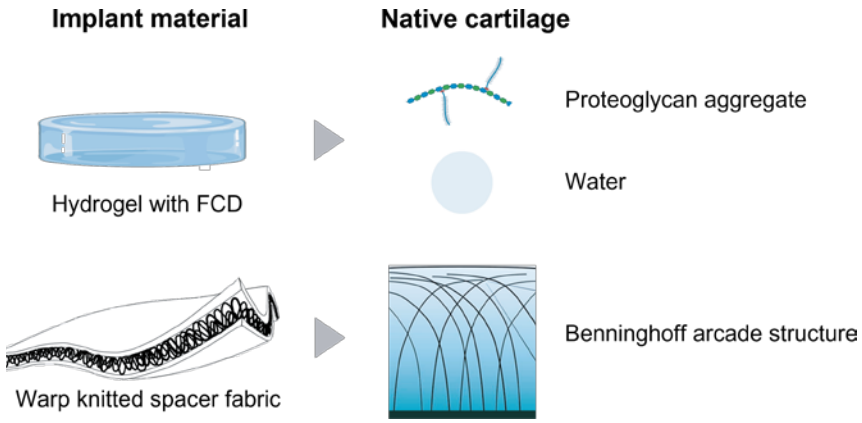

Figure 1.7: *Hypothesized implant material, consisting of a hydrogel with a FCD, mimicking the proteoglycan content of cartilage, injected within a spacer fabric, mimicking the arcade structure of cartilage. Adapted from Cooke et al.*[80] *under the terms of the Creative Commons Attribution 4.0 International License (https://creativecommons.org/licenses/by/4.0) and created with biorender.com*

1.6 Thesis outline and aim

In this thesis we aim to develop a tissue engineered, load bearing implant for cartilage replacement, based on a biomimetic restricted swelling approach. To accomplish that and achieve load-bearing properties, warp-knitted spacer fabrics are combined with high swelling hydrogels.

First, a proof of principle is described in **chapter 2** where swelling of a 2-hydroxyethyl methacrylate - sodium methacrylate (pHEMA NaMA) hydrogel would be restricted by the tension developing in a polyamide 6 (PA6) warp-knitted spacer fabric, mimicking the restricted swelling of proteoglycans in the arcade-like collagen structure in healthy cartilage. Indeed, a positive linear relationship is found between the osmotic pressure and the resulting mechanical stiffness of the implant.

The pHEMA NaMA used in chapter 2 is not suitable for chondrocyte encapsulation and thus regenerative applications. Therefore, in **chapter 3,** a biomimetic hydrogel is developed, based on native occurring polysaccharides chondroitin sulfate methacrylate (CSMA) and hyaluronic acid methacrylate (HAMA). Similar results were observed as in chapter 2, where restricted swelling by a PA6 spacer fabric significantly increased the mechanical properties. Moreover, primary bovine chondrocytes seeded within the restricted environment show promising initial cell viability.

In chapters 2 and 3, spacer fabrics are used synthesized from PA6, a non-degradable polymer. To develop a fully regenerative articular implant for focal defects, a

biodegradable spacer fabric composed of poly-4-hydroxybutyrate (P4HB) and polycaprolactone (PCL) is developed. These biodegradable spacer fabrics are used in combination with the in chapter 3 developed CSMA HAMA hydrogel to determine in **chapter 4** the wear on opposing cartilage by implanting the HydroSpacers in an osteochondral defect created in healthy bovine osteochondral plugs. Using a pin-on-plate wear apparatus, articulation of the implanted HydroSpacer is enabled against healthy bovine cartilage simulating gait. Placement of the HydroSpacer relative to the surface determines the resulting cartilage damage. Moreover, substantial load sharing of the implant with the surrounding cartilage is independent on implant placement.

PEGDMA CSMA hydrogels in combination with the P4HB spacer fabrics are used to study in **chapter 5** if induced hydrostatic pressure activates primary bovine chondrocytes to synthesize ECM components, or whether dynamic loading is required to stimulate synthesis of articular cartilage ECM in vitro. Similar effects regarding restricted swelling are observed as chapter 2 and 3. It was found that primary bovine chondrocytes express donor specific ECM synthesis in terms of type II and VI collagen independent on restricted swelling or mechanical stimulation during culture.

The pericellular matrix of chondrocytes, mainly consisting of type VI collagen, transduces biomechanical and biochemical signals to and protects the chondrocyte by stress-shielding. Moreover, results in chapter 5 might indicate a positive effect on type II collagen synthesis when a PCM is present. Therefore, it might be worthwhile to study the effect of the presence of a PCM on chondrocytes cultured in restricted swelling in a controlled manner. However, current methods to enzymatically isolate chondrons from bovine cartilage results in heterogenous cell populations. Therefore, in **Chapter 6** we developed a new isolation protocol, using type VI collagen as fluorescent active cell sorting strategy. Although a homogenous population could be obtained, the strategy leads to a low cell yield, which is more suitable for single-cell research instead of cartilage tissue engineering.

In **Chapter 7** the main findings of this thesis are discussed, including future recommendations regarding implant design, cell source and testing.

2

Towards a load bearing hydrogel: a proof of principle in the use of osmotic pressure for biomimetic cartilage constructs.

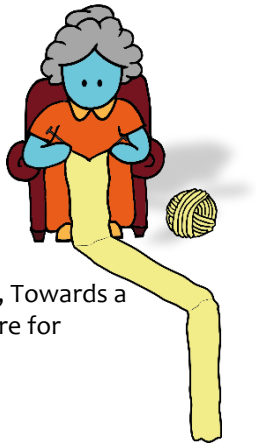

The contents of this chapter are based on:
G.H. Schuiringa, Maria Pastrama-Mastnak, Keita Ito, C.C. van Donkelaar, Towards a load bearing hydrogel: A proof of principle in the use of osmotic pressure for biomimetic cartilage constructs, vol. 137, January 2023, 105552
DOI: 10.1016/j.jmbbm.2022.105552

Abstract

Cartilage defects occur frequently and can lead to osteoarthritis. Hydrogels are a promising regenerative strategy for treating such defects, using their ability of mimicking the native extracellular matrix. However, commonly used hydrogels for tissue regeneration are too soft to resist load bearing in the joint. To overcome this, an implant is being developed in which the mechanical loadbearing function originates from the osmotic pressure generated by the swelling potential of a charged hydrogel, which is restricted from swelling by a textile spacer fabric. This study aims to quantify the relationship between the swelling potential of the hydrogel and the compressive stiffness of the implant.

Solutions with different molecular weight ratios of poly 2-hydroxyethyl methacrylate (pHEMA) and sodium methacrylate (NaMA) (20:0, 19:1, 18:2, 17:3) were used to create either plain hydrogels or HydroSpacers, which were obtained by injecting the hydrogel in a poly amide 6 (PA6) warp knitted spacer fabric. After equilibration in 0.15 M or 0.015 M sodium chloride solution, samples were mechanically tested in stress relaxation with a step deformation of 15% strain at a strain rate of 15% strain/sec and held till equilibrium was reached. Afterwards, samples were lyophilized to determine water, polymer content, fixed charge density (FCD) and osmotic pressure.

Hydrogels alone swelled up to 9-fold the initial weight, whereas HydroSpacers swelling was restricted to 1.2-fold. This restricted swelling of pHEMA-NaMA hydrogels in warp knitted PA6 spacer fabrics lead to an internal osmotic pressure. Regression analysis revealed a positive linear relationship between peak and equilibrium stress and osmotic pressure, showing that the mechanical properties of this so-called HydroSpacer can be tuned by adjusting the swelling capacity of the hydrogel via the FCD. In conclusion, a proof of principle is demonstrated using swelling hydrogels, where swelling of the hydrogel is restricted by the tension developing in the warp-knitted spacer fabric, resulted in a similar load-bearing mechanism as in healthy cartilage.

2.1 Introduction

There is a strong correlation between the load-bearing properties of articular cartilage and its total proteoglycan content [22,81–83]. In healthy hydrated cartilage in the unloaded state, the solid matrix, especially the collagen fiber network, restricts the swelling originating from the Donnan osmotic pressure, which is caused by the ion imbalance between the bathing solution and the interstitial fluid due to the negative fixed charges of the proteoglycans [20,38,84–88]. Moreover, the proteoglycan content provides both a high swelling pressure and a low hydraulic permeability, which results in a limited water loss during loading and fast recovery [20]. The osmotic pressure, dependent on the fixed charge density (FCD) and osmolarity of the bathing solution, has been shown to be the dominating factor in the equilibrium response, contributing up to 50% of the equilibrium modulus [24–27]. By modulating the Donnan osmotic pressure using different external saline concentrations of the bathing solution, cartilage stiffness is affected, showing a 50% reduction of the equilibrium modulus when bathed in a hypertonic solution [87,89]. When the tissue is depleted of proteoglycans, the modulus decreases to less than 2% of the original cartilage modulus [90]. Collagen, the other major component of the solid phase, is a crucial factor. The compressive stiffness of collagen is only significant at high compressive strains [78]. However, the specific arcade shaped and crosslinked collagen architecture in cartilage with fibers running from the cartilage-bone interface to the superficial layer [12,91], is essential for the generation of sufficient osmotic pressure by the encapsulated proteoglycan network. While the charged proteoglycans attract ions and therewith water, the tissue swells. This swelling tensions the collagen fibers, which then resist further swelling of the cartilage. Consequently, the number fixed charges per volume of water remains high, and therefore the osmotic pressure. Indeed, structural changes in collagen were shown to induce tissue swelling, suggesting failure to maintain the restricted swelling, leading to a decrease in stiffness of the tissue [29]. These results align with findings using a fibril-reinforced swelling poroviscoelastic model of articular cartilage [38,92], where the equilibrium load was found to be predominantly carried by the osmotic swelling pressure, which finds its origin in restriction against swelling by the collagen fibers [93]. In other words, the interaction between fluid, amorphous swelling proteoglycans and structured strain-resistant collagen fibers is essential for maintaining the mechanical properties and the load-bearing capacity of articular cartilage.

Due to trauma, focal cartilage defects may arise. Because cartilage has a limited

capacity of self-regeneration, focal defects are often treated to prevent cartilage deterioration into osteoarthritis (OA). Current treatments of focal defects such as osteochondral autograft transfer, autologous chondrocyte implantation and microfracture do not lead to the desired outcomes, inducing fibrous tissue formation, opposing cartilage damage and donor site morbidity and are limited to specific age groups, lesion sites or sizes [94,95]. To address this, research pertaining to the development of regenerative implants for cartilage focal defects have resulted in a broad range of new methods and materials. Due to their ease of handling and mimicking the native cell environment, hydrogels are generally considered the most promising solution [63–65].

However, the poor load-bearing capacity of most hydrogels is one of the main hurdles in creating successful regenerative cartilage implants; only a few hydrogel formulations reach the lower range stiffnesses of native cartilage [68,69]. To overcome this, fiber-reinforced hydrogels have been developed with significantly increased stiffness compared to hydrogels alone [70,71]. In hydrogels that contain woven fibers, the weave architecture, yarn diameter and friction between yarns are the key role players for guiding stiffness, with smaller pore sizes and porosities and tighter weave architectures leading to an increased stiffness of the construct [73–76]. However, the addition of alginate, fibrin or agarose hydrogels did not increase the stiffness of the composite material in comparison with the woven construct alone [77,96]. In contrast, hydrogel in a warp-knitted spacer fabrics, consisting of a knitted top and bottom layer which are connected by pile yarns, demonstrated a two to threefold increase of the Young's Modulus with non-swelling agarose or collagen-based hydrogels. Nevertheless, the Young's modulus of these spacer fabrics was still tenfold lower than of native cartilage [97]. The present study postulates that using a swelling hydrogel in a warp-knitted spacer fabric would have superior load-bearing properties. In such construct, swelling of the hydrogel would be restricted by the tension developing in the warp-knitted spacer fabric, mimicking the restricted swelling of proteoglycans in the arcade-like collagen structure in healthy cartilage. This load-bearing mechanism is similar to that of healthy cartilage, which means that not only the equilibrium stiffness, but also peak stiffness and the time-dependent behavior may mimic that of cartilage. The properties of this so-called HydroSpacer can be tuned by adjusting the density of fixed negative charges in the gel, thus adjusting the swelling potential, or the properties of the spacer fabric, such as the stiffness of the fiber or the density of pile yarns. The objective of the present study is to demonstrate the potential of using non-regenerative HydroSpacers as load-bearing cartilage replacement material, and the effect of modulating the load-

bearing capacity of the implant by tuning the swelling potential of the hydrogel.

2.2 Materials and methods

2.2.1 *Spacer fabrics*

Polyamide 6 (PA6) warp knitted spacer fabrics (Karl Mayer Textilmaschinenfabrik GmbH, Obertshausen, Germany) were used as restricting scaffold (Fig 2.1). The top and bottom layers were knitted using a multifilament yarn with a linear density of 44 dtex, applying 22.4 courses/cm and 37 wales/inch. The top and bottom parts were separated by a monofilament pile yarn with a linear density of 12 dtex, resulting in a total fabric height of 2.8 mm and fabric weight of 230.3 g/m^2. Samples of 8 mm diameter were cut from the spacer fabric using a laser cutter (VLS 3.50, Universal Laser Systems GmbH, Vienna, Austria). To visualize the macro- and microscopic morphology of the spacer fabric, a digital microscope (VHX-500F, Keyence Corporations, Osaka, Japan) was used.

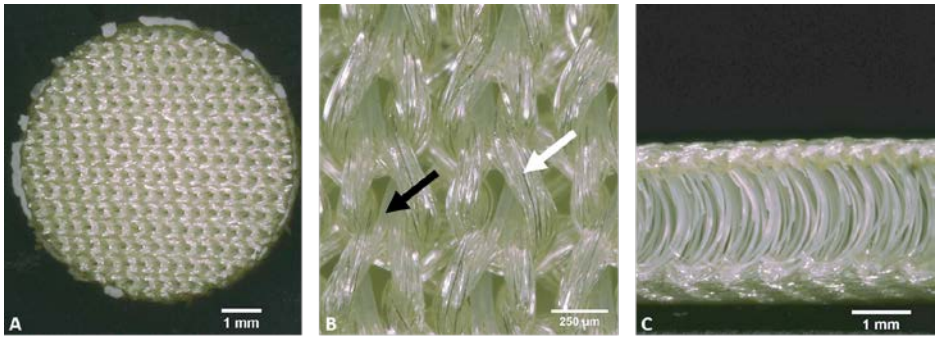

Figure 2.1: *Warp-knitted spacer fabric, without hydrogel.* ***A****) Top layer of the PA6 warp knitted spacer fabric.* ***B****) Close up of the warp knitted surface, with the multifilament indicated by the white arrow and the monofilament pile by the black arrow.* ***C****) Side view of the spacer fabric, with monofilaments separating the top and bottom layer.*

2.2.2 *Hydrogel*

To create a hydrogel with adjustable swelling potential, 20 mol% 2-hydroxyethyl methacrylate (HEMA, Sigma-Aldrich St. Louis, MO, USA) sodium methacrylate (NaMA, Sigma-Aldrich, St. Louis, MO, USA) hydrogel was used, which was created with 79.98 mol% demi water, 0.01 mol% poly(ethylene glycol) dimethacrylate (DMPEG, Sigma-Aldrich, St. Louis, MO, USA) as crosslinker, and 0.01 mol% 2,2-azobis (2-methylpropionamide)dihydrochloride (Sigma-Aldrich, St. Louis, MO, USA) to initiate the polymerization.

The fixed charge density of the gel, determining its swelling potential, depends on

the number of NaMA salt molecules that is incorporated in the copolymer. In the present study, four different compositions of the pHEMA:NaMA hydrogel were used in a 20:0, 19:1, 18:2 and 17:3 mol ratio. Unpolymerized hydrogel solution was stored at 4°C and protected from light prior to use.

2.2.3 Hydrogel and HydroSpacer polymerization

Hydrogels and HydroSpacers were prepared in a custom-made Teflon mold system with chambers of 8 mm in diameter and 3 mm in height, connected by a channel. Spacer fabrics with equal diameter were weighted, inserted in the chambers and covered with a 1 mm thick glass slide (Corning Life Sciences, Tewksbury, USA). The hydrogel was injected using a syringe, while the mold was held in a vertical position. To ensure that no air bubbles were formed, CT imaging of representative samples was performed using a µCT100 imaging system (Scanco Medical, Brüttisellen, Swisterland), with voxelsize of 14.8 µm and energy level and intensity set to 45 kVp and 88µA, respectively. The hydrogel was photopolymerized for three hours at a distance of ~5 cm, using 4 UV lamps (Nailstar professional, London, UK) resulting in an intensity of 4.8 mW/cm^2 at a wavelength of 365 nm.

2.2.4 Swelling ratio

To analyze the swelling potential of the hydrogels alone and in the HydroSpacers, the swelling ratio (SR, eq. 1), FCD and osmotic pressure were calculated from the weights of the samples after bathing in a sodium chloride (NaCl) solution of 0.15 or 0.015 M until equilibrium was reached.

$$SR = \frac{m_{wet}}{m_0} \tag{2.1}$$

with m_0 and m_{wet} as the weight prior to and after swelling, respectively.

2.2.5 FCD

After the experiment, samples were lyophilized (Freezone 2.5, Labconco, Kansas City, USA). The water content and polymer content were determined by subtracting the dry weight from the wet weight and by subtracting the weight of the spacer fabric from the dry weight, respectively. (eq 2.2 and 2.3)

$$m_{H_2O} = m_{wet} - m_{dry} \quad (2.2)$$

$$m_P = m_{dry} - m_{spacer\ fabric} \quad (2.3)$$

Using the NaMA density of the gel and polymer mass present in the HydroSpacer, the FCD of the constructs was obtained (eq 2.4) [41].

$$FCD = \frac{m_{NaMA} * \left(\frac{z_{NaMA}}{MW_{NaMA}}\right)}{m_{H_2O}} * \frac{1000\ mEq}{mol-charge} \quad (2.4)$$

with FCD in mEq/g, m_{NaMA} and m_{H_2O} respectively the mass of NaMA and total water content in mg, z_{NaMA} the mol-charge and MW_{NaMA} the molecular weight of NaMA.

2.2.6 Osmotic pressure

From the FCD, the osmotic pressure difference produced by the interactions of the bathing solution and the FCD was calculated (eq 2.5) [81].

$$\Delta\pi = \pi_{intern} - \pi_{extern} = RT\left(\sqrt{c^{F^2} + 4c^{*^2}} - 2c^*\right) \quad (2.5)$$

with R the gas constant, T the absolute temperature, c^F the FCD and c^* the osmolarity of the bathing solution.

2.2.7 Mechanical properties

To investigate the mechanical effect of the osmotic pressure on the constructs, a confined compression test was performed using a tensile tester (Model 42, MTS Criterion, Eden Prairie, USA) equipped with a loadcell of 5kN (LSB.503, MTS systems corp., Eden Prairie, USA). After polymerization, the samples were placed in a custom-made stainless-steel confined set-up with a diameter of 8 mm. A porous platen (316L stainless steel with 200 µm pore size, THN, Enschede, Netherlands), a custom-made piston and a 7 mm diameter stainless steel ball (Fabory, Tilburg, Netherlands) were placed consecutively on top of the sample, to allow fluid flow throughout the test (Fig 2.2). Subsequently, the bathing solution was added to the container and the construct was allowed to swell for ~24 h while a constant preload of 50 kPa was applied to keep the specimen in place. After the maximum height of the construct was reached, the crosshead position was fixed, and the swelling pressure induced by the construct was allowed to equilibrate prior to further testing.

To determine the mechanical properties, a stress relaxation test was performed by applying 15% strain, relative to the equilibrium height after swelling, with a strain rate of 15%/sec. The strain was held constant for 2.5 hours and stress relaxation was measured at a frequency of 10 Hz. The peak and equilibrium stresses (σ_t and σ_{Eq}), were calculated from the relaxation curve. To obtain the fast and slow relaxation response (τ_1 and τ_2), Matlab (Mathworks Inc., Natick, Massachusetts, United States) curve fitting was used (eq 2.6).

$$\sigma_t = a + b^{(-t/\tau_1)} + c^{(-t/\tau_2)} \tag{2.6}$$

where t is the test time in seconds and *a* and *b* are constants.

To calculate the hydraulic permeability k, equation 2.7 previously described by Cutcliffe and Defrate (2020) was used.

$$k = \frac{h^2}{H_A \tau_2} \tag{2.7}$$

where h is the height of the sample after swelling and H_A the aggregate modulus at 15% strain.

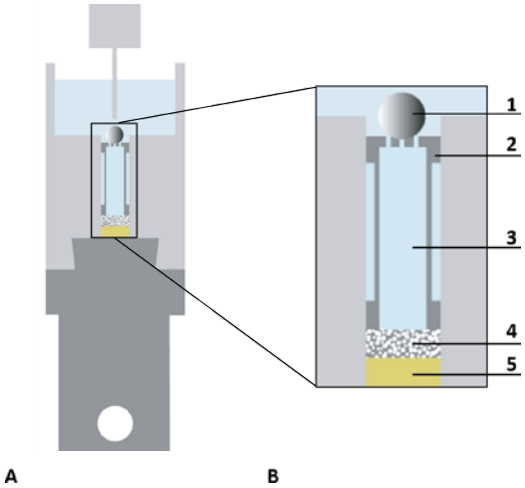

Figure 2.2: *Confined test set-up, consisting of a stainless-steel confined chamber containing the bathing solution, with the lower part mounted on the tensile tester (**A**) and the upper part containing ball on top (1), piston (2), bathing solution (3) porous platen (4) and the sample (5) (**B**).*

2.2.8 Statistical analysis

Data are presented as mean ± standard deviation. A two-way ANOVA with Tukey's multiple comparison post-hoc testing was used to compare the effect of hydrogel composition and bathing solution on the swelling and mechanical properties. A multiple linear regression model was applied to determine the effects of the dependent variables on peak and equilibrium stress. All analyses were performed using Prism GraphPad. A p-value < 0.05 was indicated as significant difference between groups (*p<0.05, **p<0.01, ***p<0.001).

2.3 Results

2.3.1 Swelling, FCD and osmotic pressure

Plain hydrogels (Fig 3A-B and left pairs of columns in Fig 2.4) swell up to 8.8 times their original volume (Fig 2.4A). Significant increase in swelling was found with increasing initial density of fixed charges (NaMA content), and with lower concentration of external saline concentration (0.15 vs 0.015 M NaCl), in agreement with osmotic swelling theories (Fig 4A). All HydroSpacers (Fig 2.3D,E and right pair of columns in Fig 2.4) containing NaMA swelled 1.2 times, independent of NaMA density or saline concentration of the bathing solution (Fig 2.4A).

With more swelling, the charges in the polymer network are diluted in a larger volume of water. Consequently, the effective FCD (mEq/L) and the osmotic pressure in equilibrium was similar between hydrogels (Fig 2.4B,C). With similar water uptake, yet different density of fixed negative charges incorporated in the polymer, the effective FCD in equilibrium of HydroSpacers significantly increased with increasing NaMA concentration up to 0.8 mEq/mg in the 17:3 composition (Fig 2.4B).

The hydrogels in 0.015 M NaCl develop slightly higher osmotic pressure compared to those in 0.15 M NaCl (Fig 2.4C), because stresses develop in the crosslinked polymeric network when it swells, and these stresses resist further swelling. For HydroSpacers, the lowest osmotic pressure can apparently stretch the pile yarns till 20% strain, but the highest osmotic pressures are unable to stretch the pile yarns much more than that. This may be explained by the bended structure of the pile yarns after warp-knitting (Fig 2.1C & 2.3C,D). During swelling until 1.2 times the original height, the pile yarns straighten (Fig 2.3E). Further swelling would strain the PA6 fibers, but the combination of all PA6 pile yarns is stiff enough to restrict swelling even for the case with the highest osmotic pressure. Consequently, there

is also a significant difference in osmotic swelling pressure depending on the amount of NaMA and on the bathing solution (eq 2.5, Fig 2.4C). CT images confirmed there were no air bubbles present in the HydroSpacers (Fig 2.3F).

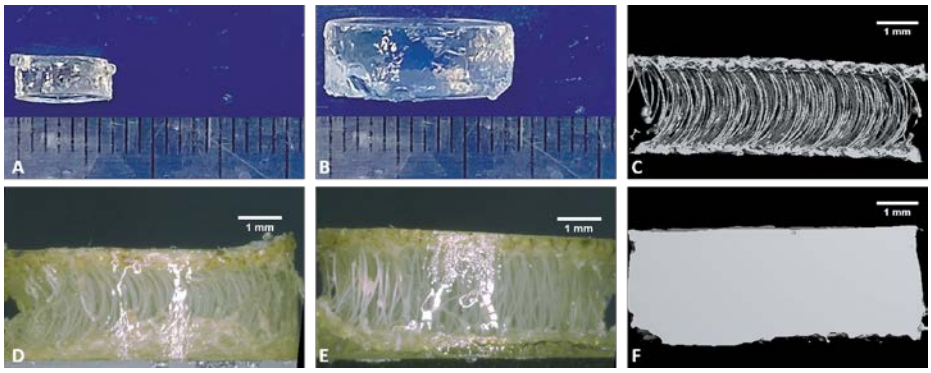

***Figure 2.3**: pHEMA : NaMA hydrogel with a 17:3 composition prior (**A**) and after swelling (**B**) in 0.15M NaCl. A difference in stretching of the pile yarns was observed in HydroSpacers directly prior (**D**) and after swelling (**E**). To confirm no air bubbles were present µCT images were taken from the construct, with an empty PA6 spacer fabric (**C**) and injected with pHEMA (**F**).*

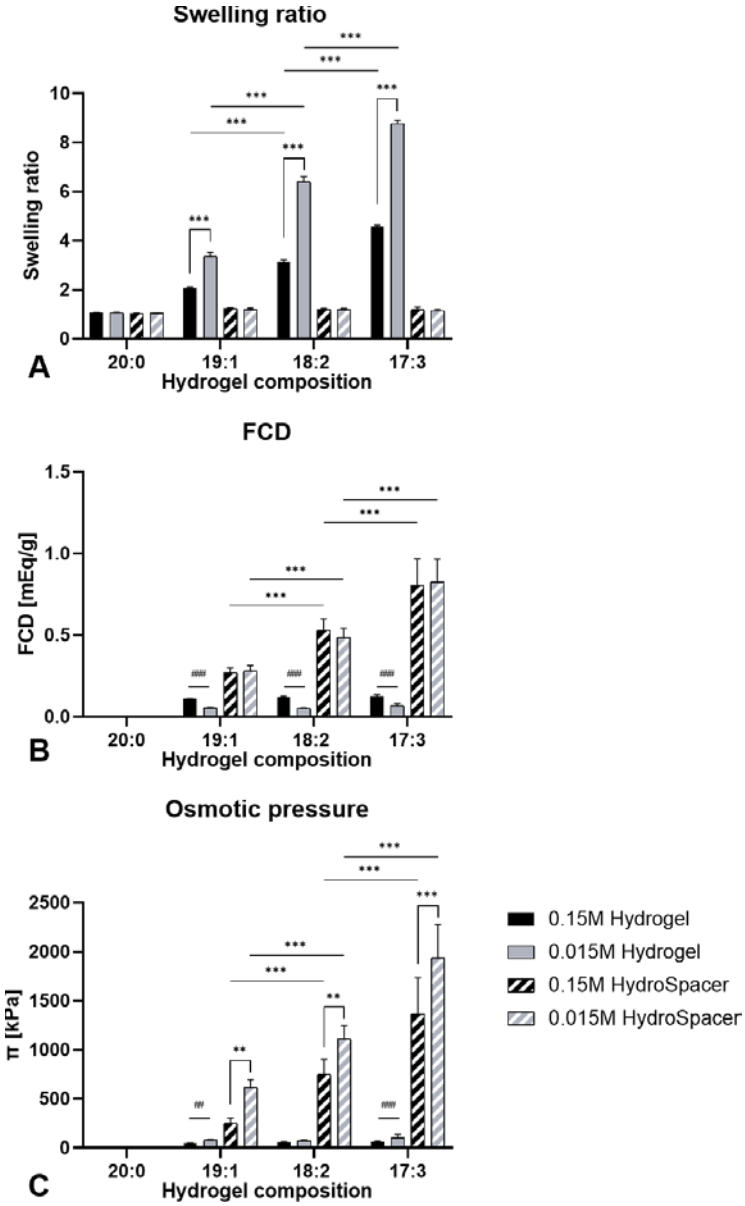

Figure 2.4: *Swelling ratios (**A**), FCDs (**B**) and osmotic pressures (**C**) of the four pHEMA-NaMA hydrogel compositions used, without and with the fiber reinforcement of a PA6 spacer fabric (HydroSpacer) bathed in 0.15M or 0.015M NaCl.*

2.3.2 Mechanical properties of the HydroSpacer constructs

With increasing NaMA concentration, the peak stress increased significantly for all HydroSpacer groups. For the equilibrium stress, significant differences were found between all groups in comparison with the 17:3 composition, for both bathing solutions. In contrast to the calculated osmotic pressures (Fig 4C), no significant differences were found in the stresses of the HydroSpacer consisting of the same hydrogel composition in the different bathing solutions. Theoretically it should be larger, following the osmotic pressure, and although the trend is clear, there is no significant difference (Fig 5).

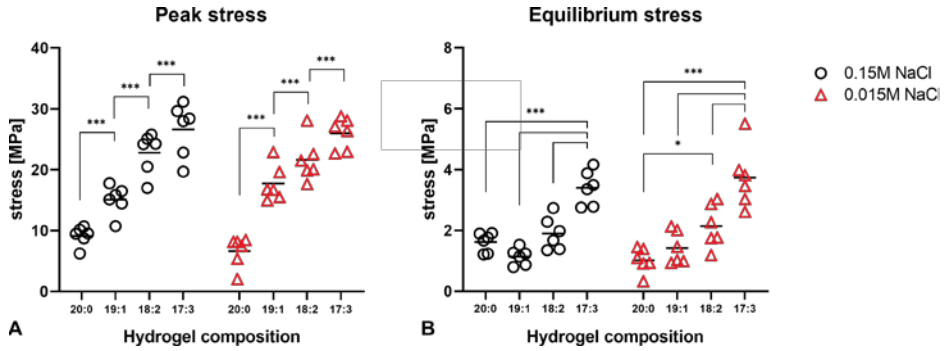

Figure 2.5: *Peak (**A**) and equilibrium (**B**) stress at 15% strain for HydroSpacers. Significant differences can be found with an increased NaMA concentration and is not dependent on bathing solution.*

A multiple linear regression was performed with the dependent variables water content (w%), polymer content (w%), osmotic pressure (kPa), and bathing solution osmolarity (M), to identify the variables that have a significant influence on the measured peak and equilibrium stress. Only the osmotic pressure had a significant effect on both stresses, whereas the composition does not significantly influence the outcome (Table 2.1).

***Table 2.1**: Multiple linear regression analysis between peak or equilibrium stress, and water content, polymer content, bathing solution or osmotic pressure.*

	Bathing solution	Adjusted squared	Osmotic pressure	Water content (w%)	Polymer content (w%)
Peak stress	0.15M NaCl	0.8103	<0.001 (***)	0.070 (ns)	0.133 (ns)
	0.015M NaCl	0.8607	<0.001 (***)	0.412 (ns)	0.613 (ns)
Equilibrium stress	0.15M NaCl	0.666	<0.001 (***)	0.545 (ns)	0.442 (ns)
	0.015M NaCl	0.734	<0.001 (***)	0.252 (ns)	0.205 (ns)

Further linear regression analysis revealed a significant linear relationship between osmotic pressure and peak (Fig 2.6A) and equilibrium stresses (Fig 2.6B) in HydroSpacers, with a R^2 of 0.48 and 0.69, respectively.

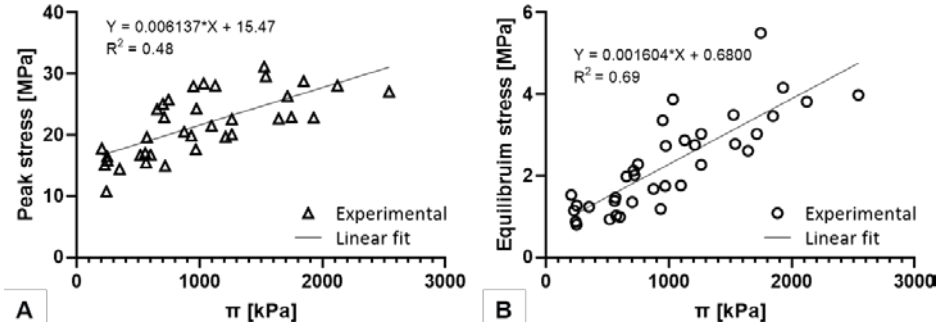

***Figure 2.6**: Regression model of the peak and equilibrium stress as a function of osmotic pressure.*

Moreover, a non-linear relationship between hydraulic permeability and FCD was observed, indicating that the hydraulic permeability decreased with an increased FCD, which was shown for both groups bathed in 0.15 M NaCl and 0.015 M NaCl (R^2=0.62 and 0.51, respectively, Fig 2.7).

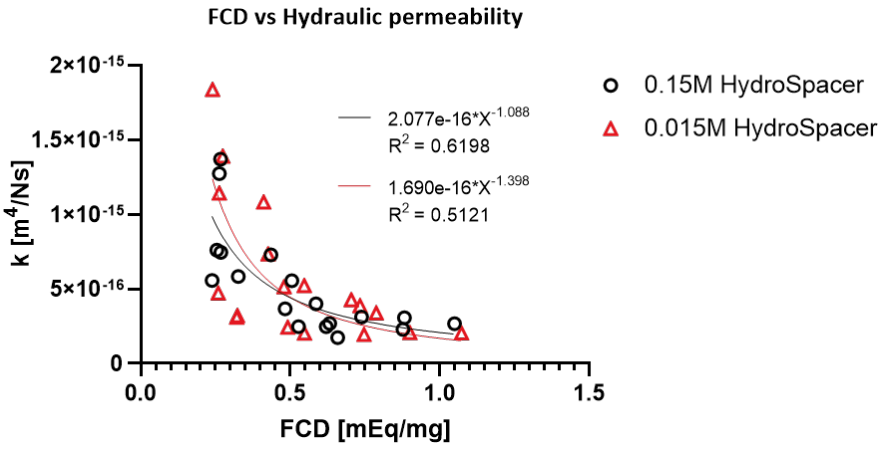

Figure 2.7: *Calculated values of the hydraulic permeabiitity plotted against the FCD. The fitted line shows a non-linear relationship between the FCD and the hydraulic permeability for both bathing solutions.*

2.4 Discussion

This study demonstrates that HydroSpacers containing hydrogels with incorporated fixed negative charges have equilibrium stiffness (1-4 MPa), peak stress (10-30 MPa) and permeability (10^{-15}-10^{-16} m^4/Ms) very similar to healthy articular cartilage (Fig 5 & 7). This load-bearing principle is identical to that in native cartilage, in which the load-bearing properties originate from the osmotic pressure induced by the FCD of the proteoglycan network and the restricting collagen network [93]. The relationship between these variables and the osmotic pressure illustrates that the mechanical properties of a HydroSpacer constructs can be tuned over a wide range by changing the FCD. Similar to cartilage [29,82,99,100], FCD and external salt concentration in the bathing solution together determine the mechanical properties of the HydroSpacers (Figure 4B). Though the osmotic pressure increases with a decreased salt concentration of the bathing solution (Fig 4C), this did not lead to significant differences of the peak and equilibrium stresses between groups with the same pHEMA:NaMA composition and FCD 0.3-1.0 mEq/mL (Fig 5). Similarly, in cartilage with FCDs of 0.3-0.4 mEq/mL the apparent Young's modulus plateaued with bathing solutions between 0.15 M and 0.015 M NaCl [82]. Finally, the reverse relationship between the FCD and the hydraulic permeability in cartilage [88,101] was also apparent in the HydroSpacers (Fig 7).

Although in the study of Schäfer et al. a significant increase of the Young's Modulus was observed with the introduction of hydrogels in warp-knitted poly (ethylene terephthalate) spacer fabrics compared to empty warp-knitted spacer fabrics, native cartilage stiffnesses were not reached [97]. The same applies for the use of chitosan nanofibers as fiber reinforced material in swelling hydrogels. By inserting nanofibers, swelling of polyacrylamide hydrogels was reduced by 75%, but a distinct difference in sustained stress between the restricted and free swelling hydrogel only occurred at non-physiological strain levels higher than 60% [102,103]. Restricted swelling up to 90% of three hydrogel compositions in woven poly(ε-caprolactone) (PCL) scaffolds led to an approximately 10-fold increase of the equilibrium modulus. The degree to which the swelling was restricted correlated with the increase in equilibrium modulus [104].
This is in line with the results shown in the present study, in which peak and equilibrium stress both depend on the amount of restricted swelling. In the study of Moffat et al., swelling hydrogels could increase volume even when restricted in fiber meshes, which was not possible in the PA6 spacer fabrics in the present study (Fig 2.3A). Apparently, the present fibers were stiffer or the pile yarns were denser. As a result of their swelling, Moffat's equilibrium moduli were less dependent on hydrogel compositions than the fully restricted HydroSpacers in the current study (Fig 2.5B) [104]. With changing the spacer fabric material, the stiffness of the pile yarns is the key factor for the stiffness of the whole construct. Using stiffer pile yarns, less swelling is allowed resulting in higher stiffnesses using the same hydrogel and vice versa. However, different spacer fabric materials might also alter the properties of the hydrogel, e.g. through chemical reactions with the hydrogel, alterations in cross-linking during the polymerization process, etc.

Restricted swelling results in high FCD and osmotic pressure, mimicking the interaction between proteoglycans and collagen in native cartilage tissue. Cartilage swelling correlates with collagen degradation in osteoarthritic cartilage [105]. Indeed, intact cartilage tissue detached from the bone swells 12% in 0.15M NaCl, while degenerate cartilage swells up to 51% [29]. This shows the importance of an intact collagen network to withstand the internal swelling pressure. In healthy cartilage, collagen in the deep zone is thought to be strained by 2-3% [92,106].

In native tissue, the FCD ranges from 0.04 to 0.3 mEq/mL [24,100]. The FCD in 19:1 pHEMA:NaMA hydrogel (0.27 mEq/g) is within this range, but the calculated FCDs in the other two hydrogel compositions is larger. Reported osmotic pressures increase with increasing FCD in cartilage and hydrogels. Cartilage with FCD between

0.08 and 0.18 mEq/mL has osmotic pressures up to 200 kPa in 0.015 M NaCl [100], the 0.27 mEq/mL 19:1 HydroSpacer in the present study reaches 250 kPa and 615 kPa in 0.15M and 0.015M NaCl, respectively (Fig 2.4B). Chondroitin sulfate (CS) solutions with an FCD of 0.5 mEq/mL reach 0.42 MPa and 0.6 MPa in 0.15 M and 0.015 M NaCl solutions, respectively [99]. This FCD is comparable with that of 18:2 pHEMA:NaMA HydroSpacers, which reach in 0.15M NaCL 0.75 MPa osmotic pressures. Hydrogels with FCD 0.8 mEq/mL reach approximately 1.3 MPa osmotic pressure in a physiological solution [41], similar to the 17:3 pHEMA:NaMA HydroSpacer.

Spacer fabrics restrict swelling in the 17:3 - 0.015 M NaCl group 8.8/1.2 = 7.3-fold, resulting in an 2000/100 = 20-fold increase in internal osmotic pressure. With the osmotic pressure taking 90% of the load bearing capacity in equilibrium [93], the load bearing capacity of the HydroSpacer is 0.9*20 = 18 times increased. With the equilibrium modulus of native cartilage ranging between 0.1 - 2 MPa [107] at 15% strain, this 90% would give estimated osmotic pressures between 13 kPa and 270 kPa, comparable to the osmotic pressure values found in HydroSpacers with the 19:1 composition (250 kPa). Finally, permeability in HydroSpacers with the lower FCDs correspond with values of native cartilage (10^{-16}-10^{-15} m^4/Ms) [107].

In this study, 2.8 mm high PA6 fabrics were used, which is in the high range of tibia plateau cartilage thickness [2]. The mechanical performance will be independent of samples size, as it is determined by the fixed charge density in the tissue, which is determined by gel composition and swelling, which is equal throughout samples. There are some major advantages of using cartilage-implants based on swelling hydrogels in which the swelling is restricted by a fiber mesh. First, they are immediately load-bearing even without neotissue formation by seeded chondrocytes. Typically, (M)ACI-type surgeries with cell-seeded gels are too soft for load-bearing immediately post-operatively. These constructs develop stiffness over time when matrix is being produced by the cells. Therefore, a significant period of non-loading is required after surgery[108]. This is not needed with HydroSpacers, as these constructs are immediately load-bearing due to their inherent osmotic pressure. Second, HydroSpacers have cartilage-mimicking mechanical properties, which means that their surface is pliable. This provides these implants with an advantage over clinically used metal resurfacing implants, which are very stiff and may consequently damage opposing cartilage, in particular when implanted at a slight angle [61,109]. Another advantage of HydroSpacers over metal implants is that MRI remains possible. The spacer fabric and hydrogel materials used in this paper were chosen based on their reproducible properties, to demonstrate the proof of

principle. In other versions, biocompatible spacer fabric (eg PCL-based) and hydrogels (eg Chondroitin sulphate-based) may be used, which allows this system to be used as a regenerative platform [110,111]. Ultimately, creating an osteochondral implant by combining a regenerative HydroSpacer adhered to a synthetic bone scaffold is desired to induce osteointegration and stabilization, which will be in the end beneficial for the treatment of osteochondral defects caused by for example trauma or osteochondritis dissecans in younger and active patients, as it allows patients to instantly load the affected joint and reduce recovery times.

In conclusion, this study is the proof of principle that it is possible to mimic the load-bearing mechanism in cartilage by injecting a swelling hydrogel in a strain-limiting spacer fabric. The positive linear relationship between peak and equilibrium stress and osmotic pressure allow the mechanical properties of this so-called HydroSpacer to be tuned by adjusting the swelling capacity of the hydrogel via the FCD. In this study non-regenerative materials were used. In the future, cell-seeded biocompatible and biodegradable swelling hydrogels may be used in combination with biocompatible warp-knitted spacers fabrics to create regenerative implants with immediate load-bearing properties.

2.5 Acknowledgements

This research was performed under the framework of Chemelot InSciTe, supported by the partners of Regenerative Medicine Crossing Borders and powered by Health~Holland, Top Sector Life Sciences & Health.

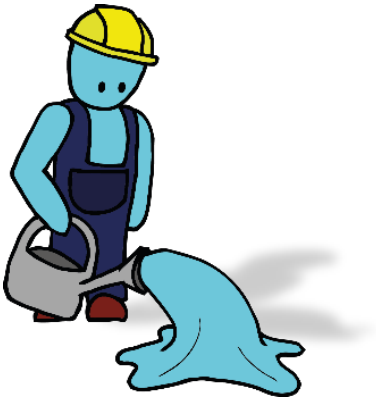

3

Creating a Functional Biomimetic Cartilage Implant Using Hydrogels Based on Methacrylated Chondroitin Sulfate and Hyaluronic Acid

The contents of this chapter are based on:
G. H. Schuiringa*, M. Mihajlovic*, C. C. van Donkelaar, T. Vermonden, K. Ito, Creating a functional biomimetic cartilage implant using hydrogels based on methacrylated chondroitin sulfate and hyaluronic Acid, vol. 8, issue 7, 2022
DOI: 10.3390/gels8070457
* These authors contributed equally to this work

Abstract

The load-bearing function of articular cartilage tissue contrasts with the poor load-bearing capacity of most soft hydrogels used for its regeneration. The present study explores whether a hydrogel based on the methacrylated natural polymers chondroitin sulfate (CSMA) and hyaluronic acid (HAMA), injected into warp-knitted spacer fabrics, could be used to create a biomimetic construct with cartilage-like mechanical properties. The swelling ratio of the combined CSMA/HAMA hydrogels in the first 20 days was higher for hydrogels with a higher CSMA concentration, and these hydrogels also degraded quicker, whereas those with a 1.33 wt% of HAMA were stable for more than 120 days. When confined by a polyamide 6 (PA6) spacer fabric, the volumetric swelling of the combined CSMA/HAMA gels (10 wt%, 6.5 × CSMA:HAMA ratio) was reduced by ~53%. Both the apparent peak and the equilibrium modulus significantly increased in the PA6-restricted constructs compared to the free-swelling hydrogels after 28 days of swelling, and no significant differences in the moduli and time constant compared to native bovine cartilage were observed. Moreover, the cell viability in the CSMA/HAMA PA6 constructs was comparable to that in gelatin–methacrylamide (GelMA) PA6 constructs at one day after polymerization. These results suggest that using a HydroSpacer construct with an extracellular matrix (ECM)-like biopolymer-based hydrogel is a promising approach for mimicking the load-bearing properties of native cartilage.

3.1 Introduction

Hydrogels are soft materials made of hydrophilic polymer networks that are able to absorb and retain water. In the past few decades, interest in these materials has increased significantly, especially in the fields of artificial implants, scaffolds, drug delivery, and wound healing [112–117]. Since they are able to mimic the extracellular matrix (ECM), hydrogels are particularly suitable for carrying and supporting cells [118–121], and are therefore applicable to tissue engineering and regenerative medicine. Naturally occurring glycosaminoglycans (GAGs), such as chondroitin sulfate (CS) and hyaluronic acid (HA), are very attractive materials for designing biomimetic hydrogels [122]. CS is a sulfated linear polysaccharide composed of glucuronic acid and *N*-acetylgalactosamine as its repeating disaccharide unit [123]. HA is also a linear polysaccharide, whose disaccharide repeating unit is composed of glucuronic acid and *N*-acetylglucosamine [124]. Both polymers are highly hydrophilic, negatively charged, and, therefore, characterized by water retention capacity and possessed of specific rheological, physiological, and biological properties. The resulting hydrogels have the potential to support encapsulated chondrocytes and are recommended for applications where chondrogenic potential is required [125–128]. However, the load-bearing function of articular cartilage tissue contrasts with the poor load-bearing capacity of most currently used and developed soft hydrogels [68,69].

The mechanical properties of native articular cartilage originate from the fact that the proteoglycans present in the tissue attract water due to an ion imbalance between the tissue and the surrounding fluid, and therefore induce tissue swelling. On the other hand, this swelling is restricted by the specific arcade-shaped, crosslinked collagen architecture present in the cartilage [12], inducing a Donnan osmotic pressure as the fixed charge density (FCD) remains high [20,38,84–88]. The more the swelling is prohibited, the higher the proteoglycan density and, therefore, the FCD are, and the better the load-bearing capacity is [22,81–83]. A drop to 2% of the original cartilage modulus was observed when the tissue was depleted of proteoglycans [28]. Moreover, the equilibrium response was found to be largely controlled by the osmotic pressure, as demonstrated by in vivo and in silico studies [24–27,38,92,93].

Both HA and CS belong to the family of GAGs that are naturally found in ECM and connective tissues, especially in articular cartilage. Therefore, these biopolymers are characterized by inherent cytocompatibility and bioactivity, which makes them suitable materials for clinical translation, e.g., for scaffolds in cartilage tissue engineering. Both methacrylated HA and CS,

referred to as HAMA and CSMA, respectively, have individually been combined with other materials (both synthetic and natural) in order to achieve blends with improved properties, such as mechanical properties, swelling, biocompatibility, or application-oriented properties, as reviewed elsewhere [110]. However, CSMA and HAMA photocrosslinkable polymers have rarely been explored when combined alone, with no other additional materials. More often than not, CSMA and HAMA, when combined together, have also been joined by other biopolymers, such as collagen [129,130], gelatin-methacrylate (GelMA) [131], or alginate [132]. In most of these cases, the goal of such combinations was to intrinsically affect the final application, mainly by enhancing and regulating the chondrogenesis, and, in some cases, improving the mechanical properties (e.g., the stiffness) [131].
To improve the stiffness of hydrogels, fiber reinforcement has often been employed [70,133]. Another method is the use of warp-knitted spacer fabrics, consisting of a knitted top layer and a bottom layer connected by pile yarns, which have been shown to have a beneficial effect on the stiffness compared to plain hydrogels [79]. Such spacer fabrics restricted the swelling of negatively charged hydrogels (pHEMA-NaMA), thus generating a high osmotic pressure[134]. A significant positive correlation between the FCD of the hydrogel and the resulting stiffness of the construct was identified, and, with respect to the physiological cartilage-like FCD, the load-bearing properties were similar to those in cartilage, both in the loading phase and in the equilibrium phase[134].

Although the abovementioned study is very promising for the creation of implants for cartilage replacement with cartilage-mimetic load-bearing properties, it used very stable hydrogels that were non-regenerative and based on cytotoxic monomers. Thus, these gels cannot be used for clinical applications. The present study explores whether hydrogels based on the natural polymers CS and HA, injected into warp-knitted spacer fabrics (Scheme 3.1), could be used to create biomimetic constructs with cartilage-mimetic mechanical properties that would be stable over a longer time-period. The mechanical properties of these constructs, referred to as HydroSpacers, are characterized as a function of swelling achieved by varying the degree of hydrogel confinement in comparison to native articular cartilage.

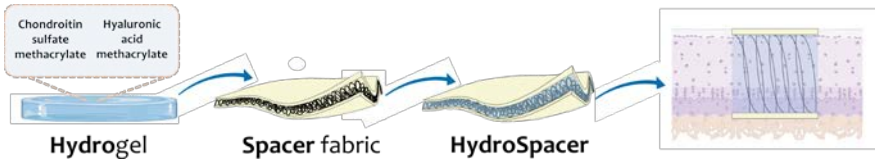

Scheme 3.1. *Hydrogel based on methacrylated chondroitin sulfate (CSMA) and hyaluronic acid (HAMA) is combined with polyamide 6 (PA 6) warp-knitted spacer fabric to form a HydroSpacer—a construct with spacer fabric material restricting hydrogel swelling and mimicking cartilage structural organization. Partially created with biorender.com.*

3.2 Materials and Methods

3.2.1. Materials

Sodium hyaluronate was purchased from Lifecore Biomedical (323 kDa as measured with GPC, Chaska, MN). Chondroitin 4-sulfate sodium salt (bovine trachea) was obtained from Sigma-Aldrich (Zwijndrecht, the Netherlands). Lithium phenyl-2,4,6-trimethylbenzoylphosphinate was obtained from TCI Europe N.V (Zwijndrecht, the Netherlands). All organic solvents and reagents were purchased from Biosolve (Valkenswaard, the Netherlands) and Sigma-Aldrich (Zwijndrecht, the Netherlands), respectively, and were used without further purification. PA6 warp-knitted spacer fabrics were obtained from Karl Mayer Textilmaschinenfabrik GmbH (Obertshausen, Germany). Collagenase type II was purchased from Worthington Biochemical Corporation (Lakewood, NJ, USA). Hyaluronidase, fetal bovine serum (FBS, BCBV7611), and Calcein AM were purchased from Sigma-Aldrich. Dulbecco's Modified Eagle Medium (DMEM, 41966-029, GibcoTM), penicillin/streptomycin (P/S, 15070063), and propidium iodide were purchased from Thermo Fisher Scientific (Landsmeer, the Netherlands/Waltham, MA, USA). Insulin/transferrin/selenium-plus (ITS+ premix, Corning) was obtained from VWR International B.V. (Amsterdam, the Netherlands).

3.2.2 Functionalization of the Biopolymers

The sodium salts of both the hyaluronic acid (HA) and chondroitin 4-sulfate (CS) were chemically modified to bear pending methacrylate moieties (Supporting information, Scheme S1). The methacrylation of HA was performed following a previously reported method [135]. Briefly, HA (4.8 g, 11.9 mmol) was dissolved in milliQ water (240 mL), and the solution was stirred overnight at 4 °C. Then, DMF (240 mL) was added, and the resulting mixture

was placed in an ice bath. Methacrylic anhydride (5.5 mL, 36.9 mmol) was added dropwise at 0 °C (over 3.5 h), while continuously adjusting the pH between 8–9 (0.5 M NaOH). Next, the reaction mixture was supplemented with NaCl (0.5 M final concentration), followed by precipitation in cold ethanol. After filtration, the white precipitate was recovered, redissolved in milliQ water (550 mL), and dialyzed against water for 3 days (cutoff 14 kDa). The final product, corresponding to methacrylated HA (HAMA), was obtained after freeze-drying for 2 days as a white, cotton-like material (yield ~80%, defined as the ratio between the number of moles of the recovered HAMA and the starting HA, adjusting the molar mass of the HAMA according to the amount of the grafted methacrylate groups). For the methacrylation of CS, a previously published protocol was used [136]. Briefly, the sodium salt of CS was firstly converted into a more lipophilic tert-butyl-ammonium (TBA) salt (CS-TBA) through resin exchange (Dowex 50 × 8 w hydrogen form and tert-butyl-ammonium fluoride). The CS-TBA was then frozen and dialyzed (for 2 days against NaCl 150 mM aqueous solution, followed by 3 days against water, cutoff 14 kDa) and freeze-dried for 2 days. The dry CS-TBA (24.5 g, 31.1 mmol) was dissolved in anhydrous DMSO (935 mL), and the solution was stirred under N_2 at 50 °C until the CS-TBA was fully dissolved. Then, 4-dimethylaminopyridne (DMAP) was added (4.5 g, 36.8 mmol), followed by glycidyl methacrylate (GMA) (5.1 mL, 37.3 mmol, feed ratio GMA:HA disaccharide 1.2), and it was allowed to stir at 50 °C for 65 h. The reaction mixture was diluted with milliQ water (water:DMSO ratio 1:1) and the pH was adjusted to 5.5 (0.2 M HCl). Finally, dialysis (for 3 days, cutoff 14 kDa) and freeze-drying for 2 days yielded the final product, chondroitin 4-sulfate methacrylate (CSMA), as a white-yellow fluffy solid (yield ~94%, defined as the ratio between the number of moles of the recovered CSMA and the starting CS, adjusting the molar mass of the CSMA according to the amount of the grafted methacrylate groups).

3.2.3 Determination of the Degree of Methacrylation with HPLC

The HAMA and CSMA polymers were accurately weighed (5 mg), placed in 2 mL of 0.02 M NaOH solution, and incubated overnight at 37 °C to allow for the basic hydrolysis of the methacrylate groups. Next, 1 mL of 2 M acetic acid was added to neutralize the solution. Methacrylic acid freed from the polymers was quantified with HPLC [137]. Specifically, the HPLC system was used (Alliance Waters), equipped with a UV-Vis detector (Dual Lambda absorbance, 210 nm) and Waters Sunfire C18 column. The eluent used had a

ratio of 15:85 acetonitrile:milliQ water (v%), supplemented with 0.1% perchloric acid. The flow rate was set at 1 mL/min, and 10 µL of each sample was injected. The quantification was performed by means of a calibration curve of the methacrylic acid standards. The degree of methacrylation (DM) was defined as the number of methacrylate groups per the disaccharide units and expressed as a percentage.

3.2.4 ^{1}H-NMR Spectroscopy

The NMR spectra of the functionalized biopolymers HAMA, CS-TBA, and CSMA were recorded on an Agilent 400-MR NMR spectrometer (Agilent Technologies, Santa Clara, CA, USA) in D_2O. The chemical shifts were reported as δ in parts per million (ppm) and were calibrated against a residual solvent peak of D_2O (δ = 4.79 ppm) or DMSO (δ = 2.50 ppm).

3.2.5 Hydrogel Fabrication

The CSMA and HAMA hydrogel disks were prepared by dissolving the polymers in PBS at the desired concentration (10 wt%). The resulting polymer solutions were supplemented with lithium phenyl-2,4,6-trimethylbenzoylphosphinate (LAP) photo-initiator (0.2 or 0.3 w/v% final concentration,) subsequently injected into a Teflon mold with cylindrical wells, and covered on both sides with quartz glass plates. The well dimensions for the free-swelling gels were 6 × 2 mm (diameter × height) and those for the confined gels were 8 × 3 mm (diameter × height). The crosslinking was achieved by UV-irradiating the samples for 15 min at distances of 3 or 5 cm from the light source for each side of the mold (UV lamp VL-4.LC, A. Hartenstein GmbH, intensity 0.58–1.49 mW/cm^2, wavelength 365 nm). The HydroSpacers were prepared by inserting the warp-knitted PA6 spacer fabric (height: ~2.7 mm, diameter 8 mm) into the mold prior to filling the wells with the CSMA/HAMA hydrogel. The UV-polymerized HydroSpacers were transferred into cylindrical resin cassettes (8 × 3 mm, diameter × height). R05 resin (Envisiontec, Dearborn, MI, USA) was used to prevent the lateral swelling of the hydrogel. The spacer fabrics and HydroSpacers were visualized using a digital microscope (VHX-500F, Keyence Corporations, Osaka, Japan).

3.2.6 Crosslinking Efficiency Determination

Methacrylation conversion (crosslinking efficiency) after photopolymerization was determined with HPLC by measuring the amount of free methacrylic acid released after basic hydrolysis, corresponding to the methacrylate groups not reacted during photopolymerization (see Section 4.3). Instead of using free polymers, prepared hydrogels were freeze-dried and their weight was recorded (~60 mg).

3.2.7 Swelling

The hydrogel swelling capacity was determined by gravimetry. The unconfined hydrogel disks and HydroSpacers with and without cassettes were placed in pre-weighed vials. The initial weight (W_0) was recorded, and the samples were incubated in 1 mL PBS (pH 7.4) at 37 °C. At designated time points, the hydrogel weight was determined (W_t). The swelling ratio, defined as the ratio of W_t/W_0, was used to characterize the hydrogel swelling capacity. All samples were measured in triplicate.

3.2.8 Bovine Cartilage Harvesting

Full-thickness cartilage was harvested from bovine patellae (3–6 years old), which were collected after slaughter and stored at –20 °C. Prior to harvesting, the patellae were thawed at 4 °C for 24 h, immersed in PBS. Cartilage without visible fissures or roughening was isolated from the underlying bone of the distal-lateral quadrants of the patellae using a razor blade. Samples were immediately punched using an 8 mm-diameter biopsy punch (Curavet, Garbsen, Germany), positioned in the resin cassettes to ensure lateral confinement, and allowed to equilibrate in PBS at room temperature prior to mechanical characterization.

3.2.9 Mechanical Characterization

To determine the stiffness of the hydrogels, HydroSpacers, and cartilage plugs, such that the measurements were free of swelling or damage at the cut edges, an indentation test was performed using a 5 mm-diameter plane-ended indenter attached to a tensile tester (Model 42, MTS Criterion, Eden Prairie, MN, USA) equipped with a 50 N loadcell (LSB.503, MTS Systems Corp., Eden Prairie, MN, USA). The hydrogels and HydroSpacers were tested within the confined resin cassettes at day 0 and day 28. HydroSpacers were already kept in these cassettes. After 28 days of swelling in PBS at 37 °C, the

free-swelling hydrogels were cut to fit into the resin cassettes using an 8 mm-diameter biopsy punch (Curavet, Garbsen, Germany).
A stress relaxation test was performed by applying 15% strain, relative to the equilibrium height after swelling, with a strain rate of 15%/sec, in PBS. The strain was held constant for 600 s and the stress relaxation was measured at a frequency of 10 Hz. The apparent peak, equilibrium moduli, and time constant τ_2 were calculated from the relaxation curve using curve fitting (Equation 3.1), using Matlab (Mathworks Inc., Natick, MA, USA):

$$\sigma_t = a + b^{(-t/\tau_1)} + c^{(-t/\tau_2)} \quad (3.1)$$

where t is the test time in seconds and *a, b and c* are constants.

3.2.10 Cell Viability

The chondrocytes were isolated from bovine metacarpal joints (aged 8–12 months, slaughterhouse material) using a previously described enzymatic digestion method [135]. After harvesting, the cells were suspended in either 10 % (*w/v*) GelMA or 10 wt% CSMA/HAMA at a concentration of 10×10^6 cells/mL, injected into the PA6 spacer fabrics and polymerized as previously described. The HydroSpacers were cultured in DMEM, 41966-029, supplemented with 1% ITS+ premix and 1% P/S for up to 7 days. The cell viability was assessed using a live/dead assay. The samples were cut in half and stained, for living cells using Calcein AM (2 µM) and for dead cells using propidium iodide (1.5 µM), in PBS for 60 min at 37 °C, and visualized using confocal microscopy (Leica TCS SP5X, Wetzlar, Germany) after 1 day and 7 days of culture.

3.2.11 Statistics

The data are presented as the mean ± standard deviation. A Shapiro–Wilk test was performed to check for normality. If the samples were normally distributed, a two-way ANOVA test with Tukey's multiple comparison post hoc testing was performed; otherwise, a Kruskal–Wallis test with a Dunn's multiple comparison test was performed. All analyses were performed using Prism GraphPad. A *p*-value < 0.05 threshold was used to indicate significant differences between the groups (* $p < 0.05$, ** $p < 0.01$, *** $p < 0.001$).

3.3 Results and Discussion

3.3.1 Biopolymer Functionalization

During the preparation of the methacrylated polymers, the presence of proton peaks in the aliphatic region in the ^{1}H-NMR spectrum (0.94, 1.32, 1.57, and 3.16 ppm) demonstrated the successful exchange of the sodium salt with TBA cations (Figure 3.1A). The following methacrylation reaction yielded CSMA polymer, as confirmed by the ^{1}H-NMR spectrum, demonstrating the presence of methacrylate group proton peaks at 1.96, 5.77, and 6.20 ppm [136], while the peaks of the aliphatic protons disappeared, confirming the successful removal of the TBA ions (Figure 3.1A). The final CSMA polymer displayed a degree of methacrylation (DM) of ca. 23%, as determined by HPLC.

The formation of HAMA was confirmed by ^{1}H-NMR with a DM of ca. 39%, where peaks corresponding to methacrylate protons were observed at 5.75 and 6.19 ppm (Figure 1B). All the detected peaks were in accordance with previously published results [135,136]. The methacrylation of both CS and HA was in line with the previously reported reactions, and both products were obtained as expected. It was important that the DM of HAMA exceeded 30%, as the crosslinking points deriving from HA methacrylate groups are considered to be responsible for the stability features of hydrogels. This notion is related to the higher stability of the ester methacrylate groups on HA polymers as compared to CSMA polymers [138].

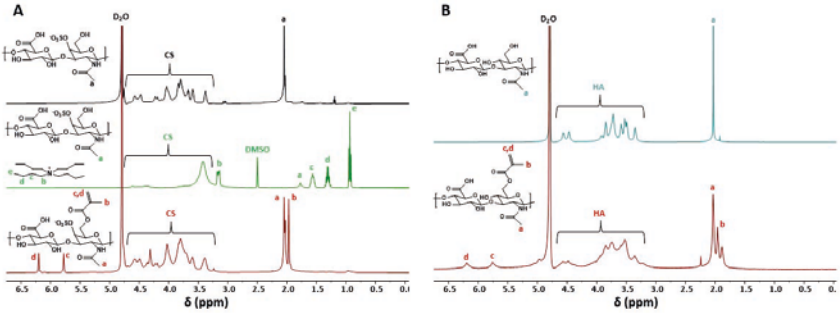

Figure 3.1 *(**A**) H-NMR spectra of CS (top) in D_2O, CS-TBA (middle) in DMSO d-6, and CSMA (bottom) in D_2O. (**B**) H-NMR spectra of HA (top) in D_2O and HAMA (bottom) in D_2O.*

3.3.2 Hydrogel Fabrication and Crosslinking Efficiency

The hydrogels were prepared via photopolymerization, and PA6 spacer fabric (Figure 3.2A) was used to confine the CSMA/HAMA hydrogels, yielding a HydroSpacer construct (Figure 3.2B). In order for the CSMA/HAMA hydrogels to be used as suitable cell carriers, the presence of unreacted methacrylate groups has to be limited [139]. The unreacted methacrylate groups, upon hydrolysis, produce methacrylic acid, which can cause cell toxicity due to its acidic character and reactivity to nucleophilic compounds [140–142]. Therefore, the crosslinking efficiency was optimized for the hydrogels and the hydrogels in spacer fabrics, where the PA6 influences the UV exposure (Table 3.1 and Figure 3.2).

Table 3.1 *Conditions tested to optimize the conversion efficiency of the methacrylate groups upon photopolymerization.*

Sample [a]	**Spacer Fabric**	**LAP (w/v%)**	**Exposure Duration (minutes)**	**UV Exposure (Direction)**	**UV Intensity (mW/cm²)**
CSMA/HAMA	No	0.3	15	One side	0.58
CSMA/HAMA	No	0.2	15 (7.5 each side)	Both sides	1.49
CSMA/HAMA	No	0.3	15 (7.5 each side)	Both sides	1.49
CSMA/HAMA/PA6	Yes	0.3	15	One side	0.58
CSMA/HAMA/PA6	Yes	0.2	15	Both sides	1.49
CMSA/HAMA/PA6	Yes	0.3	15 (7.5 each side)	Both sides	1.49

[a] *All hydrogel samples were prepared with 10 wt% polymer concentration (HAMA 1.33 wt%).*

With an LAP concentration of 0.3% and a bilateral exposure to UV at 1.49 mW/cm², the hydrogels and HydroSpacers yielded the highest methacrylate conversions, at rates of 90 and 80%, respectively (Figure 3.2). The lower conversion can be explained by the spacer fabric blocking part of the light. Therefore, these conditions were chosen for the fabrication of the hydrogels to be used in further experiments.

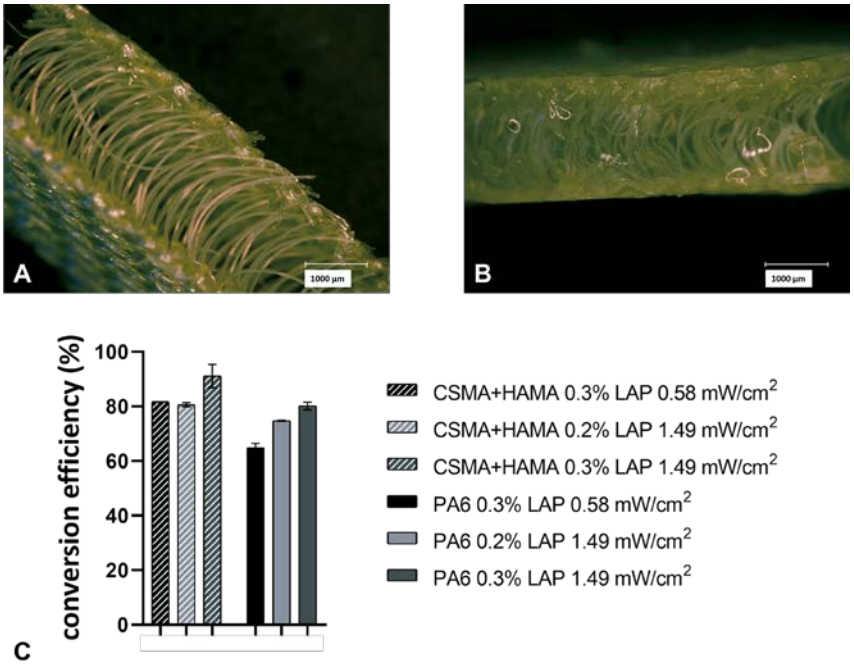

Figure 3.2 *(**A**) Empty spacer fabric (PA6), scale bar 1000 µm. (**B**) HydroSpacer construct with CSMA/HAMA hydrogel formed with PA6, scale bar 1000 µm. (**C**) Methacrylate conversion efficiency of hydrogel samples with and without the addition of a PA6 spacer fabric (10 wt% polymers, CSMA to HAMA ratio 6.5), tested under different polymerization conditions and photo-initiator concentrations. Samples polymerized with a UV intensity of 0.58 mW/cm² were exposed from one side for 15 min, whereas samples exposed to 1.49 mW/cm² were bilateral polymerized for 7.5 min from each side. Samples were tested in duplicate, except for CSMA + HAMA 0.3% 0.58 mW/cm² (n = 1). The data are presented as the mean ± SD.*

3.3.3. Hydrogel Swelling Behavior

The swelling ratio of the CSMA/HAMA hydrogels (Figure 3.3A) in the first 20 days was higher for the hydrogels with the higher CSMA content and, therefore, higher FCD and lower crosslinking density, as determined by the DM of the polymers, and these hydrogels also degraded quicker after 20–30 days (Figure 3.3C). The swelling capacity of hydrogels is dependent on the crosslinking density, the latter also being indirectly related to the methacrylate ester stability. The hydrogels based on CSMA exhibited higher swelling potential and faster degradation rates compared to those based on HAMA (at comparable DM) due to the combined effects of the higher flexibility and hydrophilicity of CSMA compared to HAMA, rendering the microenvironment around the methacrylate esters in CSMA more hydrophilic

and thus more sensitive to hydrolysis. This ester instability in CSMA eventually leads to a decreased crosslinking density, and thus causes more swelling [110,138,143–146]. The swelling profile observed in the formulations with a lower content of HAMA indicates a higher swelling capacity of the gels, which is most likely due to the more predominant CSMA component. This is also in line with previous research, where CSMA underwent a faster ester hydrolysis, which, in addition to a higher negative charge density (sulfate groups), resulted in water absorption and thus more swelling [136,147,148]. Consequently, different formulations produced different swelling profiles. The hydrogels containing 0.1–1 wt% of HAMA swelled to ~5.3 before fully degrading. The swelling profile of these gels indicates bulk degradation. The degradation of CSMA/HAMA hydrogels takes place through ester hydrolysis of the methacrylate groups [149]. These gels were stable for 30–58 days. With the incorporation of 1.33 wt% of HAMA, the hydrogels remained stable for over 120 days. This increased stability suggests that highly methacrylated HA at 1.33 wt% contributes to the stabilization of the hydrogels, as the methacrylate esters of HAMA are less sensitive to hydrolysis [150–152], and thus long-term stability can be achieved. The increased stability is also related to the limited swelling capacity observed in the formulation in question. In fact, CSMA/HAMA hydrogels with 1.33 wt% of HAMA displayed an SR of a maximum of ~2.5 within the first 30 days, after which it slowly decreased and equilibrated at ~1.9, demonstrating that, at 1.33 wt% HAMA, the network is sufficiently crosslinked to maintain a stable structure that is resistant to excessive swelling. This reduced swelling is due to the high DM of both polymers (23 and 39% for CSMA and HAMA, respectively) and in line with previously observed results in CSMA-based hydrogels [136,153]. This observation proved our hypothesis that making a hybrid hydrogel combining CSMA and HAMA could result in formulations with tunable swelling behaviors. It should be noted that CSMA-only-based gels degraded within ~3 weeks (15 wt%, pH 7.4), as reported previously [138], whereas those based on HAMA (10 wt%) could not be formulated due to the excessive solution viscosity.

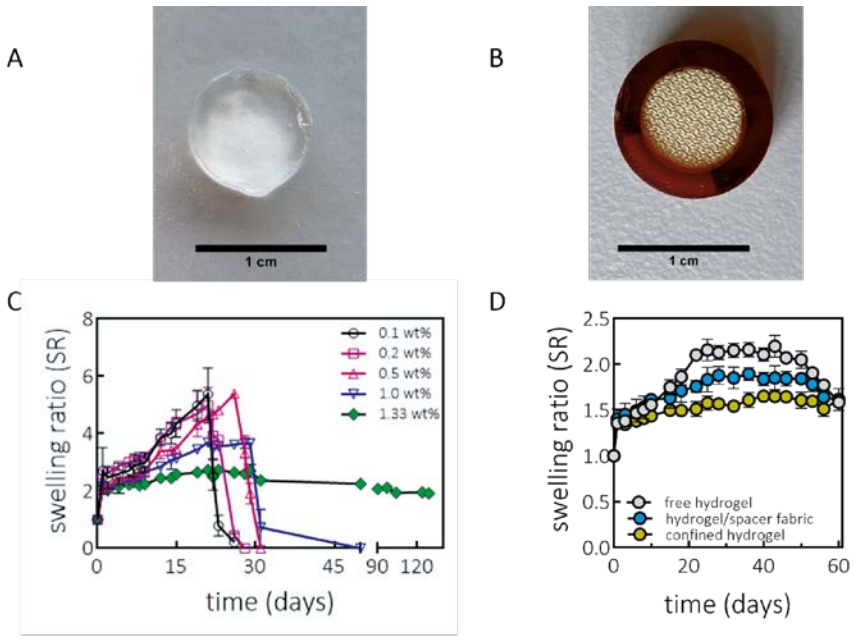

Figure 3.3 *(**A**) CSMA/HAMA hydrogel disk after photopolymerization (10 wt% polymers, CSMA to HAMA ratio 6.5). (**B**) CSMA/HAMA hydrogel incorporated into spacer fabric and a cassette (confined hydrogel, 10 wt% polymers, CSMA to HAMA ratio 6.5). (**C**) Swelling ratio and stability in time of the CSMA/HAMA gels with different concentrations of the HAMA component (total polymer concentration was kept at 10 wt%). (**D**) Swelling profile of CSMA/HAMA hydrogels: a comparison between the free-swelling hydrogel, spacer fabric-filled hydrogel (semiconfined), and confined hydrogel (hydrogels were prepared with a 10 wt% polymer concentration, CSMA to HAMA ratio 6.5). All samples were measured in triplicate. Data are presented as the mean ± SD.*

Clearly, less swelling is directly related to higher stability, which is important for supporting chondrocytes over long periods. However, higher swelling capacity is important for creating osmotically induced pressurization of the scaffold, which is essential for mechanical load-bearing. These are contradicting requirements that were best met with the most stable formulation (1.33 wt% HAMA) that still displayed significant swelling, which will be investigated in more detail in the present work. The free gel reached the maximum swelling ratio of ~2.3 under free swelling after 21 days, until it started to reduce after ~50 days, continuing for the remaining 10 days of the study (Fig. 3.3D). When confined by a spacer fabric (semi-confined), or by inserting the spacer fabric into a cassette (maximally confined, Fig. 3.3D), the volumetric swelling of the gels was reduced by ~28% or ~53%, respectively. Even though the gels were confined axially and laterally in the latter case,

there was still some swelling of the gels, as the cassette had a partially open structure. This experiment revealed that the swelling restriction did not influence the swelling significantly, except by reducing the maximum swelling in the period between days 20 and 40. Swelling then stayed constant, depending on the confinement, for another 20 days. However, interestingly, the stability was not affected by altering the swelling behavior, as between days 40 and 60, all differently confined gels had reduced swelling and each gel converged and equilibrated at ~1.6 of the swelling ratio at day 60.

The remaining question, then, is whether these confining conditions influence the mechanical properties of the materials by tuning the swelling behavior. Specifically, the stability of the hydrogels is mainly related to the swelling capacity (total water content) and also to the crosslinking density of the network[154].

3.3.4. Mechanical Characterization

Both the apparent peak and the equilibrium modulus significantly increased in the PA6-restricted constructs compared to the free-swelling hydrogels after 28 days of swelling. The more the gels swelled, the more the swelling potential was lost. If the swelling is restricted, the swelling potential is transferred into an osmotic pressure that strongly supports the load-bearing (Figure 3.4A,B). Moreover, after 28 days of swelling, the HydroSpacers showed no significant difference in the apparent peak, equilibrium modulus, and time constant τ_2 compared to the native bovine cartilage, whereas the hydrogels alone showed significantly lower moduli and higher τ_2 (p = 0.013, 0.008, and 0.032, respectively, for the apparent peak, equilibrium modulus, and τ_2, Figure 3.4A–C). The addition of the spacer fabric to the hydrogel lead to a faster and increased relaxation of the construct, which was similarly observed in the native cartilage. This time-dependent behavior was also observed when a polyacrylamide-alginate hydrogel was introduced into a woven textile [155]. The effect of the addition of the spacer fabric on the time-dependent properties was already apparent at day 0. Possible explanations for this behavior could be, firstly, that PA6 absorbs water as well as the hydrogel [156], and, secondly, as PA6 is relatively inert, the addition of the spacer fabric might introduce an interface between the fibers and the hydrogel, thus creating channels around the fibers, both of which can influence the fluid flow while being compressed. There were no significant differences observed directly after polymerization between the hydrogels

and the HydroSpacers, suggesting that the addition of the spacer fabric itself does not have a beneficial effect on the construct's stiffness initially, but does have an effect after the swelling. The spacer fabric restricts the swelling and thereby, importantly, preserves the FCD, leading to an osmotic pressure which gives the HydroSpacers their load-bearing properties[134]. This observation is in line with the outcomes of numerical data showing that the load-bearing capacity of cartilage is highly dependent on the osmotic pressure [93], which is different from other reinforcement strategies using woven scaffolds, where the stiffness of the construct was dependent on the porosity and the pore size instead of the hydrogel used, as demonstrated in this study [73,75,157].

Although the mechanical testing technique employed in this study is not a pure form of confined compression or indentation, the values found in the literature for the aggregate modulus of both human and bovine cartilage are in the range of the values found in the current study [42,44,45,49]. This observation indicates that, when using hydrogels based on CSMA and HAMA, and restricting the swelling through a PA6 spacer fabric, load-bearing properties that are similar to those of native cartilage can be generated.

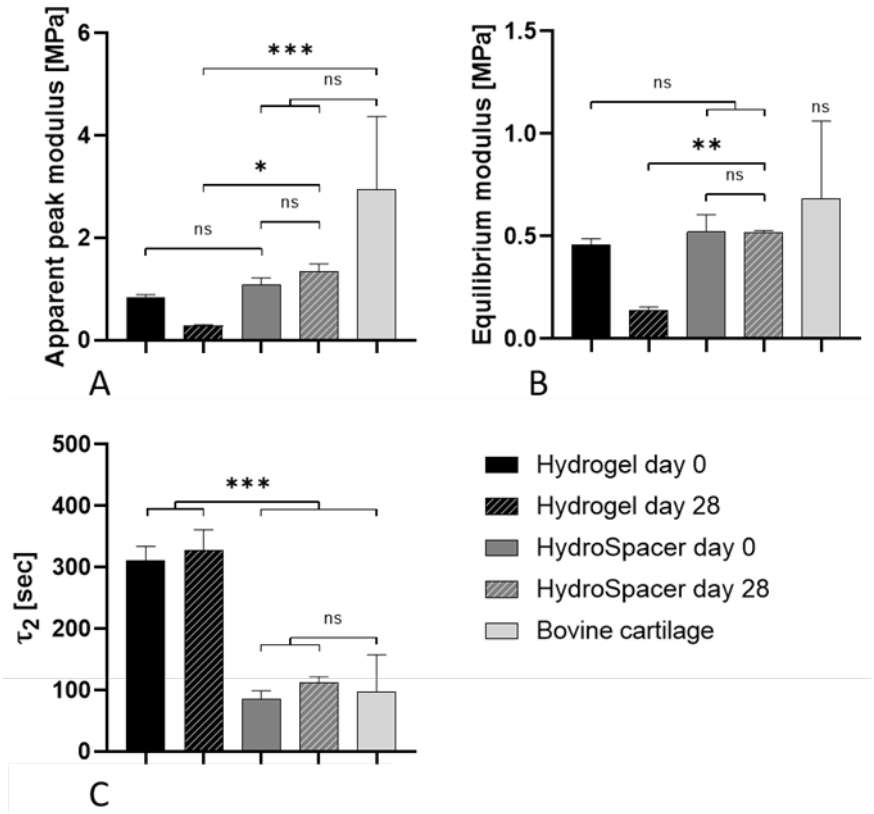

Figure 3.4 *Mechanical properties of CSMA/HAMA hydrogels and HydroSpacers (n = 5) at day 0 and day 28, and of bovine cartilage. (**A**) Apparent peak modulus. (**B**) Equilibrium modulus. (**C**) Time constant τ_2 in seconds. Data are presented as the mean ± SD. A Kruskal–Wallis test was performed using Prism GraphPad. The significance is indicated with *, ** or ***, with single signs referring to a p-value < 0.05, double signs referring to a p-value < 0.01 and triple signs referring to a p-value < 0.001.*

3.3.5 Cell Viability

On day 1, the cell death in the CSMA/HAMA HydroSpacers is concentrated at the outer edge, whereas in the GelMA HydroSpacers, it is diffused throughout (Figure 3.5A). However, no significant differences were observed in the overall cell viability between the CSMA/HAMA and GelMA HydroSpacers at day 1, reaching approximately 73% (Figure 3.5B). Cell viability increased over 7 days of culture in the GelMA constructs to 87%; however, this was not observed within the CSMA/HAMA HydroSpacers (63% viability), leading to a significant difference between the GelMA and CSMA/HAMA constructs at day 7. This difference might be caused by a stiffness-induced

restricted cellular motility [158]. No effect of the PA6 spacer fabric itself was observed, as the cell viability was not hampered in the GelMA group, as compared to findings from the literature [159,160]. Nevertheless, the cell viability was sufficient to further investigate the CSMA/HAMA HydroSpacer as a potential strategy and as a regenerative application in cartilage tissue engineering. Moreover, the aim of this research was to demonstrate the initial cell viability, and an optimized cell culture system might lead to a higher cell viability which is more in line with previous research using chondroitin sulfate and hyaluronic acid-based hydrogels [161,162].

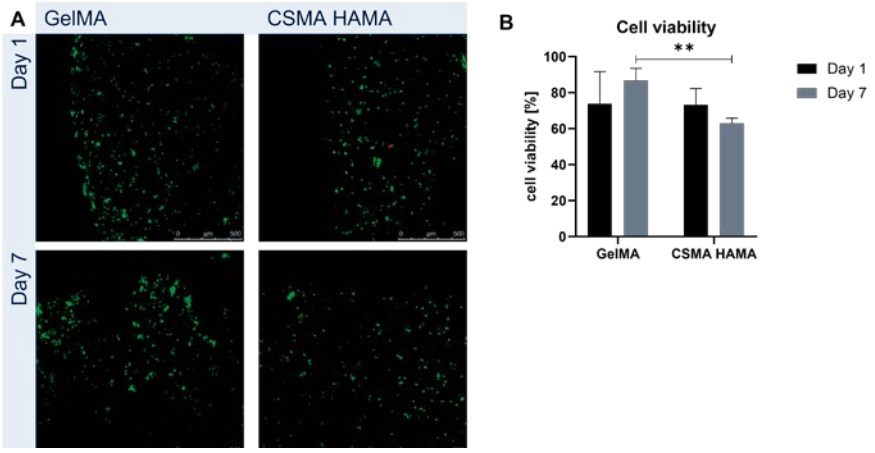

Figure 3.5. *(**A**) Cell viability of gelatin–methacrylamide (GelMA) and CSMA/HAMA HydroSpacers after 1 and 7 days of culture. Viable cells are stained in green, dead cells in red. (**B**) Percentage of living cells embedded in the GelMA and CSMA/HAMA HydroSpacers (n = 5). The significance is indicated with **, with double signs referring to a p-value < 0.01.*

3.4 Conclusions

In this work, the naturally occurring polysaccharides CS and HA were successfully methacrylated and used for hydrogel fabrication. The swelling potential of the resulting hybrid CSMA/HAMA hydrogels was investigated as a function of the HAMA weight fraction. Hybrid hydrogels characterized by long-term stability (over 4 months) were prepared with a 1.33 wt% HAMA content (total polymer content 10 wt%). Moreover, the photopolymerization conditions of the hydrogels within the spacer fabric materials were optimized in order to ensure that the methacrylate conversion, and thus the crosslinking efficiency, would be as high as possible. A crosslinking efficiency of ~80% was achieved when the CSMA/HAMA hydrogels were fabricated

within PA6 spacer fabric scaffolds, with no influence on cell viability compared to the GelMA HydroSpacers at one day after polymerization. The use of these PA6 spacer fabrics led to the restricted swelling of the CSMA/HAMA hydrogels, which resulted in the maintenance of the FCD within the CSMA/HAMA PA6 constructs. When using the osmotic pressure generated by the FCD of the CS and HA, the load-bearing properties were similar to those of native cartilage. The results demonstrated in this work suggest that the use of a HydroSpacer construct (with an ECM-like biopolymer-based hydrogel) is a promising regenerative approach for mimicking the load-bearing properties of native cartilage.

Supplementary Materials: The following supporting information can be downloaded at: www.mdpi.com/xxx/s1, Scheme S1: Synthesis route for HAMA and CSMA polymers.

Author Contributions: Conceptualization, G.S., M.M., C.v.D., T.V., and K.I.; methodology, G.S., M.M., C.v.D., T.V., and K.I.; validation, G.S. and M.M.; formal analysis, G.S. and M.M.; investigation, G.S. and M.M.; writing—original draft preparation, G.S. and M.M.; writing—review and editing, G.S., M.M., C.v.D., T.V., and K.I.; visualization, G.S. and M.M.; supervision, C.v.D., T.V., and K.I.; funding acquisition, C.v.D., T.V., and K.I. All authors have read and agreed to the published version of the manuscript.

Funding: This research was funded by the framework of Chemelot InSciTe (Project MimiCart), supported by the partners of Regenerative Medicine Crossing Borders (www.regmedxb.com) and powered by Health~Holland, Top Sector Life Sciences & Health.

4

The effect of HydroSpacer implant placement on the wear of opposing and adjacent cartilage

The contents of this chapter are based on:
A.H.A. Damen, **G. H. Schuiringa,** K. Ito, C. C. van Donkelaar, The effect of HydroSpacer implant placement on the wear of opposing and adjacent cartilage, Journal of Orthopaedic Research, Volume 41, Issue 7, Pages 1397-1406
DOI: 10.1002/jor.25487

Abstract

A HydroSpacer implant, i.e. a swelling hydrogel confined by a spacer fabric, was developed to repair focal cartilage defects and to prevent progression into osteoarthritis. The present study evaluated the effect of implant placement on wear of the opposing and adjacent cartilage.

Three-dimensional warp-knitted spacer fabrics, polycaprolactone (PCL) with poly(4-hydroxybutyrate) (P4HB) pile yarns, were filled with a hyaluronic acid methacrylate (HAMA) and chondroitin sulfate methacrylate (CSMA) hydrogel. After polymerization of the hydrogel, these HydroSpacers were implanted in osteochondral (OC) defects (ø 6 mm) created in healthy bovine OC plugs (ø 10 mm) and allowed to swell to equilibrium. A custom-made pin-on-plate wear apparatus was used to apply articulation against healthy bovine cartilage, simulating gait in the knee, i.e. simultaneous compression (260 N and 26 N) and sliding (2.5 mm/s and 3.75 mm/s) over 6 mm.

Cartilage damage, visualized with Indian ink, was only seen for the group in which the HydroSpacer was placed flush with the surrounding cartilage. A significant increase in average surface roughness of the sliding path compared to the adjacent cartilage confirmed surface damage for this group. When the implants were recessed (with and without extra hydrogel layer on top of the implant), this damage was not observed, but the cartilage surrounding the implants was compressed (without damage) indicating substantial load sharing with the implant. Furthermore, it was shown that all defects treated with a HydroSpacer implant resulted in shear forces comparable to intact cartilage.

In conclusion, the present study suggests that placing a HydroSpacer implant recessed into the surrounding cartilage would decrease wear of the opposing cartilage and that adding an extra hydrogel layer would not be necessary. Altogether, this study supports the development of textile-constraining hydrogels for cartilage replacement.

4.1 Introduction

Cartilage lesions are found in more than half of knee arthroscopies performed in middle-aged patients [163–165]. A recently developed treatment that relieves pain and preserves joint kinematics and function is a focal knee resurfacing implant (FKRI). Nowadays, these implants are made of metals. These materials are much stiffer than the native cartilage it replaces and the articulating surface of these implants lacks lubricating properties leading to damage of the opposing and adjacent cartilage [166–169]. Especially when the implant protrudes above the surrounding surface or is placed at an angle [109,170–172].

As an alternative to rigid metal implants, hydrogels are gaining attention as a matrix material for soft tissue replacement. In addition, hydrogels can be biocompatible and biodegradable allowing for their use as carriers for chondrocytes or allowing for endogenous cell infiltration, enabling regenerative therapies [63–65,173]. However, hydrogels typically lack mechanical strength and stability, especially those which promote tissue growth within it, and these are necessary characteristics of an implant whose purpose is to functionally replace load-bearing cartilage [63,64].

To overcome this, woven textile structures have been developed to reinforce hydrogels [96]. However, these constructs require much higher fiber content than that found in natural cartilage leaving little volume for tissue regeneration. As an alternative, a more structurally similar implant was developed to mimic the load bearing mechanism of natural articular cartilage. Recent work of Schäfer *et al.* (2020) showed that a three-dimensional (3D) warp-knitting technique can be used to mimic the arcade-like collagen structure of healthy cartilage [79]. More specifically, this involves a spacer fabric consisting of a warp-knitted top and bottom sheet which are connected by pile yarns. The fabric can be filled with hydrogels and cells, resulting in a promising platform technology to biofabricate textile-constraining hydrogels. A recent study showed that filling with a hydrogel with strong swelling potential led to superior load-bearing properties, mimicking not only the equilibrium stiffness but also peak stiffness and time-dependent behavior of cartilage [174]. The osmotic pressure generated by the swelling potential when a charged hydrogel is restricted from swelling by a textile spacer fabric, significantly increases the stiffness of the entire construct.

Various polymers can be used to create swelling hydrogels, amongst others chondroitin sulfate (CS) and hyaluronic acid (HA), which are highly negatively charged polysaccharides found in cartilage extracellular matrix and synovial fluid [138]. To obtain a hydrogel, functional methacrylate groups can be used to covalently cross-link the polymers triggered by light exposure resulting in a 3D polymer network. Recent work of Mihajlovic *et al.* (2022) showed promising swelling and mechanical properties of a CS/HA-based double-network hydrogel [173].

However, besides having load-bearing properties, these scaffolds should also protect the opposing cartilage that slides over the scaffold. It is already known that implant positioning of rigid, impermeable implants has a substantial influence on the opposing and adjacent cartilage [109,170–172]. Previous studies have shown that a protruding implant should be avoided and most studies advise to place such an implant flush with, or just below, the adjacent cartilage surface [175–177]. Though, several animal studies have also shown damage to the opposing cartilage when an implant was placed too deep into the surrounding cartilage [170,172]. Besides, Manda *et al.* (2011) showed using finite element simulations that a too deep positioned implant leads to high shear stress in the cartilage edges around the implant [175]. However, these studies were all performed with stiff, impermeable implants and less is known about the tribological properties of the HydroSpacer implant, let alone the effect of implant placement. Therefore, the objective of the present study was to investigate the feasibility of using HydroSpacers for cartilage replacement by examining its influence on the opposing and adjacent cartilage.

As far as we know, this is the first study to investigate the influence of three appropriate surgical positions of a HydroSpacer implant (flush, recessed and with additional hydrogel layer) on opposing cartilage wear using a physiologically relevant loading regime. The tribological response of a HydroSpacer implant was evaluated by sliding-indentation experiments in which the implant was placed at various heights in an osteochondral (OC) plug and articulated against healthy cartilage. It was hypothesized that a HydroSpacer implant placed flush with the surrounding cartilage would be most protective for the surrounding cartilage. However, as it is in direct contact with the opposing cartilage, it might damage the opposing cartilage. Whereas an implantation just below the surrounding surface might avoid wear of the opposing cartilage but cause damage to the surrounding

cartilage due to higher compression. Therefore, a third group was investigated in which the empty space between recessed implant and surrounding cartilage surface was filled with an additional hydrogel layer.

4.2 Materials and methods

4.2.1 Warp-knitted spacer fabrics

Spacer fabrics were made out of polycaprolactone (PCL) (EMS-Griltech AG, Domat/Ems, Switzerland) and poly-4-hydroxybutyrate (P4HB,Becton, Dickinson and Company, Franklin Lakes, USA) fibers using a double Raschel warp-knitting machine (Karl Mayer GmbH Doubleraschel, DR 16 EEC/EAC, Obertshausen, Germany). Twisted PCL multi-filaments with a linear density of 55 dtex were knitted in a Samt-Franse pattern and functioned as top and bottom sheets (Fig. 4.1A). These sheets were connected to each other using USP 7-0 P4HB monofilaments as pile yarns in a X-shape fashion in full density (100%, Fig. 4.1B). The spacer fabric constructs were knitted in long strips of fabric 20 mm wide with a height of 1.87 mm.

The warp-knitted textile underwent heat treatment for 20 minutes in a 45 ˚C oven (Carbolite, Hope, United Kingdom) in order to remove residual stresses of the fabric. Subsequently, circular samples (ø = 6 mm) were cut out of the fabric sheet using a laser cutter (VLS 3.50, Universal Laser Systems GmbH, Vienna, Austria). To reduce heat-related damage, the power was set to 15% and the cutting procedure was repeated ten times.

4.2.2 Hydrogel

Methacrylation of CS and HA was performed as described by Schuiringa *et al.* (2022b) and stored at -20 ˚C until use [178]. Chondroitin sulfate methacrylate (CSMA, 8.6 wt%) and hyaluronic acid methacrylate (HAMA, 1.3 wt%) were dissolved in phosphate buffered saline (PBS) (Sigma-Aldrich, Zwijndrecht, the Netherlands) and left on a tube roller at 4 ˚C overnight. Lithium phenyl-2,4,6,-trimethylbenzoylphosphinate (LAP) (TCI, Tokyo, Japan), used as photoinitiator, was dissolved in PBS and added to the polymer solution to reach a final concentration of 0.3 w/v% after which the hydrogel was immediately used.

4.2.3 HydroSpacer formation

The spacer fabrics were placed in a custom-made Teflon mold with inter-connected cylindrical wells (ø = 6 mm, h = 1.90 mm) (Fig. 4.1C-D). The top and bottom of the wells were covered with quartz glass plates after which the CSMA-HAMA hydrogel was injected into the mold, allowed to flow through and fill the cylinders and polymerized using UV light (VL-4.LC, A. Hartenstein GmbH, France) for 15 minutes at a distance of 3 cm, using an intensity and wavelength of 1.49 mW/cm² and 365 nm, respectively.

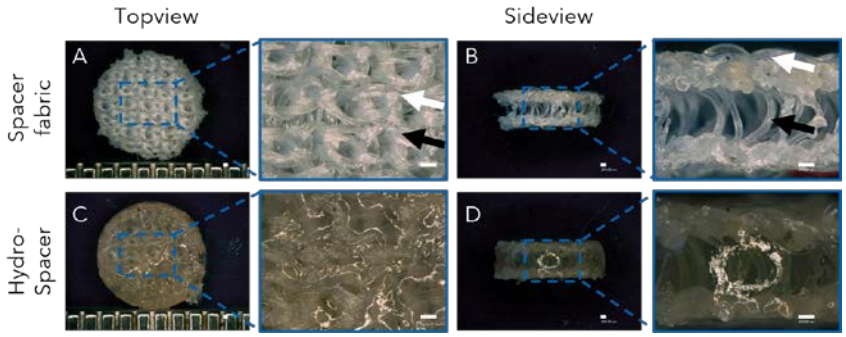

Figure 4.1: *Top (**A, C**) and side (**B, D**) view of the P4HB-PCL spacer fabric alone (**A, B**) and of a hydrogel-filled spacer fabric: HydroSpacer (**C, D**). The black arrows indicate a P4HB monofilament and the white arrows a PCL multifilament. Scale bars are 250 µm.*

4.2.4 Osteochondral sample preparation

Bovine patellae (from 3 - 6 year-old cows) were obtained from the slaughterhouse and stored at -20 °C until use. Prior to harvesting, patellae were thawed at 4 °C overnight while being completely submerged in PBS. OC blocks (~25 x 15 x 10 mm, l x b x h) and plugs (ø = 10 mm, h = 10 mm) were obtained from the distal-lateral quadrant of the patella using an electric handsaw (Universal multi12, Bosch, Stuttgart, Germany) and a core-drill (MF dental, Weiherhammer, Germany). The cranial-caudal direction was marked on both the blocks and plugs to ensure that the direction of movement during the sliding-indentation test coincided with the normal gait cycle.

The OC plugs were divided into five experimental groups (n = 5 each, Fig. 4.2). The intact OC plugs served as negative control. In all the other plugs, a cylindrical (osteo)chondral defect (ø = 6 mm, h = 2 – 2.5 mm) was drilled at the center of the OC plugs using a custom-made reamer and drill guide. The HydroSpacers were either manually press-fitted flush with respect to the level of the surrounding cartilage or ~0.5 mm below the surrounding

cartilage. Half of the latter group stayed like this, forming the recessed group while for the other half, an extra layer of CSMA-HAMA hydrogel was added on top of the implant, filling the empty gap. This hydrogel layer was covered with a glass plate and UV polymerized (5 min). The fifth group served as positive control and consisted of OC plugs with an empty defect. All OC plugs were left in PBS at 4 ˚C overnight to allow hydrogel swelling to equilibrium.

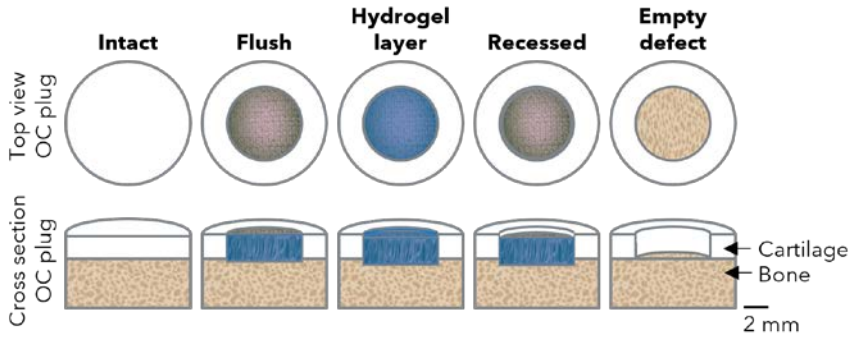

***Figure 4.2**: Schematic illustration of the five experimental groups including an intact osteochondral (OC) plug, a HydroSpacer placed with the surrounding cartilage, a HydroSpacer placed recessed into the surrounding cartilage with and without an extra hydrogel (blue colored) layer on top and an OC plug with an empty defect.*

Prior to the wear experiment, the cartilage surface of the OC blocks and plugs was stained with Indian ink (Royal Talens, Apeldoorn, the Netherlands) for 30 seconds, washed under running tap water, and photographed using a digital microscope (VHX-500F, Keyence Corporations, Osaka, Japan) to ensure that there were no visible fissures present.

4.2.6 Synovial fluid collection

Synovial fluid was collected from bovine stifle joints (from 8 – 12 months-old cows) with an 18G spinal needle (BD Microlance 3, Fraga, Spain). On average 2.8 mL (range 1 – 5.5 mL) of synovial fluid was aspirated from each joint. The synovial fluid was centrifuged at 1500 rpm for 15 minutes, pooled (eight joints) to eliminate biological variations in composition between animals, and then divided into aliquots of 33% synovial fluid in PBS and stored -80 ˚C until further use [179].

4.2.7 Sliding-indentation wear experiment

A custom-made pin-on-plate sliding-indention apparatus was used to perform 1-hour (900 cycles) wear experiments (Fig. 4.3A). For each cycle, 60% was high-loaded moving with a relatively low sliding velocity in the cranial-to-caudal direction, mimicking the stance phase while the other 40% was low-loaded moving with a relatively high sliding velocity in caudal-to-cranial direction, mimicking the swing phase of the gait cycle during normal walking (Fig. 4.3B). The OC square block was placed in a container while exposing the cartilage layer (23 x 15 mm, l x b). The container was placed in a bath and fixed to a movable stage. The bath was filled with 9 mL of diluted synovial fluid which was thawed at 4 ˚C overnight. The movable stage was powered by an Arduino controlled stepper motor and executed a sliding distance of 6 mm using sliding velocities of 2.5 mm/s and 3.75 mm/s for the stance and the swing phase of the cycle, respectively. The OC plug was placed with its bone part into an indenter holder, leaving the cartilage layer sticking out. The axial load that was applied by pressing the OC plug onto the OC block using the dead weight of the system for the swing phase and an additional air-pressure controlled dynamic load for the stance phase, resulting in a normal force of 26 N and 260 N respectively (0.33-0.52 MPa and 3.18-4.97 MPa). A load cell (MV-NA27-5KG, Mavin, Xiamen, China) which was attached to the upper part of the system, constantly measured the shear force between the opposing bodies.

After the wear experiment, the top view of the OC blocks and the top and side view of the OC plugs were immediately photographed after which the samples were allowed to re-equilibrate in PBS at 4 ˚C overnight.

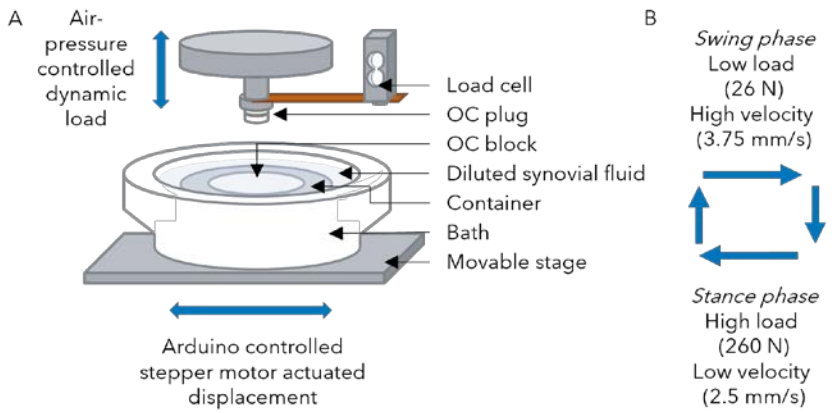

***Figure 4.3**: (**A**) Schematic illustration of the sliding-indentation setup and (**B**) the corresponding loading cycle mimicking the stance and the swing phase of the gait cycle.*

4.2.8 Roughness measurements

Cartilage surface roughness was measured with an optical surface profiler (Sensofar Plμ 2300, Terrassa, Spain) using a 20x objective. For each measurement, a random field in the area of interest covering approximately 640 x 480 μm^2 was imaged and corrected for tilt using a third-order polynomial fit. The arithmetic average surface roughness (S_a), peak-to-valley height (S_t), surface polarity skewness (S_{sk}) and kurtosis (S_{ku}) were determined as explained by Aşık *et al.* (2022) [180]. Measurements were taken at the ring of the OC plug and at the sliding-indentation pathway as well as adjacent to the sliding-indentation pathway of the OC block. The average of three measurements at different locations on each sample was used for further analysis.

4.2.9 Macroscopic evaluation

After re-equilibration, the cartilage surfaces were again stained with Indian ink and photographed. The top view images obtained immediately after wear and after re-equilibration were evaluated by a blinded observer and classified as intact or showing some type of damage (Fig. 4.4). The inner and outer diameter of the cartilage ring and the cartilage thickness of the OC plugs were measured using ImageJ (version 1.52n).

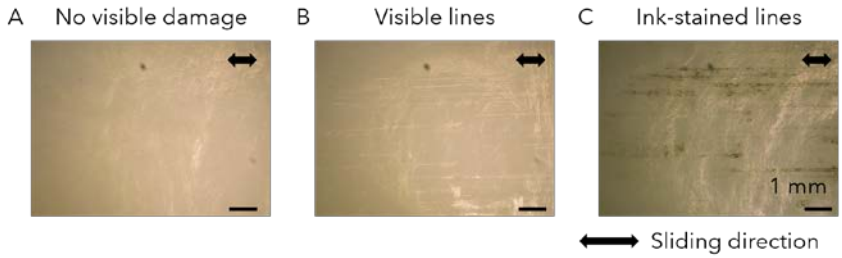

***Figure 4.4**: Macroscopic photographs of the cartilage surface of the opposing OC block showing (**A**) no visible damage, (**B**) visible lines and (**C**) ink-stained lines. Scale bars are 1 mm.*

4.2.10 Statistical analyses

Statistical analyses were performed with GraphPad Prism 8.02. A one-tailed Wilcoxon matched-pairs signed rank test was used to assess increases or decreases in roughness parameters between the sliding-path and the

adjacent cartilage of the OC blocks. The same test was used to assess a decrease in cartilage thickness and increase in diameter of the OC plugs before and immediately after the wear experiment. Differences between groups regarding cartilage thickness and roughness parameters were analyzed using a Kruskal-Wallis test with Dunn's posthoc for multiple comparison. *P*-values lower than 0.05 were considered statistically significant.

4.3 Results

4.3.1 Macroscopic cartilage evaluation

All the cartilage surfaces that articulated against an implant placed flush with the surrounding cartilage revealed visible lines oriented in the sliding direction immediately after the experiment. For the group in which an extra hydrogel layer was placed on top of the implant, three out of five of the opposing OC blocks showed these visible lines in the sliding direction. For all other samples, the opposing cartilage surface stayed visually undamaged. After overnight recovery in PBS, three out of five cartilage surfaces that articulated against an implant placed flush with the surrounding cartilage showed Indian ink stained lines in the sliding direction. None of the other samples showed Indian ink uptake on the cartilage surface of the OC block (Table 4.1).

Table 4.1 *The number of samples that showed visible lines immediately after the wear experiment and after recovery for each group*

# samples showing visible lines on cartilage surface of opposing OC block	**Division of OC plugs**				
	Intact	**Flush**	**Hydrogel layer**	**Recessed**	**Empty defect**
Immediately after wear experiment	0/5	5/5	3/5	0/5	0/5
After 24h recovery in PBS and Indian ink staining	0/5	3/5	0/5	0/5	0/5

4.3.2 Surface roughness

None of the roughness parameters of the cartilage adjacent to the sliding-path on the OC blocks did significantly differ between groups. The only significant difference between the sliding-path and the adjacent cartilage within a group was found for the average surface roughness when articulated against an implant placed flush with the surrounding cartilage ($P = 0.03$) (Fig. 4.5, Table 4.2). Also, the largest difference in peak-to-valley height was visible for the group in which the implant was placed flush with the surrounding cartilage, however, this was only a trend and just not statistically significant ($P = 0.06$) (Fig. 4.5, Table 4.2).

All sides surrounding the sliding-path had an average positive skewness. The average skewness value in the sliding-path was lower for all groups containing an implant and was even negative for the groups that had an implant placed flush or recessed to the surrounding cartilage, however, this was not significantly different from the adjacent cartilage ($P > 0.16$). No significant differences were found for the kurtosis value between the sliding-path and the adjacent cartilage for any of the groups ($P > 0.22$).

Roughness parameters of the cartilage ring of the OC plugs did not significantly differ between groups (data not shown).

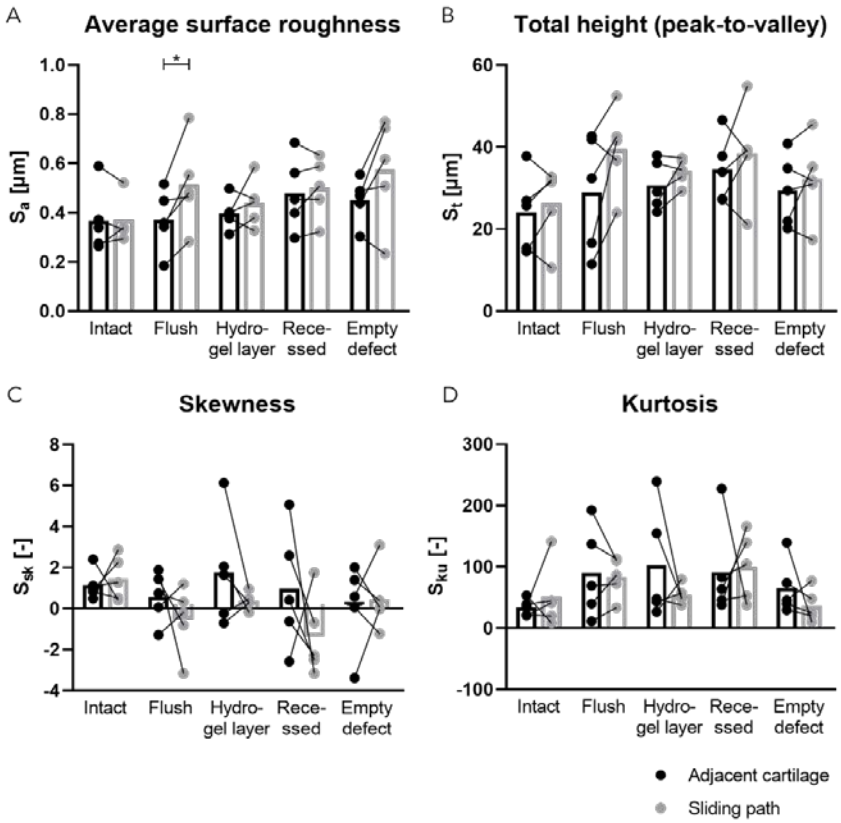

Figure 4.5: *Paired surface roughness analysis of the OC blocks measured in the sliding path (grey dots) and adjacent to this path (black dots) for each individual group. Including (**A**) the average surface roughness, (**B**) total height (peak-to-valley), (**C**) skewness and (**D**) kurtosis of the cartilage surfaces. Bars represent the average value. * P < 0.05.*

***Table 4.2**: P-values comparing the surface of the sliding-path and the adjacent cartilage of the OC blocks for each roughness parameter and each group. # P < 0.1, *P < 0.05.*

	Intact	Flush	Hydrogel layer	Recessed	Empty defect
S_a	0.50	**0.03 (*)**	0.22	0.31	*0.09 (#)*
S_t	0.31	*0.06 (#)*	0.16	0.31	0.31
S_{sk}	0.41	0.31	0.16	0.22	0.41
S_{ku}	0.31	0.50	0.31	0.31	0.22

4.3.3 Cartilage thickness of the adjacent cartilage

No significant difference in cartilage thickness of the OC plugs between the groups was observed prior to the wear experiment (P = 0.45). The cartilage adjacent to the implants that were recessed into the surrounding cartilage (hydrogel layer and recessed) significantly decreased in height immediately after the wear experiment compared to before the experiment (P = 0.03, Fig. 4.6A).

4.3.4 Diameters of the OC plug

Both the inner and the outer diameter of the cartilage ring in which the implant was placed flush with the surrounding cartilage was significantly larger immediately after the wear experiment compared to before the experiment (P = 0.03, Fig. 4.6B-C). None of the other groups showed a significant increase in outer diameter of the OC plug. The inner diameter of the ring significantly increased in the hydrogel layer and recessed groups (P = 0.03, Fig. 4.6B-C).

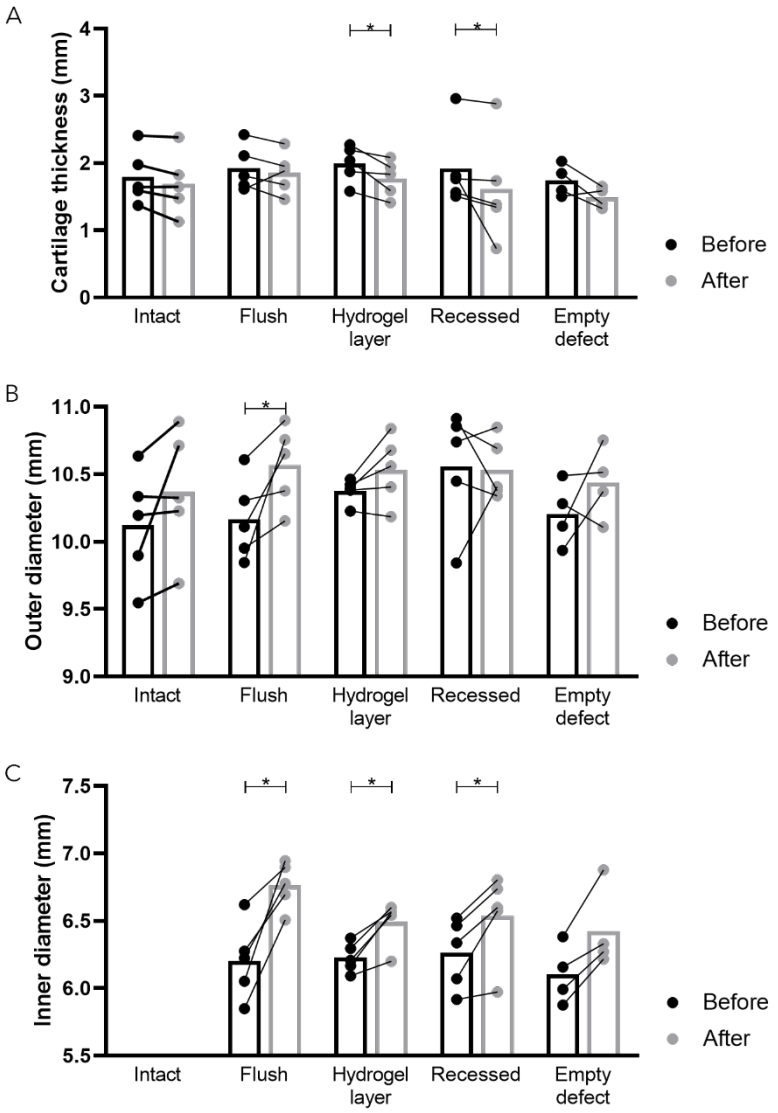

Figure 4.6: *(**A**) The cartilage thickness, (**B**) outer diameter and (**C**) inner diameter of the OC plug before (black dots) and after (grey dots) the wear experiment for each group.* ******* *$P < 0.05$.*

4.3.5 Shear force

Higher shear forces were experienced during the stance phase compared to the swing phase for all groups (Fig. 4.7). The highest average shear force, ~5 N, was experienced between the OC block and the intact OC plugs while the lowest shear force, ~2 N, was measured for the OC plugs that had an implant that was covered with an extra hydrogel layer.

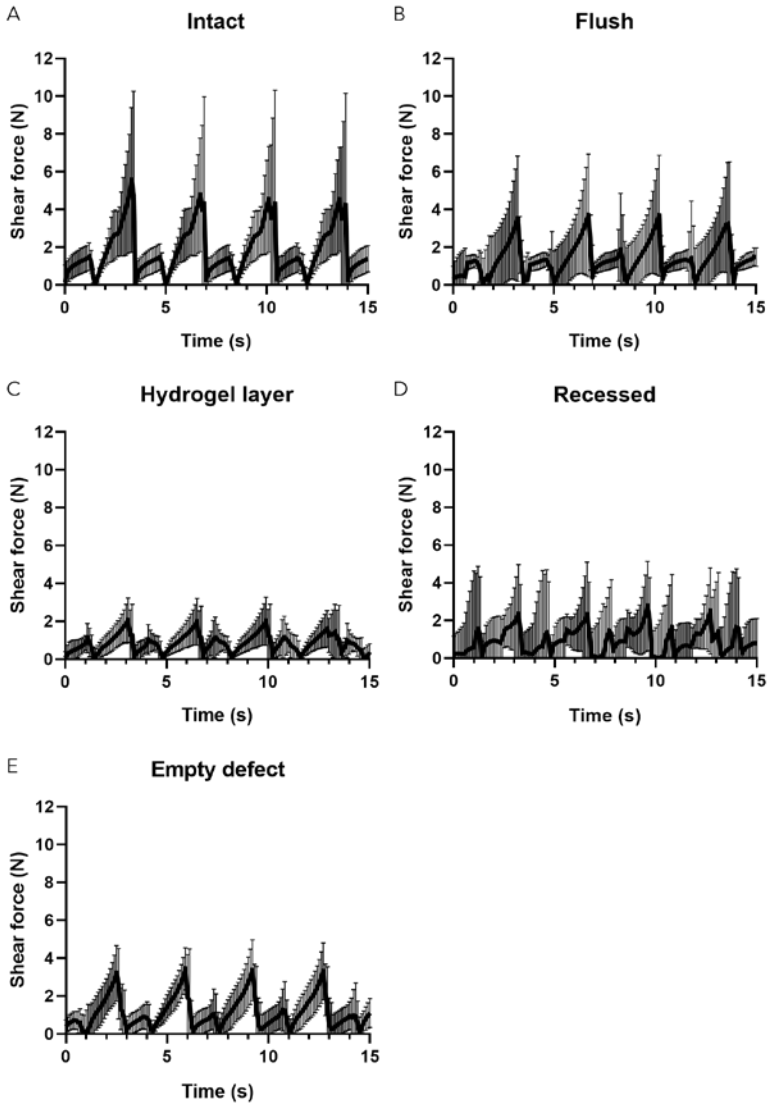

Figure 4.7 *Average shear force (solid line) ± standard deviation (bars) for 5 samples over time of the last six loading cycles for each group. Each graph starts at the swing phase.*

4.4 Discussion

The present study presented a HydroSpacer, i.e. a swelling hydrogel confined by a warp-knitted spacer fabric, as a potential cartilage resurfacing implant. The aim of the present study was to evaluate the effect of implant placement on wear of the opposing and adjacent cartilage. It was demonstrated that the implant best be placed recessed in the surrounding cartilage to avoid wear on the opposing cartilage. In fact, a HydroSpacer implant placed flush with respect to the adjacent cartilage led to visible surface damage and an increased surface roughness of the opposing cartilage.

After one-hour of cyclic sliding-indentation, eight out of twenty-five samples showed visible lines in the sliding direction on the cartilage surface of the OC block (Fig. 4.4). These included all the samples of the flush group and three out of five samples of the hydrogel layer group. These lines were visible due to an optical diffraction pattern which can be caused by indentation and deformation or by removal of material. After an overnight recover period in PBS, the cartilage surfaces were stained with Indian ink. Surprisingly, only three samples showed black stained stripes indicating that these surfaces contained deep scratches, all belonging to the group in which the implant was placed flush. The damage found in the present study is expected to have been caused by direct contact between the PCL-P4HB fibers and the opposing cartilage. The interpretation is that the wear with the recessed implant is less, as the sliding area under the implant is less loaded compared to the flush implant. Indeed, the cartilage thickness of the surrounding cartilage ring of the recessed group significantly decreased, indicating that it carried more load, and that there was also some direct contact between the PCL-P4HB fibers and the opposing cartilage in this group (Fig. 4.6A). However, the load between implant and opposing cartilage is lower in the recessed case than with the flush implant, and therefore the PCL-P4HB fibers did not cut into the opposing cartilage when placed recessed whereas they did when placed flush to the adjacent surface.

The change in surface topography was not only visualized with Indian ink but also quantified by roughness analysis. Supportive to the macroscopic data, a significantly higher average roughness was measured in the sliding-path opposing a flush placed implant compared to the adjacent cartilage of these OC blocks (Fig. 4.5A). Also, the difference in peak-to-valley height was largest for this group and the average skewness turned out to be negative, indicating that the surface predominantly consisted out of valleys which could held the Indian ink particles (Fig. 4.5B-C). The average skewness in the

sliding-path of cartilage opposing an implant that was placed recessed was also negative (Fig. 4.5C). However, no ink particles stuck to any of these cartilage surfaces after the wear experiment (Fig. 4.3D). This supports the idea that there was some direct contact between the PCL-P4HB fibers and the opposing cartilage, thereby deforming the cartilage surface. However, because the load was mainly carried by the surrounding cartilage ring, the fabric was unable to bite into the tightly packed collagen fiber structure of the superficial zone of the cartilage, preventing it from causing scratches.

Not only the opposing cartilage, but also the surrounding cartilage was affected by the different implant placements. There was a significant decrease in cartilage thickness for both the hydrogel layer and recessed group, probably because of fluid release from the cartilage ring (Fig. 4.6A). It was previously shown, with a similar hydrogel, that when in unconfined stage it is not very stiff [173]. Therefore, it is believed that the thin hydrogel layer on top of the implant does not support much load. Consequently, the cartilage rings in the recessed and hydrogel-layer groups carried comparable loads and decreased in height equally. While the cartilage thickness stayed the same, both the outer and inner diameter of the cartilage ring in which an implant was placed flush to the adjacent cartilage increased, indicating outward deformation of ring (Fig. 4.6). This is probably caused by the internal pressure of the implant since all other inner diameters of groups containing a HydroSpacer implant also significantly increased. Furthermore, the cartilage ring of one empty defect sample bulged sideways into the defect, in the direction of sliding (data excluded from height and diameter measurements). It seemed like the cartilage ring surrounding the defect was overloaded as previously suggested by Heuijerjans *et al.* (2018) [109]. The present study showed that treating an OC defect with a HydroSpacer implant, regardless of implant placement (flush or recessed), prevented bulging of the surrounding cartilage.

Based on the previous mentioned results, it was expected that the flush placed HydroSpacer would experience the highest shear loads since it was cutting into the opposing cartilage. However, no correlation could be found between the shear loads and the Indian ink staining or surface roughness. All groups demonstrated very low equilibrium shear forces, at the same level or even lower than cartilage-on-cartilage. The hydrogel layer group was the most slippery, as expected (Fig. 4.7). The highest friction was surprisingly in the intact cartilage samples, probably because the cartilage surface is able to deform more in comparison to the exposed implant surface, resulting in a

larger contact area between the two opposing surfaces, and therefore leading to a higher shear force. Although the shear force was highest for this group, the amount of visible and measurable surface topography change was negligible (Fig 4.4-5). Overall, the very low friction illustrates the suitability of the HydroSpacer as a cartilage implant.

The present study used an *in vitro* pin-on-plate setup to mimic the swing and stance phase of the gait cycle. Although this is a commonly used setup type to evaluate cartilage-on-implant articulation, it is several limitations. Firstly, it is unable to mimic the rolling movement experienced in the knee joint *in vivo*. Including this specific motion in the test setup, even as using pure synovial fluid instead of diluted synovial fluid, may result in an even more reliable loading pattern and lubrication regime using slightly more specific contact areas and loading magnitudes comparable to regular knee loading. However, it is expected that this will not significantly change the findings of this study with regards to the opposing cartilage. Secondly, another notable difference between this *in vitro* setup and the *in vivo* situation is the volume of the cartilage surrounding the implant. In this experimental setup, the implant was placed in an OC plug with a surrounding cartilage ring of 2 mm in width. The width of the ring increased during loading, which is prohibited *in vivo* by the surrounding cartilage. Also, some water and glycosaminoglycans (GAGs) may have been lost from the outer sides of the cartilage ring during the experiment. When this implant will be placed in an entire knee joint, this will not be possible and potentially the cartilage will be less indented as was now seen by a decrease in cartilage thickness for the hydrogel layer and recessed group (Fig. 4.6A). Lastly, all OC explants had the same outer diameter, and the load was chosen identical in all groups. As a consequence, however, depending on the positioning of the implant, the five experimental groups differed in contact surface area. Thus, the cartilage adjacent to the recessed implants and the empty OC plug experienced more load during sliding-indentation (4.97 MPa instead of 3.18 MPa). It was believed that this best mimics the *in vivo* case, where the same force is distributed over the joint area that is in load-bearing contact, with increased contact pressures on the edges [109]. Furthermore, both values are within the range of physiological values experienced within the human gait [181].

4.5 Conclusion

To conclude, the present study supports the idea of using a hydrogel-filled warp-knitted spacer fabric for the treatment of focal cartilage defects. It was shown that all defects treated with a HydroSpacer implant resulted in shear forces comparable to intact cartilage. This suggests that the hydrogel limits friction and shear to native values. However, macroscopic Indian ink and surface roughness analysis showed that placement of the HydroSpacer implant flush to the adjacent cartilage leads to visible surface damage and an increased surface roughness of the opposing cartilage. Likely, exposed fibers of the HydroSpacer construct bite into the opposing cartilage, thus resulting in local wear. This problem was solved when the implant was placed slightly recessed relative to the adjacent cartilage, which reduces the compressive force through the implant, yet assuring the mechanical support of the surrounding cartilage on the defect side. The idea to fill the empty spot, on top of the implant, with an additional layer of hydrogel to protect the surrounding cartilage did not reveal any additional benefits and was therefore deemed unnecessary.

Acknowledgements

This work was supported by the framework of Chemelot InSciTe, supported by the partners of Regenerative Medicine Crossing Borders and powered by Health~Holland, Top Sector Life Sciences & Health. We acknowledge Kai-Chieh Kuo (ITA Institut für Textiltechnik, RWTH Aachen University) for producing the spacer fabrics and Marko Mihajlovic (Utrecht Institute for Pharmaceutical Sciences, Utrecht University) for producing the hydrogel. We are grateful to Jurgen Bulsink for his assistance in developing the test setup.

5

Donor-dependent articular cartilage matrix formation in CSMA-PEGDMA hydrogels embedded in spacer fabrics to restrict swelling

This chapter was written in collaboration with C.C. van Donkelaar and Keita Ito.

Abstract

Three-dimensional warp-knitted spacer fabrics were developed to confine a swelling hydrogel. This system mimics the osmotic pressure in native cartilage, generated by the proteoglycans in and arcade-like collagen network. The chondrocytes in such system experience a constant osmotic pressure. It is not known how they respond to that. It may activate them, or they may become passive. This study addresses the question if the induced hydrostatic pressure activates primary bovine chondrocytes to synthesize ECM components, or whether dynamic loading is required to stimulate synthesis of articular cartilage ECM *in vitro*. Poly(ethyleneglycol) dimethacrylate (PEGDMA) was co-polymerized with methacrylated chondroitin sulphate (CSMA) within a spacer fabric composed of polycaprolactone (PCL) with poly(4-hydroxybutyrate) (P4HB) pile yarns. After 48 hours of culture, mechanical stimulation was induced by a flat-bottomed indenter for the loaded HydroSpacer group. As a control, free swelling PEGDMA CSMA hydrogels were included. After both 48 hours and 19/26 days of swelling in culture medium, significant lower ($p<0.001$) swelling ratio was revealed for the HydroSpacer groups, demonstrating the restricted environment. This restricted swelling resulted in a 5 times higher stiffness for HydroSpacers compared to free swelling hydrogels, after 48 hours of culture. Directly after cell encapsulation, a small portion of chondrocytes were already surrounded by type VI collagen, indicating the presence of chondrons with pericellular matrix (PCM). After 19 days of culture, Type II collagen deposition was most abundant in one out of three HydroSpacers. Therefore, it might be that collagen deposition was not impeded by the restricted swelling, whereas dynamic loading enhanced matrix production in one donor, but had no effect in others.

5.1 Introduction

Although tissue engineering of cartilage started decades ago with autologous chondrocyte transplantation in 1987[182], mimicking the native environment to provide biological, physical and mechanical support to chondrocytes in load-bearing cartilage constructs is still a challenging exercise and shows inconsistencies. In native cartilage, the composition of the extracellular matrix (ECM) reflects the loading pattern, with the highest proteoglycan content in the most loaded regions[183], and collagen orientation is thought to depend on the strain direction[184]. Chondrocyte morphology and ECM synthesis depend on stiffness of the 2D or 3D substrate or environment: on a stiff substrate chondrocytes lose their rounded shape morphology and start spreading, indicated by the deposition of actin stress fibers[185,186]. In 3D hydrogel environment such as gelatin methacryloyl (GelMA, stiffness 29.9 kPa), chondrocytes retain their phenotype and produce cartilage-specific ECM [187]. *In vitro* cultured chondrocytes embedded in a chitosan-hyaluronic acid based hydrogel using chondrogenic medium produce more favorable ECM components in stiffer hydrogels (±180 kPa), whereas chondrocytes cultured in soft hydrogels (±130 kPa) maintain a more chondrogenic phenotype (rounded shape) and higher viability[188]. It is also shown that not agarose concentrations (and therefore initial stiffnesses) but the addition of transforming growth factor beta (TGF-β) in the culture medium determines the ECM quantity, whereas the agarose concentration determines the homogeneity of the ECM deposition and therefore an increased stiffness after a culture period of 42 days[189]. Type II collagen production is independent on hydrogel stiffness, and increased proliferation and GAG production is observed in softer agarose hydrogels when no TGF- β is added the culture media[190]. Moreover, the ability of monolayer-expanded dedifferentiated chondrocytes to redifferentiate into chondrocytes is not dependent on the elasticity of a 3D environment, but the availability of more adhesions sites within the hydrogel hampers the redifferentiation, diminishes production of glycosaminoglycans (GAGs) and increases production of type I versus type II collagen[191]. Using mesenchymal stemcells (MSCs), increases substrate stiffness and leads to differentiation of MSCs and towards the formation of fibrocartilage[192]. Moreover, MSCs cultured in agarose hydrogels with ascending stiffnesses show that stiffer hydrogels suppress cartilage matrix synthesis and related gene expression, but enhance the mechanotransduction of hydrostatic pressure[193]. In monolayer

cultures, both static and intermittent hydrostatic pressure during culture lead to increased expression of TGF- β, aggrecan and type II collagen[194,195].

For *in vivo* applications, stiffer and tougher hydrogels are required than those commonly used *in vitro,* because these hydrogels face mechanically challenging environments. *In vivo*, stiffer substrate materials have shown more promising results than softer substrate materials, up to an elastic modulus of 10 MPa[196]. Chondrocytes retain phenotype when cultured in a mechanical environment comparable to native cartilage, based on a polyelectrolyte hydrogel and collagen scaffold mimicking the osmotic and electrostatic surrounding[197]. To further enhance matrix synthesis in cartilage tissue engineering, dynamic axial loading can be used. Whereas static compression inhibits synthesis of ECM components, dynamic axial compression stimulates matrix production[198]. The effects of dynamic stimulation during culture depends on the applied strain and frequency[199], and on the nature of loading. For instance, a sliding loading regime enhances collagen deposition and results in a depth-dependent matrix organization[200]. Dynamic stimulation of natural polymer-based hydrogels also has shown to have beneficial effects in terms of ECM synthesis, mechanical properties and the attenuation of hypertrophy, for example of MSCs-laden hyaluronic acid (HA) hydrogels and photoclickable poly(ethylene glycol) (PEG) hydrogels containing chondroitin sulfate [201,202]. In general, co-polymerization of methacrylated chondroitin sulphate (CSMA) with poly(ethyleneglycol) dimethacrylate (PEGDMA) shows beneficial effects in terms of stiffness and ECM production, compared to PEGDMA hydrogels[147,203,204]. Interestingly, pure CSMA based hydrogels inhibit biosynthetic activity by freshly isolated bovine chondrocytes[204]. Moreover, unconfined dynamic loading increases the proteoglycan and collagen synthesis in CSMA-PEG hydrogels compared to unloaded samples, but simultaneously inhibits cell proliferation and decreases proliferation depending on CSMA concentration[205]. Physiological negative fixed charge densities (FCD), obtained in cultures by modulating the CSMA concentration in hydrogels, leads to matrix synthesis while non-physiological FCD's shows decreased matrix synthesis when dynamically loaded[205]. This suggests that mimicking the native environment can lead to beneficial effect on ECM production. However, in these studies, free swelling hydrogels were used with compressive moduli of ~78 kPa, much softer than native cartilage[205].

An approach to mimic the natural mechanism for load bearing in cartilage is the HydroSpacer system, in which fluid pressure is created by sandwiching a swelling hydrogel in a warp-knitted spacer fabric. Consequently, hydrogel swelling is restricted, and the osmotic pressure remains high, similar to the interaction between proteoglycans and collagen in native cartilage. The resulting construct stiffness is in the range of native cartilage using both synthetic and natural occurring polymers[174,178], which makes such a construct immediately load bearing. A preliminary study with swelling hydrogels in restricted swelling conditions shows high viability after 1 week of restricted swelling, demonstrating that primary isolated bovine chondrocytes survive such high hydrostatic pressures in vitro[178]. However, this study used a hydrogel based on CSMA and methacrylated hyaluronic acid (HAMA) which is not stable for longer culture duration. Therefore, it is impossible to use this system for exploring effects of culture conditions and mechanical stimulation in relation with ECM synthesis. Hydrogels based on PGDMA and CSMA are more stable and behave similarly in HydroSpacers under restricted swelling conditions.

This study therefore uses the HydroSpacer system with restricted swelling of a PEGDMA CSMA hydrogel to address the question if the induced hydrostatic pressure activates primary bovine chondrocytes to synthesize ECM components, or whether additional dynamic loading is required to stimulate synthesis of articular cartilage ECM *in vitro*.

5.2 Materials and Methods

5.2.1 Bovine chondrocyte harvesting

Chondrocytes were freshly isolated from bovine metacarpal joints (n=6). Cartilage was removed from the underlying bone and digested overnight at 37°C in DMEM (Gibco™, Thermo Fisher Scientific, Landsmeer, the Netherlands) supplemented with 0.15% collagenase type II (LS0004174, Worthington Biochemical Corporation, Lakewood, NJ, USA) and 0.01% hyaluronidase (CAS 37326-33-3, Sigma-Aldrich, Zwijndrecht, the Netherlands), 10% fetal bovine serum (FBS, BCBV7611, Sigma-Aldrich) and 1% penicillin/streptomycin (P/S, 15070063, Thermo Fisher Scientific). After digestion, the cell suspension was filtered through a 70 µm cell strainer and kept in suspension (DMEM supplemented with FBS (10%) and P/S (1%)) and directly used for cell encapsulation.

5.2.2 Spacer fabric

PCL-P4HB warp-knitted spacer fabric scaffold (height: ~1.8 mm) were prepared as described previously[206]. In short, spacer fabrics were produced (ITA GmbH, Aachen, Germany) of top and bottom sheets of knitted multifilament polycaprolactone (PCL) (EMS-Griltech AG; Domat/Ems) and connected to each other with monofilament poly-4-hydroxybutyrate (P4HB,Becton, Dickinson and Company, Franklin Lakes, USA) pile yarns using a double Raschel warp-knitting machine (Karl Mayer GmbH Doubleraschel; DR 16 EEC/EAC). After heat treatment, 20 min in a 45°C oven (Carbolite, Hope U.K.), samples were laser cut in 8 mm diameter discs, sterilized for 1 hour in 70% EtOH, washed overnight in sterile PBS and dry-blotted prior to placement in Teflon molds.

5.2.3 Cell laden hydrogel and HydroSpacer fabrication

PEGDMA (20 kDa, Polysciences, Hirschberg an der Bergstrasse, Germany) - CSMA (synthesized in-house by partners from Utrecht University, The Netherlands[178]) hydrogels were prepared by dissolving the polymers in PBS at desired concentration (9 wt% PEGDMA, 1 wt% CSMA). The resulting polymer solution was supplemented with lithium phenyl-2,4,6-trimethylbenzoylphosphinate (LAP) photoinitiator (0.2 w/v% final concentration). Prior to polymerization, freshly isolated chondrocytes were suspended in a desired volume of polymer solution (10 wt% PEGDMA-CSMA) to a final concentration of $10*10^6$ cells/mL, and subsequently injected in a Teflon mold with cylindrical wells (1.8 mm in height and Ø 8 mm with side injection ports) and sandwiched between quartz glass plates. Crosslinking was achieved by UV irradiating the samples for 25 minutes at a distance of 5 cm from the light source (UV lamp VL-4.LC, A. Hartenstein GmbH, intensity 0.58-1.49 mW/cm^2 wavelength 365 nm); samples were turned around after 12.5 minutes and UV exposure of the otherside was carried out in similar fashion. PEGDMA-CSMA confined hydrogel samples were prepared in the same way, PCL-P4HB warp-knitted spacer fabrics were first placed in the cylindrical wells of the mold prior to injection of the polymer solution.

5.2.4 In vitro culture

HydroSpacers were placed inside circular PEEK cassettes (Ø 8 mm, with permeable bottom, silicon ring and silicon band, Fig 5.1A, B), or PEEK confined mechanical stimulation units (Ø 8 mm, with permeable bottom), to prevent lateral swelling of the HydroSpacer. 3.5 mL high glucose DMEM (Gibco™, 21969), supplemented with 10% Glutamax (Gibco™), 1% Insulin-Transferrin-Selenium-Plus (ITS+ premix, Corning, Thermo Scientific), 1% Penicillin/Streptomycin (Lonza) and 0.2 mM L-ascorbic acid-2-phosphate (Sigma-Aldrich, Zwijndrecht, the Netherlands) was added to all conditions, and changed two times per week. The three groups (PEGDMA-CSMA free swelling hydrogel ('FS'); PEGDMA-CSMA PCL P4HB restricted swelling ('HydroSpacer'); PEGDMA-CSMA PCL P4HB with mechanical stimulation ('HydroSpacer-loaded')) were cultured for 28 days at 37°C, 5% CO_2. After 48 hours of culture without stimulation, PEGDMA-CSMA PCL P4HB constructs were mechanically stimulated using a custom-built dynamic confined compression bioreactor system using flat pistons (Ø 7.9 mm, adapted from previously described system (Figure 5.1C)[207]. In short, PEGDMA-CSMA PCL P4HB constructs were inserted within a confined stimulation unit, which were housed in a water bath at 37°C that was placed in a dynamic testing device (MTS Acumen, USA). All the stimulation units were loaded simultaneously by using individual spring-based pistons. A regime of 0-0.8 N force (verified equiv. to 10~15% strain) in a sinusoidal waveform at a frequency of 1 Hz, 2 hours per day, 5 days a week was applied through a 7.9 mm flat-bottomed indenter. In between the 2 hour loading periods, stimulation units with HydroSpacers were kept in the incubator unloaded, with the piston suspended a few mm from the HydroSpacer surface. Upon loading, pistons were lowered on the HydroSpacer individually, till a change in force was measured and therefore contact to the sample secured. During the whole culture period, nutrition and fluid flow was enabled by the porous bottom of the confined units.

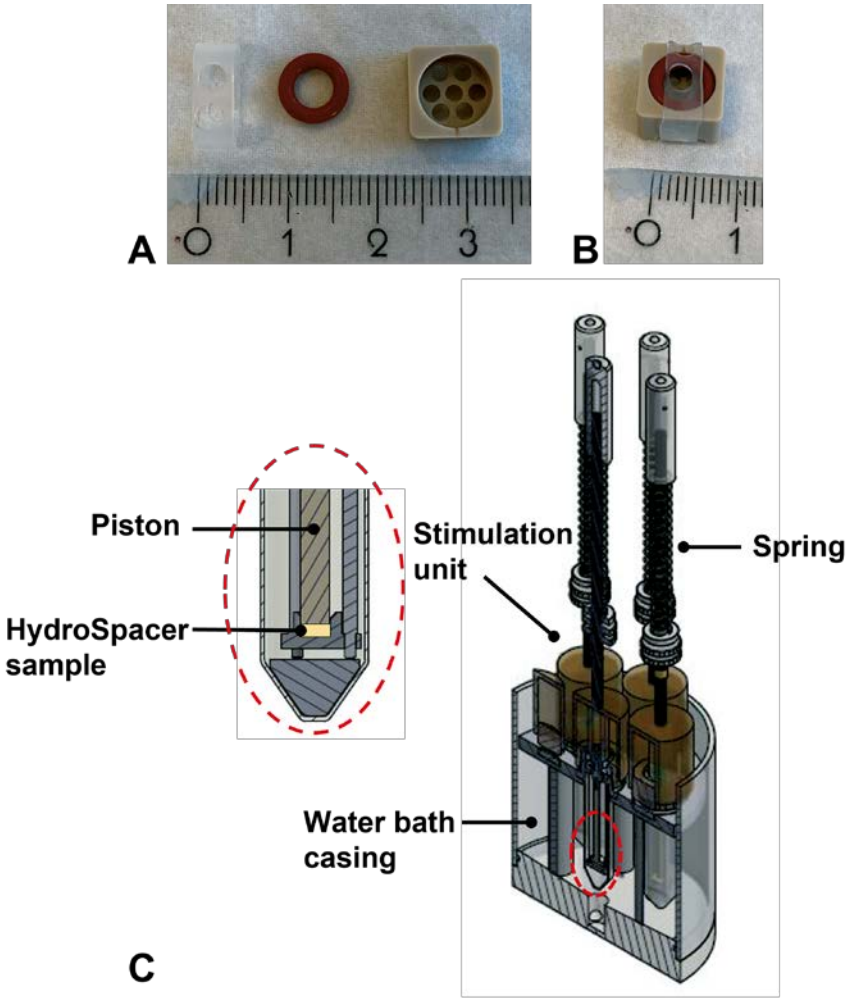

Figure 5.1: *PEEK cassettes with silicon ring and band (**A**) and assembled (**B**), Confined mechanical stimulation set-up, consisting of a water bath, 7 stimulation units with pistons loaded by springs (**C**).*

5.2.5 Swelling

The wet and dry weight (after 24 hours of lyophilization, Freezone 2.5, Labconco, Kansas City, USA) of both hydrogels and HydroSpacer were measured after swelling for 48 hours and after the culture period, in culture medium at 37°C (W_{wet}) and directly after freeze-drying (W_{dry}). The mass swelling ratio was defined as W_{wet}/W_{dry}.

5.2.6 Mechanical characterization

After 48 hours and 28 days of culturing, a confined compression test was performed using a tensile tester (Model 42, MTS Criterion, Eden Prairie, USA) equipped with a loadcell of 50 N (LSB.503, MTS systems corp., Eden Prairie, USA) inserted with a custom-made stainless-steel confined set-up, as described previously[174]. Prior to placing the samples within the confined compression set-up (Ø 8 mm), free swelling hydrogels were cut with an 8 mm diameter biopsy punch to fit into the container. After the hydrogels or HydroSpacers were inserted, a porous platen (316L stainless steel with 200 µm pore size, THN, Enschede, Netherlands), a custom-made piston and a 7 mm diameter stainless steel ball (Fabory, Tilburg, Netherlands) were placed consecutively on top of the sample, to allow fluid flow throughout the test. Subsequently, the PBS was added to the container. To determine the mechanical properties of the constructs, a stress relaxation test was performed by applying 15% strain, with a strain rate of 15%/sec and was held constant for 900 seconds. The stress relaxation was measured at a frequency of 10 Hz. The apparent peak modulus ($E_{app\ peak} = \frac{\sigma_{peak}}{\varepsilon_{peak}}$) and equilibrium modulus ($E_{eq} = \frac{\sigma_{eq}}{\varepsilon_{eq}}$) were calculated from the relaxation curve.

5.2.7 (Immuno)histochemical analysis

To gain more insight in collagen deposition during the culture period, picrosirius red staining was performed. Hydrogels and HydroSpacer halves (N = 1 per donor) were fixed in 3.7 % neutral buffered formaldehyde overnight and left in PBS. Samples were embedded in Tissue Tek® (Sakura), quickly frozen with liquid N_2 and cryosections of 15 µm thick were prepared. To visualize collagen deposition, cryosections were stained with Picrosirius Red. In short, sections were soaked in Weigert's Iron Hematoxylin (HT1079, Sigma-Aldrich) solution for 10 min, washed in running tap water for 10 min, and stained in 1 % w/v Sirius Red (36,554–8, Sigma-Aldrich) in picric acid solution (36,011, Sigma-Aldrich) for one hour. Subsequently, sections were washed in

two changes of 0.5 % acetic acid and dehydrated in 70 %, 96 %, 3 times 100 % EtOH, and 2 times xylene. Sections were mounted with Entellan (107,961 Sigma-Aldrich). Images were made using a bright field microscope (Zeiss Axio Observer Z1, 10×/0.45 Plan-Apochromat objective).

To gain more insight in the presence of different collagen sub types, immunohistochemistry was performed for Types II and VI. In short, cryosections (N = 1 scaffold per donor) were rehydrated in PBS for 10 minutes, permeabilized for 5 minutes in 0.5 % Triton X-100 in PBS prior to an antigen retrieval using 0.05% pepsin in HCl. Subsequently, sections were blocked in 10 % normal donkey serum in PBS for 30 min. Primary antibodies (Col VI: Rabbit polyclonal ab6588, Abcam, Col II: monoclonal MA5-12789, ThermoFisher) were incubated overnight at 4 °C in 1 % normal donkey serum in PBS, secondary antibodies (respectively donkey-anti-rabbit alexa 647, Jackson ImmunoResearch Europe, Ely, UK and donkey-anti-mouse alexa 488, Jackson ImmunoResearch Europe) were incubated together with DAPI for 1 h at room temperature. Imaging was performed using an epi-fluorescence microscope (Zeiss Axio Observer 7, X-cite Xylis XT720L light source, 20×/0.4 and 40x/0.6 LD Plan-Neofluor objectives).

5.2.8 Statistical analysis

Swelling and mechanical properties are presented as mean (± standard deviation). To test for normality, a Shapiro-Wilk test was done for all datasets. For comparisons between swelling, an unpaired t-test was performed. For the mechanical properties, a two-way ANOVA with Tukey post-hoc test was performed with the significance level set to $p < 0.05$. All statistical analyses were performed with GraphPad Prism (v 8.0.2, San Diego, CA, USA).

5.3. Results

5.3.1 Swelling of hydrogels and HydroSpacers

After both 48 hours and 19/26 days of swelling in culture medium at 37°C, significant differences ($p<0.001$) in swelling ratio between hydrogels and HydroSpacers was revealed, demonstrating the restricted environment of a PEGDMA CSMA hydrogel by a PCL P4HB spacer fabric (Fig. 5.2). The mass swelling ratio of free swelling hydrogels significantly ($p<00.1$) increased over the length of the culture period. No significant differences in mass swelling ratio between time points were observed for HydroSpacers and loaded HydroSpacers.

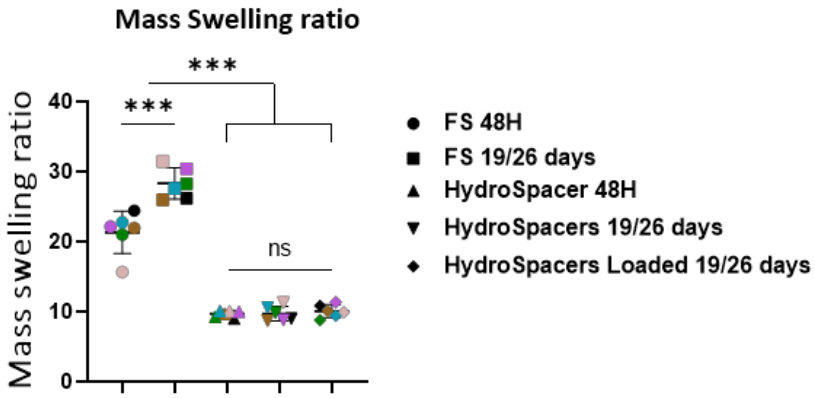

Figure 5.2: *Mass swelling ratio of PEGDMA CSMA hydrogel with and without the addition of a PCL P4HB spacer fabric after 48 hours 19 and 26 days of culture (n=6). Different donors are indicated by color (Black: D1; brown: D2; light rose: D3; purple: D4; green: D5; blue: D6)*

5.3.2 Mechanical analysis

A significant effect of the restricted swelling for both the apparent peak modulus ($p=0.001$) and equilibrium modulus ($p=0.0001$) was observed after 48 hours of equilibration (Fig 5.3A, 5.4A). HydroSpacers were more than 5 times stiffer than free swelling hydrogels (Fig 5.4A). After 19 (for donor 4, 5 and 6) and 26 (for donor 1, 2 and 3) days of culture, a yeast infection was observed in free swelling hydrogels and HydroSpacers without mechanical stimulation, and the culture was immediately aborted. Samples were harvested and handled as described in the materials and methods.

After 19 days the apparent peak modulus was increased for the free swelling hydrogels, and the modulus remained constant until day 26 (Fig 5.3A,B,C).

The HydroSpacers reached the same higher peak modulus already after 48 hours (Fig 5.3A), and the modulus did not change with time of culture, regardless mechanically stimulated (Fig 5.3B,C).

The equilibrium modulus of the HydroSpacers was higher after 48 hours. However, unlike the apparent peak modulus, the free swelling hydrogel did not increase stiffness and the HydroSpacers softened during 19 or 26 days of culture.

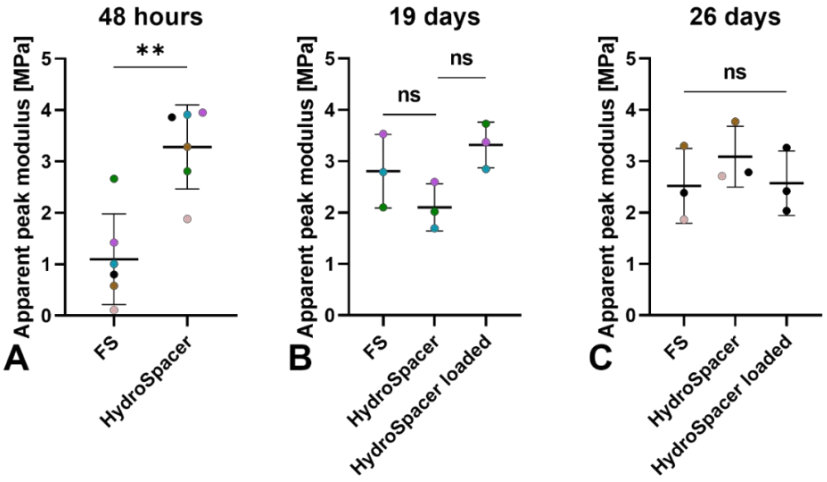

***Figure 5.3**: Apparent peak modulus of PEGDMA CSMA hydrogels and HydroSpacers with and without mechanical stimulation (MS) after 48 hours, 19 days and 26 days. Different donors are indicated by color (Black: D1; brown: D2; light rose: D3; purple: D4; green: D5; blue: D6)*

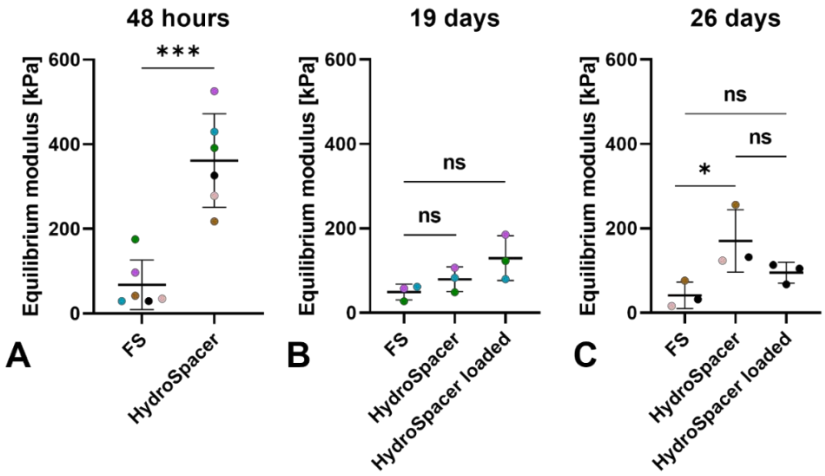

Figure 5.4: *Equilibrium modulus of PEGDMA CSMA hydrogels and HydroSpacers with and without mechanical stimulation (MS) after 48 hours, 19 days and 26 days. Different donors are indicated by color (Black: D1; brown: D2; light rose: D3; purple: D4; green: D5; blue: D6).*

5

5.3.3 Collagen deposition

Directly after cell encapsulation, collagen was present around chondrocytes in all donors, and in both hydrogels and HydroSpacers (Fig 5.5), which indicates incomplete digestion of the ECM or PCM surrounding chondrocytes. After 48 hours of culture (Fig 5.6) more cells were encapsulated with collagen, especially HydroSpacer samples of donor 4.

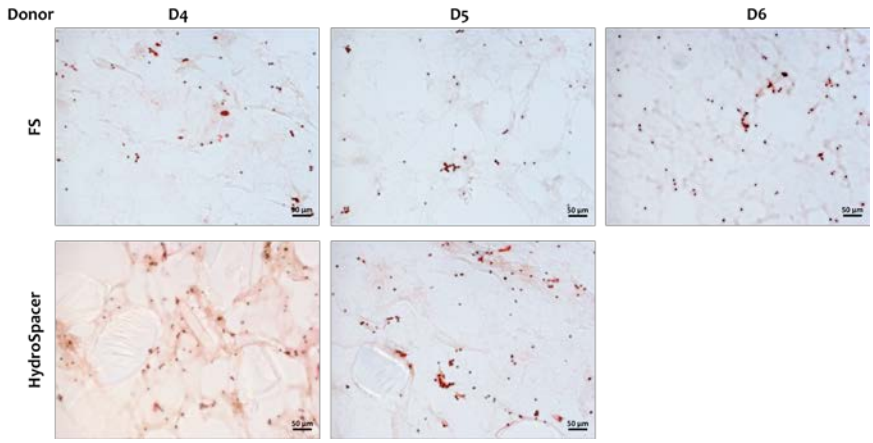

Figure 5: *Picrosirius red staining of PEGDMA CSMA hydrogels and HydroSpacers directly after cell encapsulation*

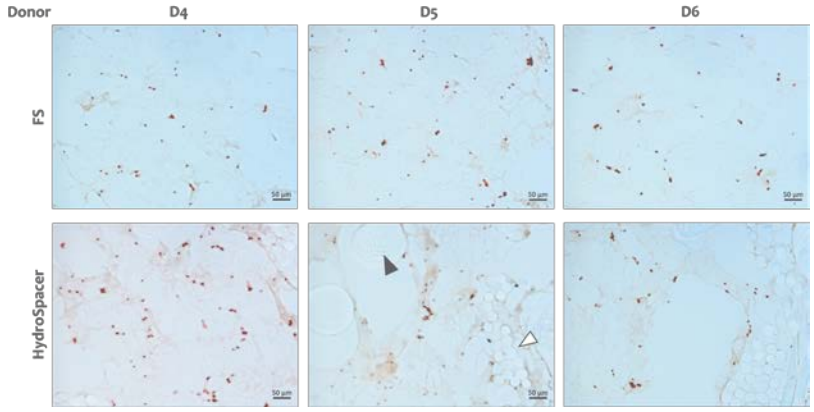

Figure 5.6: *Picrosirius red staining of PEGDMA CSMA hydrogels and HydroSpacers after 48 hours of culture. A cross section of a P4HB monofilament is indicated with a black arrow, and a cross section of the PCL multifilament by a white arrow.*

After 19 days of culturing (Figure 5.7), the free swelling hydrogels showed minor differences with the early timepoints. In the HydroSpacer samples collagen deposition was observed around more cells. This was most apparent in donor 4, with rings of collagen surrounding all cells. Adding mechanical stimulation to HydroSpacers enhanced collagen deposition in donors 5 and 6, but not in donor 4.

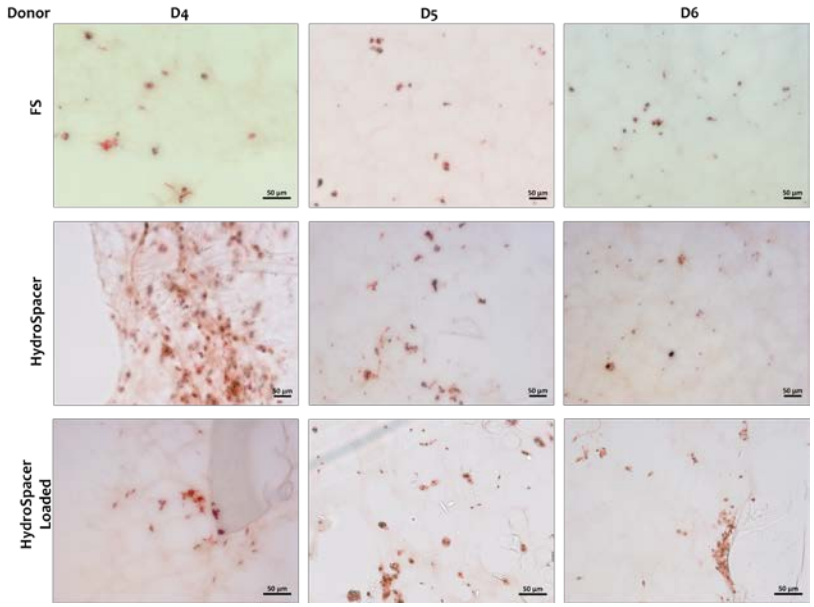

Figure 5.7: *Picrosirius red staining of samples after 19 days of culture, with and without PCL P4HB spacer fabric and mechanical stimulation. The more intense red staining, the more collagen deposition. In black cell nuclei.*

5.3.4 Type VI and II collagen deposition

Confirming the outcomes of the picrosirius red staining, it was demonstrated that directly after encapsulation a small portion of chondrocytes were surrounded by type VI collagen, indicating the presence of chondrons with pericellular matrix (PCM). These chondrons were present in all groups, but they were more abundant in donor 4 (Fig. 5.8).

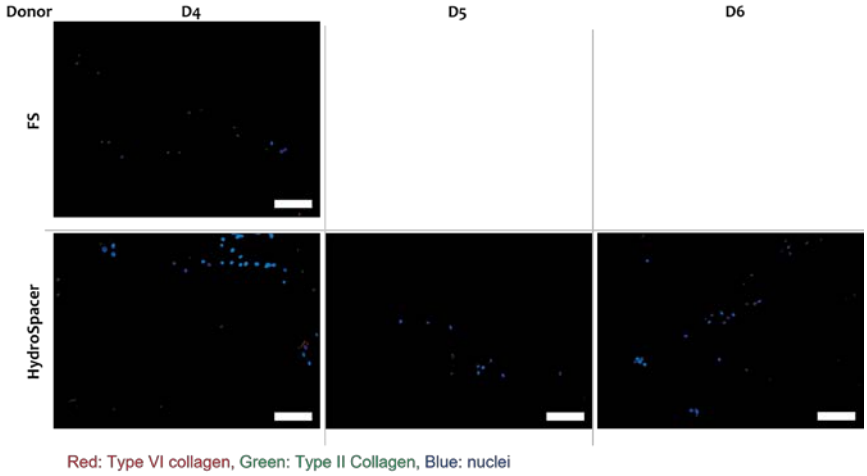

***Figure 8**:4 fluorescent imaging of samples directly after polymerization at day 0. From PEGDMA CMSA hydrogels of donor 5 and 6, no samples were present. Scale bars 50 µm.*

After 48 hours of culturing (Fig. 5.9) the number of type VI collagen positive cells increased, and the expression was more pronounced in both free swelling samples and HydroSpacers of donor 4 and 6. Collagen II was absent.

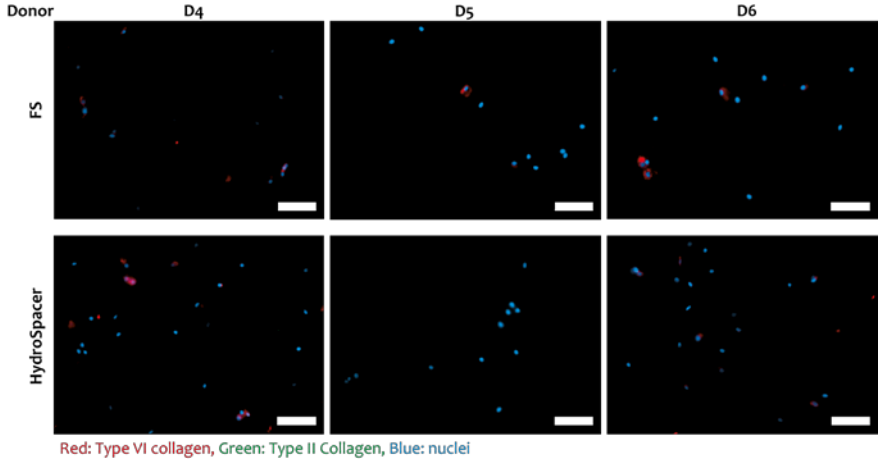

***Figure 5.9:** Fluorescent imaging of free swelling and restricted PEGDMA CSMA hydrogels after 48 hours of swelling. Scale bars 50 µm.*

After 19 days of culture, type VI and type II collagen was present in all groups (Fig. 5.10). Type II collagen deposition was most abundant in donor 4 HydroSpacers, followed by mechanically stimulated HydroSpacers of donor 5 and free swelling samples of donor 5 and 6 (Fig. 5.10-11). Col II deposition was not observed in donor 4 free swelling surrounding cells, as was seen in free swelling in the other 2 donors. Similarly, in HydroSpacers (unloaded and loaded), only in one donor per group cell and cell clusters were surrounded by col II, donor 4 and 5 respectively. In both free swelling and HydroSpacers, type II collagen seemed deposited in the pericellular region, however, donor 4 HydroSpacer synthesized larger amounts of collagen type II, which diffused a bit further away from the pericellular region (Fig. 5.10, D4 HydroSpacer). Using higher magnification (40x), a clear boundary was observed for the type VI collagen surrounding the cell, for both donor 4 and 5 in the restricted and mechanical stimulation groups (Fig. 5.11). Some cells did neither express col II nor VI, some contained only col VI. Collagen II deposition was more often observed when collagen VI was present surrounded cells and cell clusters, compared to cells without collagen VI. Day 26 samples showed similar results and were not taken along.

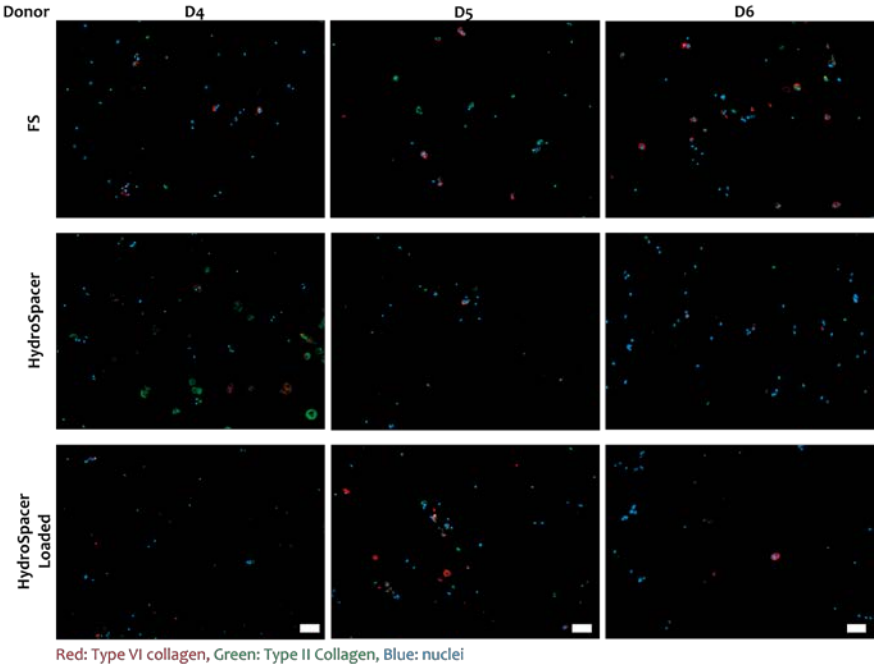

Figure 5.10 *Fluorescent imaging after 19 days in culture, with and without a PCL P4HB spacer fabric and mechanical stimulation. Scale bars 50 µm.*

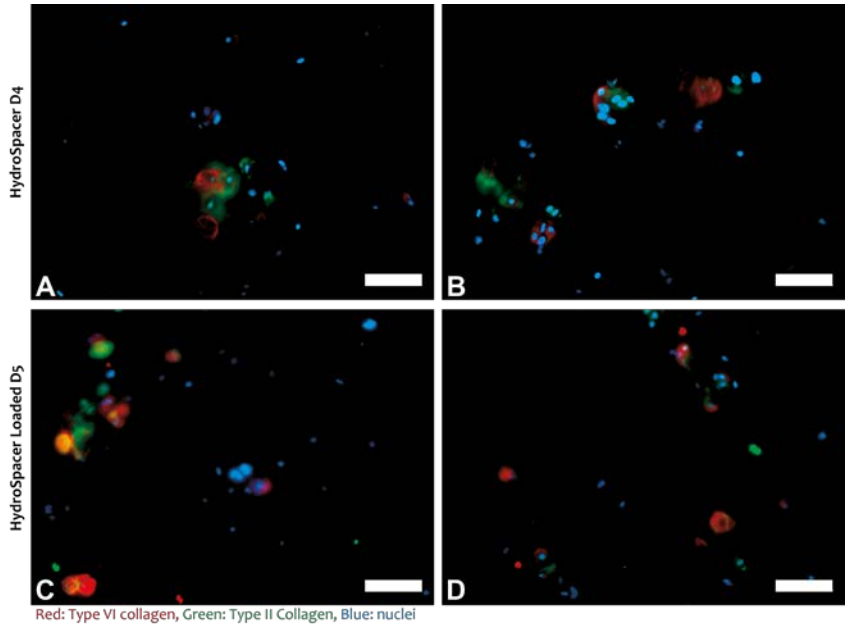

Figure 5.11: *Higher magnification images of cells from donor 4 (A and B) and donor 5 (C and D) in HydroSpacers (PEGDMA CSMA hydrogel restricted by a PCL P4HB spacer fabric) without (A and B) and with mechanical stimulation (C and D). Scale bars 50 µm.*

5.4. Discussion

It was hypothesized that the hydrostatic pressure originating from the restricted swelling, might impede ECM production of primary bovine chondrocytes but that dynamic loading would stimulate ECM synthesis. It was found that PEGDMA-CSMA Hydrogels swell less when embedded in a biodegradable PCL P4HB spacer fabric compared to free swelling (2-fold decrease in mass swelling ratio) and had a 5 times higher equilibrium modulus after 48 hours of swelling, indicating a restricted swelling environment in the restricted hydrogel.

Collagen synthesis was observed both in free and restricted swelling hydrogels, whereas one donor showed a more extensive collagen deposition in a HydroSpacer compared to a free swelling hydrogel, meaning that collagen deposition might not be impeded by the restricted swelling. Dynamic loading showed variable outcomes, in which both an increase and decrease in collagen deposition was observed. With these outcomes, no conclusions can be drawn, other than that donor variability might influence

the outcomes. Primary bovine chondrocytes formed PCM and deposited collagen type II in both free swelling and HydroSpacer system, which was donor dependent and independent on mechanical loading. The presence of PCM appeared essential for the synthesis of type II collagen in a restricted swelling environment.

The clinically relevant biodegradable PCL P4HB spacer fabric was developed based on previously studied non-degradable polyamide 6 spacer fabrics and showed similar restricting properties when filled with a swelling hydrogel[174,178]. The same PCL P4HB HydroSpacers implanted in bovine osteochondral defects showed substantial load sharing of the implant with the surrounding cartilage, and decreased wear on the opposing cartilage when the HydroSpacer was placed slightly recessed[206]. These load bearing properties of HydroSpacers were also observed in the current study with a significant increase in stiffness with the addition of the PCL P4HB spacer fabric compared to free swelling hydrogels after 48 hours.

In the current study, it seemed that chondrocytes produce more coll II and coll VI in HydroSpacers than in free swelling hydrogels. However, this was variable between donors. In previous research, success of tissue engineered cartilage was mainly attributed to the initial stiffness of the construct. For example, when primary human chondrocytes were cultured in fibrin hydrogels mimicking the elasticity of the perichondral space (30 kPa), they embedded themselves in a PCM-like spherical environment and a cartilaginous matrix composed of sGAGs and collagen type II to a much larger extend than in softer hydrogels (1 kPa)[158]. Effects of restricted swelling have not been reported often in literature. Culturing a hydrogel in a constrained cage did not lead to a quantitative difference in collagen and proteoglycan content compared to free swelling as measured biochemically[208], but the close examination of immunohistochemistry in the present study reveals increased collagen type II and type IV deposition. In support of an effect of restricted swelling on collagen metabolism, Nims et al (2017) observed an improved collagen maturation when constrained culture was used[208].

CSMA and other natural polymers have been used frequently as free swelling hydrogels in cartilage tissue engineering, with positive effects on ECM production as result. In the free swelling PEGDMA CSMA hydrogels, only very little type II and VI collagen deposition was observed after 19 days of culture.

Similar results were seen in free swelling hydrogels where the addition of CSMA to PEGDMA inhibited proteoglycan and collagen production[205]. In the study of Villanueva et al. (2010) a clear effect of the addition of 20% CS (creating a physiological ranges in terms of FCD) to a PEGDMA hydrogel was detected combined with dynamic loading, whereas in pure PEGDMA hydrogels dynamic loading didn't affect the cellular response[205]. Also, dynamic compressive loading showed superior mechanical properties and ECM production in HA-based hydrogel constructs[201]. In the current study, where hydrogels were restricted from swelling in the HydroSpacers, there was no beneficial effect of dynamic loading regarding stiffness, type II or type VI collagen deposition. This may indicate that the internal swelling pressure overrules the effect of additional external loading. However, further study is required to confirm this, because the large variation between donors and the small sample size limits the statistical power.

Immunohistochemical analysis revealed the presence of type VI collagen positive cells directly after polymerization in all donors (4-6), which implies that the digestion method yielded both chondrocytes and chondrons. The PCM enables cell signaling between the chondrocyte and the extracellular matrix[9–11] and influences the cellular response to osmotic, hydrostatic pressure and mechanical loading[193,209–211]. Growth factors which play an important role in mechanotransduction, such as TGF-β[209,212,213], bind to the PCM. With the presence of chondrons at day 1, it was expected that in response to dynamic compression, chondrons would upregulate the expression of type II collagen and aggrecan more than chondrocytes[214,215]. In previous studies it was already observed that after 1 day of culture a PCM could be formed in a PEGDMA CSMA hydrogel. In response to dynamic compression type II collagen and aggrecan expression increased compared to chondrocytes without PCM[205,214,215]. Moreover, the synthesis of PCM by chondrocytes in stiff hydrogels suggested that the PCM protected the chondrocyte from the applied pressure[216,217]. On the other hand, it seems that there was a co-expression/ synthesis of Type VI and II collagen, in which type II collagen is present more in the close surrounding of type VI collagen positive cells.

During the culture period, the mechanical properties of HydroSpacers (loaded and unloaded) decreased. Most likely, the CSMA content decreased during the culture period, caused by the susceptibility of methacrylate esters

of CSMA for hydrolysis at pH 7.4 and 37 °C[138]. The decreased CSMA content led to lower FCD, and consequently to a partial loss of swelling pressure of the hydrogel. Moreover, hydrogels with higher weight percentages of CSMA were more stable[178]. However, free swelling hydrogels did not decrease in equilibrium modulus under the same conditions (Figure 5.4), which might indicate that another mechanism caused the weakening of the HydroSpacer samples. Maybe hydrogel crosslinking was compromised by the insertion of the spacer fabric, which then resulted in gradual degradation of the hydrogel. The addition of the CSMA to pure PEGDMA led to a decreased mass swelling ratio, opposite to observations by Villanueva[205]. This contrast can be explained by the difference in molecular weight of the PEGDMA (20 kDa in the current study vs. 3kDa in the study of Villanueva[205]). Smaller 3kDa monomers form a tighter network with high density crosslinking, that didn't allow swelling. Incorporating CSMA loosened the network and allowed it to swell more. In contrast, a hydrogel with larger 20 kDa PEGDMA was able to swell several times its own volume (data not shown). As a result of the swelling, these hydrogels became more susceptible for degradation. The addition of CSMA monomers stabilized the 20 kDa PEGDMA gel by the higher degree of methacrylation crosslinking. The mass swelling ratio of PEGDMA was twice as high as the PEGDMA CSMA hydrogels under free swelling (data not shown). Moreover, other research showed that PEGDMA CSMA in a 8:2 ratio resulted in a physiological FCD, whereas in the current research a ratio of 9:1 was used[205]. This might suggest that the 9:1 ratio might be too low to induce the beneficial effects of mechano-regulators such as streaming potential and dynamic osmolarity changes on chondrocytes.

The low matrix synthesis in all groups might have a few reasons. First, throughout the culture period, basic medium was used, without the addition of TGF-β. TGF-β is essential in regulating its homeostasis and joint lubrication of articular cartilage[218,219], and in many cartilage tissue engineering cultures aiming for chondrogenesis and ECM production, TGF-β is supplemented to the culture media[220]. In general, this addition resulted in enhanced chondrocyte proliferation and ECM synthesis, which led to superior mechanical properties *in vitro*[221–223]. Indeed, studies of Bachman, et al and Kock, et al., showed that matrix synthesis was stimulated by addition of TGF-β3, and was independent of initial hydrogel stiffness[158,189]. However, the effect of TGF-β3 is complex and not fully understood. For instance, simultaneously exposure dynamic loading and TGF-β3 was less effective than

applying dynamic loading after TGF-β3 supplementation was discontinued[224]. Also, it was previously shown that TGF-β supplementation in combination with static mechanical compression inhibited matrix production[222]. The latter effect may exist under hydrostatic pressure conditions due to restricted swelling[225]. Therefore, in the current study TGF-β3 was not added to the culture media.

A second explanation for the low matrix synthesis is the possibility that the above effects are part of a natural feedback regulation system in chondrocytes, which control their PCM, Coll II and proteoglycan environment such that they experience a healthy environment. Such mechanism would depend on an interplay between dynamic and static mechanical conditions and may be controlled through cytokines. For instance, dynamic loading in the present study may have stimulated TGF-β expression[218], but the existing hydrostatic pressure in the HydroSpacers may have induced degradation of (newly formed) PCM, Coll II and proteoglycan[226]. Hypothetically, the chondrocytes may sense excessive hydrostatic pressure by the swelling polymer in the HydroSpacers and respond by secreting chondroitin sulphate degrading enzymes. These may then induce degradation of newly synthetized chondroitin sulphate, resulting in degradation products of CS that in turn further enhance the catabolic phenotype of chondrocytes[227,228]. Such mechanism would explain why aggrecan immunohistochemistry showed little to no aggrecan in the present samples, why the mechanically loaded HydroSpacers of donor 4 show very little matrix proteins, and also the decrease in GAG content in PEGDMA CSMA hydrogels between 2 and 4 weeks of culture[204].

Finally, the original cell density was identical in all prepared samples. However, due to the swelling of the PEGDMA CSMA hydrogel, the cell seeding densities became different between restricted and free swelling groups during culture. This might alter cell-cell or matrix-matrix interactions, and negatively affect the assembly of matrix molecules in some groups[201,229–232]. In addition, due to the final crosslinking density, synthesized collagens were deposited within the pericellular region in HydroSpacers. This concurs with former observations and predictions *in vitro* and *in silico,* where more less homogeneous ECM deposition was observed in denser hydrogels[233–236].

All presented data should be carefully interpreted, as the yeast infection at the end of the culture could have influenced the mechanical and cellular outcomes. Moreover, because of the heterogeneity of the cell population, it is impossible to conclude if differences in the initial presence of PCM between groups (i.e. initial chondrocytes/chondron ratio) influenced the results. For further studies, a homogenous population of either chondrocytes or chondrons could be used, to distill the effects of the PCM in a restricted swelling environment. Noteworthy, obtaining a homogenous population of chondrons with a high yield is challenging, and not very different between protocols that are thought to isolate either chondrocytes or chondrons[237,238]. Therefore, it is important to check the cells prior to such studies and specify the nature of the cell population.

Chondroitin sulfate present in the hydrogel was picked up using GAG histology and measured in GAG assays. Because to this, we were not able to distinguish between hydrogel and newly synthesized matrix, unfortunately. Therefore, both data on GAG histology and biochemical data was disregarded.

Further research may include gene analysis, in particular for the expression of catabolic genes in relation to the presence of hydrostatic swelling pressure in the HydroSpacers. Additionally, control groups without CSMA may be included to conclude on the effects of dynamic and FCD-influenced hydrostatic loading. When appropriate insight on matrix synthesis is obtained, a dynamic compression-sliding *ex-vivo* osteochondral explant defect model may be used to explore the effects of dynamic loading and swelling pressure on integration with the surrounding tissue[239]. To achieve long-term success, the degradation mechanism of the PEGDMA CSMA hydrogel should be evaluated as well, in order to optimize the material as well as the photopolymerization method to obtain a hydrogel that is initially stable but is slowly degraded and replaced by newly synthesized cartilage matrix in the long term.

In conclusion, a PCL P4HB spacer fabric was able to constrain the swelling of a PEGDMA CSMA hydrogel, which significant increased mechanical properties after 48 hours of swelling by generating an internal hydrostatic swelling pressure. With the embedding of primary bovine chondrocytes, donor specific ECM synthesis in terms of type II and VI collagen synthesis

were observed in free swelling, as well as in constrained and dynamically loaded constrained hydrogels. Dynamic loading of HydroSpacers did not lead to an increase in matrix production, compared to free swelling hydrogels. As ECM synthesis seems slow, a prolonged culture time is advised, in which mechanical stability should be maintained.

Acknowledgement
We would like to thank Marko Mihajlovic and Tina Vermonden (Utrecht University) for the synthesis of the CSMA and Kai-Chieh Kuo and Charlotte Büchter (ITA RTWH Aachen), for the production of the PCL P4HB spacer fabric. This research was performed under the framework of Chemelot InSciTe, supported by the partners of Regenerative Medicine Crossing Borders and powered by Health~Holland, Top Sector Life Sciences & Health.

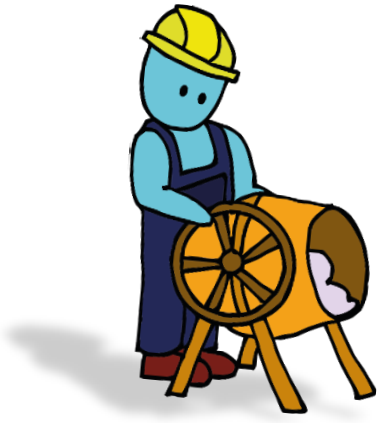

6

Enzymatic Isolation of Articular Chondrons: Is It Much Different Than That of Chondrocytes?

The contents of this chapter are based on:
M. van Mourik*, **G.H. Schuiringa***, L.P. Verhagen, L.A. Vonk, C.C. van Donkelaar, K. Ito, J. Foolen, Enzymatic Isolation of Articular Chondrons: Is It Much Different Than That of Chondrocytes?, Tissue Engineering Part C: Methods, vol. 29, issue 1, 2023
DOI: 10.1089/ten.tec.2022.0176
* These authors contributed equally to this work

Abstract

In native articular cartilage, chondrocytes are completely capsulated by a pericellular matrix (PCM), together called the chondron. Due to its unique properties (w.r.t. territorial matrix) and importance in mechanotransduction, the PCM and chondron may be important in regenerative strategies. The current gold standard for the isolation of chondrons from cartilage dates from 1997. Although previous research already showed the low cell yield and the heterogeneity of the isolated populations, their compositions and properties have never been thoroughly characterized. This study aimed to compare enzymatic isolation methods for chondrocytes and chondrons and characterize the isolation efficiency and quality of the PCM. Bovine articular cartilage was digested according to the 5-hour gold standard chondron isolation method (0.3% dispase + 0.2% collagenase II), an overnight chondron isolation (0.15% dispase + 0.1% collagenase II), and an overnight chondrocyte isolation (0.15% collagenase II + 0.01% hyaluronidase). Type VI collagen staining, fluorescence-activated cell sorting (FACS) analysis, specific cell sorting and immunohistochemistry were performed using a type VI collagen staining, to study their isolation efficiency and quality of the PCM. These analyses showed a heterogeneous mixture of chondrocytes and chondrons for all three methods. Although the 5-hour chondron isolation resulted in the highest percentage of chondrons, the cell yield was significantly lower compared to the other isolation methods. FACS, based on the type VI collagen staining, successfully sorted the three identified cell populations. To maximize chondron yield and homogeneity, the overnight chondron enzymatic digestion method should be combined with type VI collagen staining and specific cell sorting.

Impact statement

Since chondrocytes are highly dependent on their microenvironment for maintaining phenotypic stability, it is hypothesized that using chondrons results in superior outcomes in cartilage tissue engineering. This study reveals the constitution of cell populations obtained after enzymatic digestion of articular cartilage tissue and presents an alternative method to obtain a homogeneous population of chondrons. This data can improve the impact of studies investigating the effect of the PCM on neocartilage formation.

6.1 Introduction

Articular cartilage regeneration is a large and fast-growing research field within orthopaedics. During the past 10 years alone, over 2200 research papers have been published on cartilage regeneration and repair, with the number of articles increasing each year. Considering the clinical problems and socio-economic burdens associated with damage to articular cartilage, the growing interest in finding solutions for cartilage regeneration is well supported.

Regenerative strategies aim to recreate the cartilage extracellular matrix, mimicking the biomechanical, biochemical, and structural properties of the native tissue. Most of these are cell-based approaches, [240] and the cell type is very important. The use of stem cells like mesenchymal stem cells (MSCs) and adipose-derived stem cells (ASCs) has been widely explored since these are accessible cell sources.[241,242] However, depending on their original differentiation line, stem cells often do not differentiate well and have tendencies towards the bone lineage.[243] Chondrocytes, the native cell type of articular cartilage, are therefore often preferred. Within cartilage, chondrocytes are responsible for maintaining the ECM, which mainly consists of type II collagen and proteoglycans.

However, current clinical procedures using chondrocytes, for example autologous chondrocyte implantation (ACI) and matrix-induced autologous chondrocyte implantation (MACI), often result in fibrocartilage or hypertrophy.[94,244] Less than half of the procedures leads to hyaline-like cartilage or hyaline-like cartilage with fibrocartilage, and in 9% of the cases, re-operation is needed.[245] This is caused, in part, by the inability of chondrocytes to overcome de-differentiation during *in vitro* monolayer expansion.[245,246]

In native cartilage, chondrocytes are completely encapsulated by a pericellular matrix (PCM), together called the chondron. The main collagen in the PCM is type VI collagen, which plays an important role in the chondron's integrity and cell signaling between the chondrocyte and the extracellular matrix.[9–11]

Using these chondrons, considered as the functional unit of articular cartilage, may be advantageous for cartilage regeneration. Using an enzymatic isolation method developed by Lee, et al (1997)[238], it has been shown that the PCM of the chondrocyte can be preserved. This resulted in a significant increase of matrix production and led to a mechanically functional neocartilage construct *in vitro*.[247–249] During ACI in osteoarthritic (OA)

patients, human OA chondrons, obtained using a 5-hour isolation method with 0.18% Dispase II and 0.2% collagenase, outperformed OA chondrocytes in terms of cell survival and biosynthesis[250], which can be explained by the protecting and mechanosensing role of the PCM.[10,211,251] Autologous chondrons, obtained with a rapid isolation method for 45 minutes, mixed with MSCs showed to have similar or even superior outcomes compared to ACI, suggesting a stimulatory effect of MSCs on chondrons in regenerating cartilage.[252,253] Not only a significant increase in GAG content and GAG/DNA was found when chondrons were co-cultured with MSCs compared to chondrocytes co-cultured with MSCs *in vitro*, also the loss of type VI collagen of the PCM of the chondrons when co-cultured with MSCs was reduced.[254,255] Similarly, co-culturing chondrons and chondrocytes in a 1:1 ratio led to increased levels of aggrecan and type II collagen gene expression and GAG production *in vitro* and improved outcomes after implantation.[256] Using chondrons over chondrocytes in cartilage regenerative strategies is therefore hypothesized to provide superior outcomes.

As previously described, chondrons are mostly isolated via enzymatic digestion of cartilage tissue. The current gold standard for isolation of chondrons from articular was described by Lee et al in 1997, proposing a mild 5-hour enzymatic isolation protocol using a mix of dispase and collagenase type II.[238] However, both chondron and chondrocyte isolation methods result in a heterogeneous mix of chondrons and chondrocytes, respectively 62% and 29% of cells were Col VI positive.[251] Although this heterogeneity can influence their use, the properties and compositions of these cell populations have never been thoroughly characterized. The aim of this study is to compare enzymatic isolation methods for chondrons and chondrocytes and characterize the results based on isolation efficiency and structural quality of the PCM.

6.2 Materials & Methods

6.2.1 Experimental design

Cell populations resulting from different enzymatic isolation methods were analyzed using type VI collagen immunostaining to discriminate chondrons (with PCM) from chondrocytes (without PCM). Flow cytometry was used to collect quantitative data of the population composition and to sort the different cell populations. The stained cells were visualized using microscopy to assess the structure of the PCM. Additionally, the sorted cell populations

were imaged to validate the composition of the cell populations identified with flow cytometry.

6.2.2 Cell isolation

Articular chondrocytes and chondrons were isolated from fresh bovine articular cartilage from multiple donors (N = 4, age 8-12 months from slaughterhouse material). Articular cartilage was harvested from the metacarpophalangeal joint, weighted, minced (1-3 mm) and divided into three groups. Chondrocytes (Chy) were isolated by overnight enzymatic digestion at 37 °C in 0.15% collagenase type II (LS0004174, Worthington Biochemical Corporation, Lakewood, NJ, USA) and 0.01% hyaluronidase (CAS 37326-33-3, Sigma-Aldrich, Zwijndrecht, the Netherlands) in Dulbecco's Modified Eagle Medium (DMEM, 41966-029, Gibco™, Thermo Fisher Scientific, Landsmeer, the Netherlands), supplemented with 10% fetal bovine serum (FBS, BCBV7611, Sigma-Aldrich) and 1% penicillin/streptomycin (P/S, 15070063, Thermo Fisher Scientific). Chondrons were isolated using an overnight (Chn ON) or a 5-hour (Chn 5H) protocol[238] , using 0.15% dispase II (17105-041, Gibco™) and 0.1% collagenase type II in DMEM, supplemented with 1% P/S or 0.3% dispase and 0.2% collagenase II in DMEM, supplemented with 1% P/S, respectively.

Undigested tissue remnants were filtered out using a 70 or 100 µm cell strainer (542070/542000, Greiner Bio-One, Alphen aan den Rijn, the Netherlands) for the chondrocyte and chondron isolations, respectively. All cells were washed twice with phosphate-buffered saline (PBS, P4417, Sigma-Aldrich) and cell counts were measured using a NucleoCounter® NC-100™ (ChemoMetec, Allerod, Denmark), according to the standard manufacturer protocol, to determine the total number of cells obtained from each isolation. The cell yield was calculated by dividing the total number of cells by the weight of cartilage of each sample. The collected cells were centrifuged at 150 g for 5 min and kept overnight in a loose pellet culture in a 50 mL Falcon tube with DMEM, supplemented with 10% FBS and 1% P/S, at 4 °C.

6.2.3 Type VI collagen staining

To analyze the cell populations, all cells were labelled with a conjugated type VI collagen antibody. Cells were resuspended after loose pellet culture and washed with 3% bovine serum albumin (BSA, 10735086001, Sigma-Aldrich) in Ca^{++} and Mg^{++} free PBS (DPBS, 14190250, Gibco™). Cells (10^6) were labelled

with FITC-conjugated rabbit anti-type VI collagen polyclonal antibody (50-199-23-71, Life Technologies Europe, Bleiswijk, the Netherlands) at a dilution of 1:100 for 30 min at 4 °C. Cells were washed twice using the BSA/DPBS solution and were finally resuspended in 500 µL of 0.5% BSA and 2 mM ethylenediaminetetraacetric acid (EDTA) in DPBS, resulting in a final concentration of $2x10^6$ cells/mL.
A positive control for the type VI collagen staining was obtained using bovine cartilage tissue cryosections of 5 µm thickness.

6.2.4 Flow cytometry
To analyze and sort the full cell population, flow cytometry was used. Prior to sample analysis, 1 µL of propidium iodide (PI, P4864, Sigma-Aldrich) was added to selected samples to discriminate between viable and dead cells upon analysis. Flow cytometry was performed using a FACS Aria III (BD Biosciences, Franklin Lakes, NJ, USA). Of each sample a total of 10,000 events were analyzed.

To validate the PCM structure of the present cell populations, cell sorting was performed with the FACS AriaIII based on the intensity of the type VI collagen staining. Using a type VI collagen-FITC-A, three distinct cell populations could be defined. The cells were collected into Eppendorf tubes containing 500 µL DMEM and were kept at 4 °C until analysis. After sorting, the resulting cell populations were characterized with flow cytometry.

Flow cytometry data were analyzed with FlowJo (BD Biosciences v10.6.1). First, cells were separated from debris using a FSC/SSC dot plot (Fig. 6.1A). Dead cells marked by the PI staining were excluded from analysis (Fig. 6.1B). Based on the intensity of the type VI collagen staining, the cells were characterized as chondrocytes or chondrons (Fig. 6.1D). Within the type VI collagen positive cell population, two separate populations of chondrons with low- (partial) and high-intensity (intact) type VI collagen staining were found. (Fig. 6.1E). The relationship between FSC-A and FSC-H was used to define single-cell and multicellular events (Fig. 6.1C). To obtain the cell yield of all analyzed samples, the results of the flow cytometry analysis were normalized to the calculated cell yield.

6.2.5 Microscopy

To analyze the structural integrity of the PCM, the type VI collagen stained cells were visualized using microscopy. Following the staining, cells were fixed in suspension using 1 mL of 4% paraformaldehyde at room temperature for 15 min. Cells were washed with DPBS and permeabilized with 0.5% Triton X-100 in PBS for 10 min. Cells were washed with DPBS, cell nuclei were stained with 4',6-diamidino-2-fenylindool (DAPI) at a 1:500 dilution, and cells were resuspended at a concentration of 10^7 cells/mL. Prior to visualization, a droplet of cell suspension was put on a microscopy slide and covered with a cover glass. A general overview of PCM structure was obtained using widefield fluorescent microscopy (20x, 0.4 NA, Axio Observer 7, Zeiss, Oberkochen, Germany) and detailed images were obtained with confocal laser scanning microscopy (40x, 1.1 NA, SP5X, Leica Microsystems, Wetzlar, Germany).

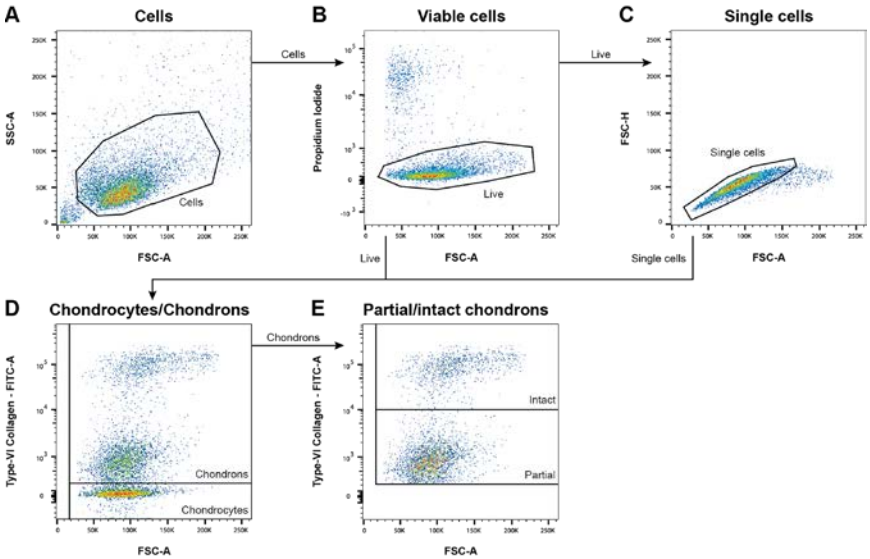

Figure 6.1: *Gating strategy of flow cytometry data analysis. First, cells were separated from debris (**A**). Viable cells are gated from dead cells (**B**). From the live cells, single cells (**C**) and chondrocytes and chondrons (**D**) are gated. From chondrons, cells with low- and high intensity type VI collagen staining, partial and intact chondrons respectively, are gated (**E**).*

6.2.6 Statistical analysis

Data are presented as mean (± standard deviation). To test for normality, a Shapiro-Wilk test was done for all datasets. For comparisons between digestion methods when analyzing cell yield, viability and different cell populations, a two-way ANOVA with Tukey post-hoc test was performed with the significance level set to $p < 0.05$. All statistical analyses were performed with R (v4.1.1, http://www.r-project.org) and GraphPad Prism (v 8.0.2, San Diego, CA, USA).

6.3 Experiment

6.3.1 5-hour chondron isolation had a much lower cell yield compared to other isolation methods

Articular chondrocytes and chondrons were successfully isolated from bovine articular cartilage. Cell yield of each isolation method, determined using the weight of the cartilage prior to digestion and the resulting cell count, was significantly different. The total cell yield for the Chy method was 14.2×10^6 cells/g cartilage (± 4.1×10^6; n=4), Chn ON was 20.1×10^6 cells/g cartilage (± 2.1×10^6; n=4), and Chn 5H was 2.8×10^6 cells/g cartilage (± 1.8×10^6; n=4) (Fig. 6.2). The cell yield of Chn 5H was an order of magnitude lower compared to both Chy ($p < 0.001$) and Chn ON ($p < 0.0001$). Cell viability, based on PI staining (Fig. 6.3), was highest for the Chy method (91.2% ± 3.27; n=4), which was significantly higher when compared to Chn 5H (77.2% ± 8.42%; n=4; $p < 0.05$). There were no significant differences between the viability of Chn ON (78.8% ± 15.2; n=4) and the other two isolation methods.

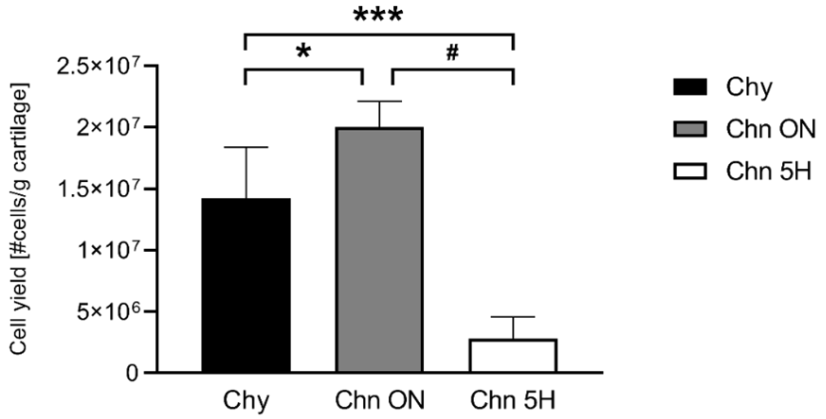

Figure 6.2: *Cell yield after chondrocyte (Chy) isolation using 0.15% collagenase type II and 0.01% hyaluronidase in DMEM, supplemented with 10% FBS and 1% P/S overnight and chondron (Chn) isolation using 0.15% dispase II and 0.1% collagenase type II in DMEM, supplemented with 1% P/S overnight (ON) or 0.3% dispase and 0.2% collagenase II in DMEM, supplemented with 1% P/S for 5 hours (5H)). *, p < 0.05; **, p < 0.01; ***, p < 0.001; #, p < 0.0001.*

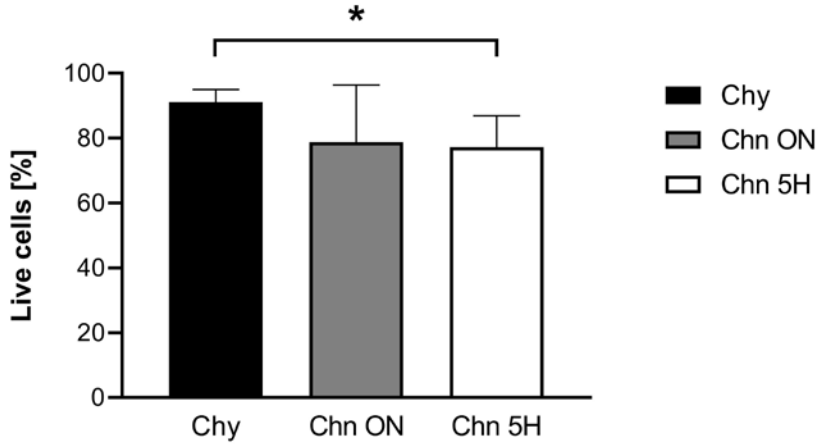

Figure 6.3: *Flow cytometry analysis of PI staining shows lower cell viability when using the Chn 5H isolation method. *, p < 0.05; **, p < 0.01; ***, p < 0.001; #, p < 0.0001.*

6.3.2 Enzymatic digestion of articular cartilage results in a heterogeneous mixture of chondrons (partial and intact) and chondrocytes, efficiency depends on the isolation method

All isolation methods resulted in a heterogeneous mixture of chondrocytes and chondrons. Three cell populations could be defined with flow cytometry, based on the intensity of the type VI collagen staining (Fig. 6.4A-C). The group containing the lowest intensity of type VI collagen, was identified as chondrocytes, and classified as the 'type VI collagen negative (Col-VI neg) population'. The low-intensity and high-intensity type VI collagen positive cells were classified as partial and intact chondrons, respectively.

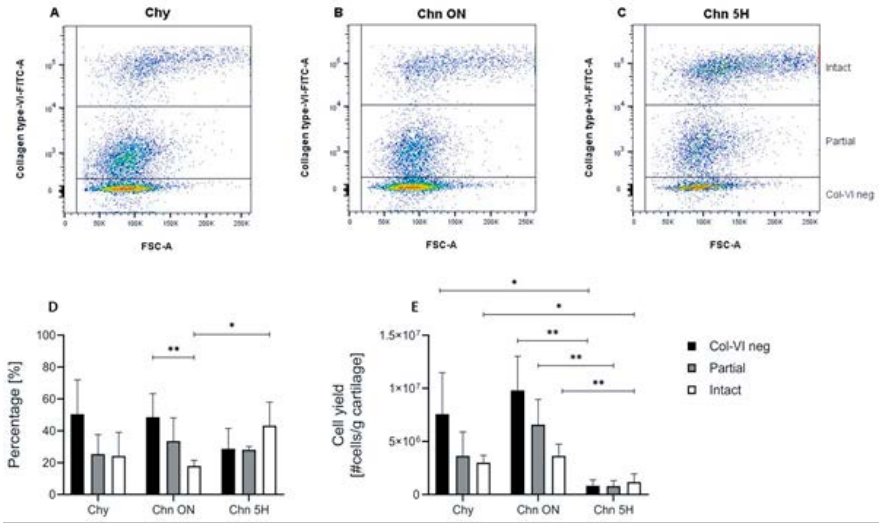

***Figure 6.4**: Enzymatic digestion of articular cartilage results in a heterogeneous mixture of chondrons (partial and intact) and chondrocytes, efficiency depends on the isolation method. Flow cytometry data of isolation efficiency of the enzymatic isolation methods Chy (**A**), Chn ON (**B**) and Chn 5H (**C**). Three distinct cell populations are seen after all isolation methods. FSC-A represents relative size of the cells. FITC-A represents the relative intensity of the type VI collagen staining. Total number of events was 10,000 for all measurements. Bar graphs representing the percentages of Col-VI negative cells, partial chondrons, and intact chondrons of the total cell population as analyzed with flow cytometry (**D**). Percentages were normalized to the cell yield, resulting in the number of Col-VI negative cells, partial chondrons, and intact chondrons per gram of cartilage tissue (**E**). *, $p < 0.05$; **, $p < 0.01$; ***, $p < 0.001$; #, $p < 0.0001$.*

Analysis of the flow cytometry data resulted in the percentages of Col-VI neg, partial chondrons, and intact chondrons after the three isolation methods (Fig. 6.4D, Table 6.1). The Chn 5H isolation method resulted in the highest percentage of intact chondrons, which was significantly higher compared to the Chn ON isolation method ($p < 0.05$). Chn ON resulted in significantly more Col-VI negative cells than intact chondrons ($p < 0.01$). No other significant differences were found between the isolation methods ($p > 0.05$).

Table 6.1: *Summary of the percentage of Col-VI negative, partial chondrons, and intact chondrons after all three isolation methods. Data is shown as mean (±SD).*

	Chy (n = 4)	**Chn ON (n = 4)**	**Chn 5H (n = 4)**
Col-VI negative	50.4% (±21.6%)	48.6% (±14.7%)	28.7% (±12.9%)
Partial chondrons	25.4% (±12.2%)	33.5% (±14.6%)	28.1% (±2.05%)
Intact chondrons	24.2% (±14.8%)	17.9% (±3.55%)	43.2% (±14.8%)

Normalization of this data to the yield of each sample, resulted in the yield of each population after the three isolation methods (Fig 6.4E, Table 6.2). When considering the yield of the isolation methods, the relative distribution over the three isolation methods changed (Fig. 6.4E). All three cell populations were significantly lower after Chn 5H isolation compared to Chn ON ($p < 0.01$). When comparing the Chy and Chn 5H isolations, the Col-VI neg and intact chondron population was significantly lower after the Chn 5H isolation ($p < 0.05$).

Table 6.2*: Summary of the total number of cells and the number of Col-VI negative cells, partial chondrons, and intact chondrons after all three isolation methods, per gram of cartilage tissue used for isolation. Data is shown as mean (±SD).*

	Chy (n = 4) [*10^6 cells/g]	**Chn ON (n = 4) [*10^6 cells/g]**	**Chn 5H (n = 4) [*10^6 cells/g]**
Total population	14.2 (±3.58)	20.0 (±1.80)	2.80 (±1.52)
Col-VI negative	7.57 (±3.91)	9.82 (±3.21)	0.82 (±0.56)
Partial chondrons	3.64 (±2.26)	6.59 (±2.38)	0.80 (±0.52)
Intact chondrons	3.01 (±0.68)	3.65 (±1.11)	1.18 (±0.76)

To validate our assumption on the existence of three different populations (intact and partial chondrons, and chondrocytes), immunocytochemistry was performed after the different isolation methods. This indeed showed a heterogeneous mixture of chondrons and chondrocytes. Overall, Chy (Fig. 6.5A, D) and Chn ON (Fig. 6.5B, E) showed more chondrocytes without a PCM when compared to the Chn 5H method (Fig. 6.5C, F). Besides intact chondrons, partially digested chondrons were observed, with PCM's not fully encapsulating the cell. This was observed after all isolation protocols in all conditions.

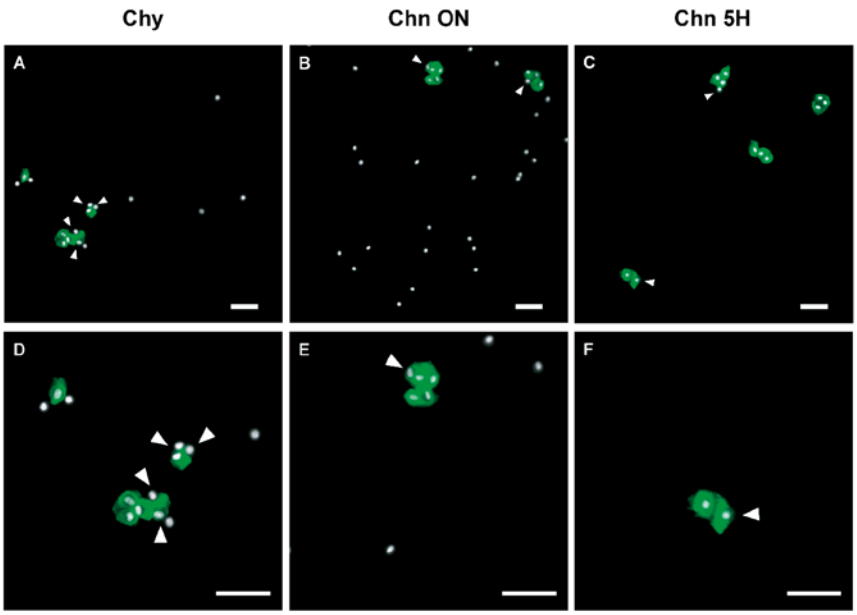

Figure 6.5: *Immunocytochemistry of cell populations obtained after different methods of enzymatic isolation, show a heterogeneous mixture of chondrons and chondrocytes.* ***D, E, and F*** *are magnifications of* ***A, B, and C****, respectively. Besides full chondrons and chondrocytes without PCM, chondrons with partially digested PCM's were found as indicated by the arrowheads. Type VI collagen was associated with FITC (green) and cell nuclei were stained with DAPI (white). Scale bar = 50 µm.*

6.3.3 Intact chondrons mainly consist of multicellular chondrocyte clusters

Microscopy data revealed the existence of single cells and clustered cells, which could indicate the regional origin of the chondron. By using the relation between the FSC-A and FSC-H of the flow cytometry data, the events

with a single cell and multiple cells were analyzed. All isolation methods resulted in a similar distribution of events and mixture of single-cell and multicellular events (Fig. 6.6A-C). Previously, the flow cytometry data showed that there was a heterogeneous mixture of type VI collagen negative, partial chondrons, and intact chondrons (Fig. 6.2 and 6.4, Table 6.1 and 6.2). When combining the values of FSC-H, FSC-A and intensity of the type VI collagen staining (FITC-A), the distribution of the three groups (chondrocytes, partial and intact chondrons) was very different when comparing the single-cell and multicellular events (Fig. 6.6D-E, Table 3 and 4).

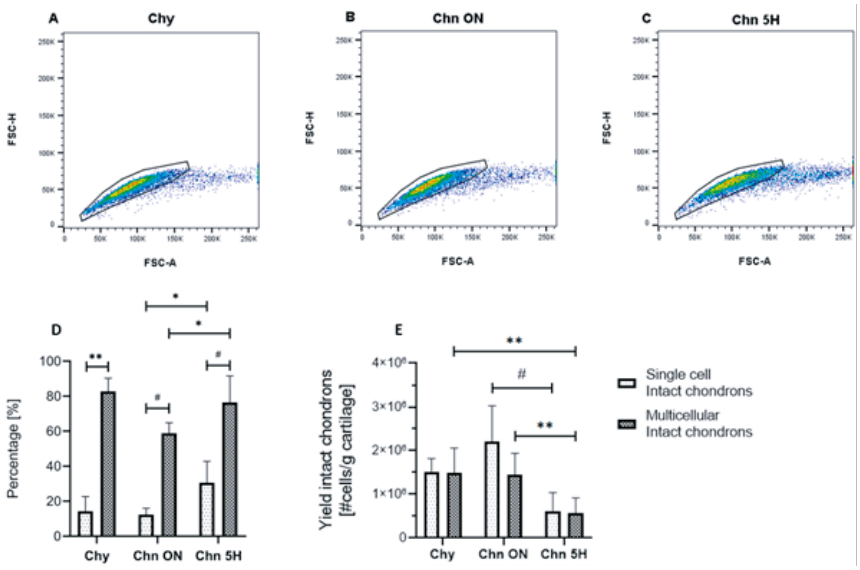

Figure 6.6: *Intact chondrons mainly consist of multicellular chondrons. Selection of single-cell and multicellular events in the flow cytometry data using the relation between FSC-A and FSC-H after the Chy (**A**), Chn ON (**B**), and Chn 5H (**C**) enzymatic isolation methods, gated for single cells. Total number of events was 10,000 for all measurements. Bar graphs representing the percentages of intact chondrons in the total population of single-cell and multicellular events as analyzed with flow cytometry (**D**). Percentages were normalized to the yield, resulting in the number of cells with an intact PCM in the populations of single-cell and multicellular events per gram of cartilage tissue (**E**). Trends change after normalization due to differences in cell yield between single donors. Total number of events was 10,000 for all measurements. *****, $p < 0.05$; ******, $p < 0.01$; *******, $p < 0.001$; #, $p < 0.0001$.*

When comparing the percentages of intact chondrons in these populations, there was a significantly higher percentage of intact chondrons in the multicellular population compared to the single-cell population for all

isolation methods (Fig. 6.6D, Table 6.3). This difference was smaller for the Chn 5H isolation ($p < 0.01$) than for the Chy ($p < 0.0001$) and Chn ON ($p < 0.0001$) isolations. When comparing the isolation methods, there were significantly more intact chondrons in both the single-cell ($p < 0.05$) and multicellular ($p < 0.05$) populations after the Chn 5H isolation compared to the Chn ON isolation.

***Table 6.3**: Summary of the percentage of Col-VI negative, partial chondrons, and intact chondrons in the single-cell and multicell populations after all three isolation methods. Data is shown as mean (±SD).*

	Chy (n = 4)		**Chn ON (n = 4)**		**Chn 5H (n = 4)**	
	Single-cell	Multicellular	Single-cell	Multicellular	Single-cell	Multicellular
Total	85.5% (±9.87%)	14.6% (±9.86%)	88.1% (±2.60%)	11.9% (±2.60%)	71.6% (±8.29%)	28.4% (±8.29%)
Col-VI negative	60.9% (±16.9%)	10.9% (±5.87%)	59.0% (±19.9%)	29.2% (±11.9%)	37.9% (±11.6%)	10.5% (±7.79%)
Partial chondrons	20.9% (±10.3%)	6.28% (±3.46%)	28.7% (±18.9%)	12.0% (±12.9%)	31.6% (±0.90%)	13.1% (±7.61%)
Intact chondrons	14.3% (±8.40%)	82.8% (±7.51%)	12.4% (±3.64%)	58.9% (±6.00%)	30.5% (±12.3%)	76.5% (±15.2%)

To get insight into the yield of the isolation methods, the flow cytometry data was normalized to the number of cells yielded per gram of cartilage (Fig. 6.6E, Table 6.4). This resulted in a shift of the distributions among the populations and isolation methods due to differences in yields between donors. There were no significant differences between the amount of intact chondrons in the single-cell and multicellular populations after all isolation methods (Fig. 6.6E). Comparison of isolation methods showed that the Chn ON isolation yields significantly more single-cell intact chondrons compared to the Chn 5H isolation ($p < 0.0001$). Additionally, significantly more multicellular intact chondrons were yielded by both the Chy ($p < 0.01$) and Chn ON ($p < 0.01$) isolations than by the Chn 5H isolation.

***Table 6.4**: Summary of the number of Col-VI negative, partial chondrons, and intact chondrons in the single-cell and multicell populations after all three isolation methods. Data is shown as mean (±SD).*

	Chy (n = 4) [*10⁶ cells/g]		**Chn ON (n = 4) [*10⁶ cells/g]**		**Chn 5H (n = 4) [*10⁶ cells/g]**	
	Single-cell	Multicellular	Single-cell	Multicellular	Single-cell	Multicellular
Total	12.4 (±4.57)	1.78 (±0.49)	17.6 (±1.42)	2.42 (±0.74)	2.08 (±1.41)	0.72 (±0.38)
Col-VI negative	8.44 (±4.04)	0.17 (±0.08)	10.5 (±3.71)	0.75 (±0.41)	0.81 (±0.58)	0.07 (±0.04)
Partial chondrons	2.48 (±1.49)	0.11 (±0.06)	4.95 (±2.99)	0.23 (±0.16)	0.65 (±0.44)	0.08 (±0.03)
Intact chondrons	1.52 (±0.30)	1.50 (±0.56)	2.21 (±0.81)	1.44 (±0.50)	0.61 (±0.42)	0.57 (±0.35)

6.3.4 Fluorescence-activated cell sorting shows the different cell populations present after enzymatic digestion of articular cartilage.

Finally, a cell sorting procedure was adopted to confirm the validity of our classification system, i.e., the presence of three distinctly different groups (chondrocytes, and chondrons with a partial or intact PCM). Therefore, the three cell populations were sorted based on the intensity of the type VI collagen staining (to note, only the Chy isolation procedure was used for this validation step, as a proof of concept). The settings used for sorting resulted in a purity between 98-99%. FITC histograms, based on type VI collagen intensity, reveal that there was some overlap to the other groups after sorting (Fig. 6.7A, D, G, J).

Immunocytochemistry confirmed that FACS could separate the cell populations. A heterogeneous population for the unsorted cell population was observed (Fig. 6.7B, C), as shown before (Fig. 6.5). Confocal microscopy showed that characteristics of all three cell populations were present before FACS. After sorting, the type VI collagen negative cells were devoid of type VI collagen staining, although some sporadic remnants of type VI collagen could be observed (Fig. 6.7E, F). The partial chondrons showed small type VI collagen rich PCM but this did not envelop the cells (Fig. 6.7G-I). The population of intact chondrons showed a thin PCM enveloping the cells and

mainly consisted of clustered chondrons (Fig. 6.7K) with also some single chondrons (Fig. 6.7L).

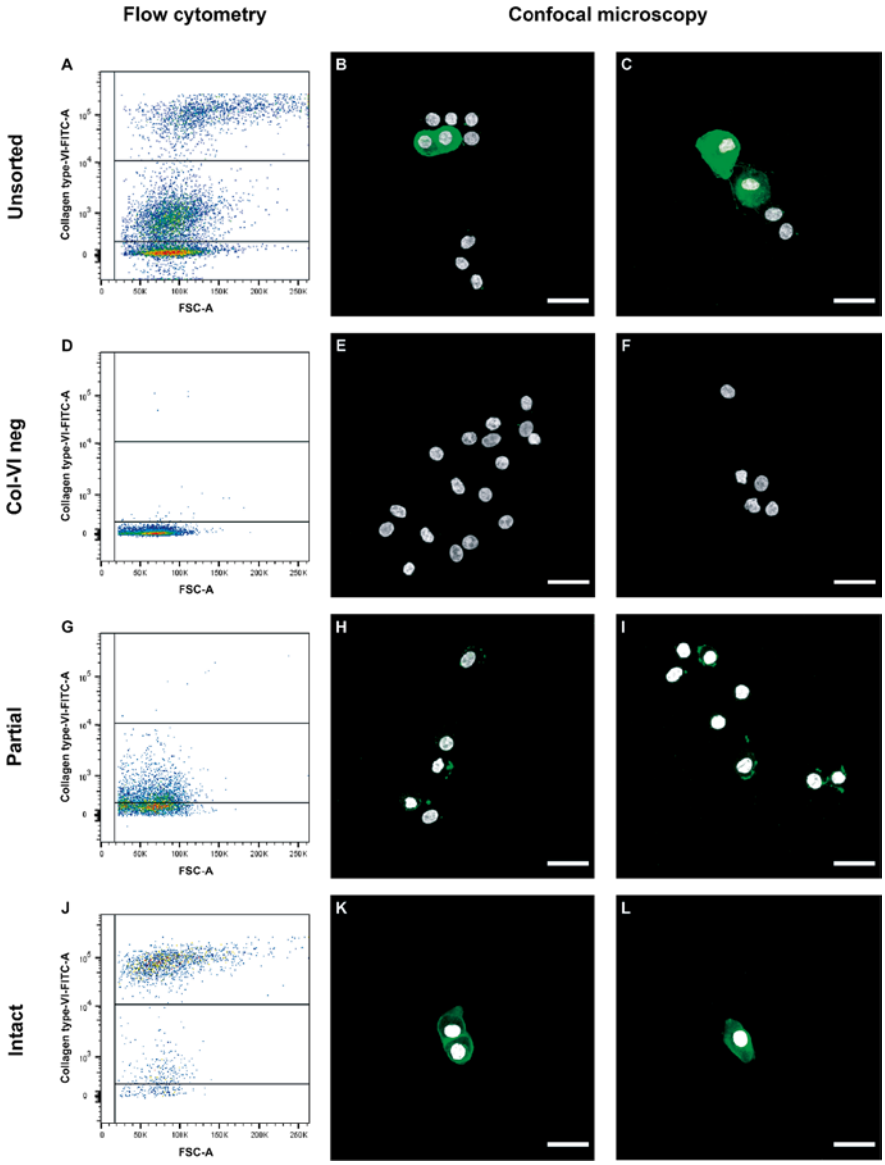

***Figure 6.7**: FACS can separate three distinctly different cell populations based on type VI collagen staining, which can be confirmed with confocal microscopy. Flow cytometry analysis before (**A**) and after (**D, G, J**) cell sorting reveal three distinctly different populations, i.e., chondrocytes, partial chondrons and intact chondrons. Representative*

*confocal microscopy images of the unsorted cell population (**B, C**) and the populations sorted for type VI collagen negative cells (**E, F**), partial chondrons (**H, I**), and intact chondrons (**K, L**). Type VI collagen was labelled with FITC (green) and cell nuclei were stained with DAPI (white). Figures H and I were digitally enhanced post acquisition such that the type VI collagen staining could be observed at this magnification. Scale bar = 20 µm.*

6.4 Discussion

This study quantified the presence of chondrocytes and chondrons within cell populations obtained after different enzymatic isolation protocols to digest articular cartilage, which were designed to preferentially isolate either chondrocytes or chondrons. It was shown that all isolation methods result in a heterogeneous mixture of chondrons and chondrocytes, using a combination of flow cytometry and microscopy. A new insight was that two populations of type VI collagen positive cells exist, which were considered to be partial and intact chondrons. Using FACS-sorting, a homogenous population of intact chondrons was isolated from bovine articular cartilage for all three different enzymatic isolation methods using a type VI collagen staining, however leading to a very low cell yield.

Peters *et al.*, already revealed the heterogeneity of the isolated chondron/chondrocyte population using the Lee protocol.[251] They however did not show the population of partial chondrons as shown in this research. When adding up the partial and intact chondrons, the percentage of chondrons from the current study are similar to that of Peters *et al.*[251], meaning that this partial population was likely present in the study of Peters. Moreover, the current study showed the presence of a chondron population containing multiple chondrocytes within the PCM. Within this group of multicellular chondrons, most type VI collagen positive cells were grouped as intact chondrons (Fig. 6.6D, Table 6.3, 6.4). Although these methods have existed since decades, this outcome is not surprising. Enzymatic isolation is a variable process and is highly dependent on the number of active units, size of the tissue to be digested, the exact composition of the ECM and digestion time. The data of this study suggest that certain regions of the cartilage tissue are either under- or overrepresented in the chondron population, since not all parts of the tissue will digest at an equal rate. Considering that chondrocytes from different cartilage zones express particular phenotypes[257], this could potentially affect study outcomes. Uncovering the

native zonal location of chondrons obtained using enzymatic isolation could improve the interpretation of future studies.
From the current study, it is clear that without proper sorting of enzymatically isolated cells, a mixture of chondrons and chondrocytes always exists, the exact ratio depending on the used isolation protocol. This heterogeneous mixture is believed to influence the interpretation of the results of previous studies. When a pure population of chondrons is compared to chondrocytes, the beneficial results of chondrons are expected to become more pronounced. However the specific application is key, as earlier studies have shown that the ratio between cell types when co-culturing chondrons with chondrocytes or MSCs affects the outcomes both *in vitro* and *in vivo*.[252,254–256] This stresses the importance of the homogeneity of the initial cell population and thus the isolation method, as the underlying mechanisms remain elusive. Moreover, using chondrons to study cell – PCM interactions on cellular level can also benefit from the suggested isolation method presented in this current study.

For the application in cartilage tissue engineering, high yields are required to reach the necessary high cell seeding densities.[258–260] From the current study, it is suggested to use the overnight chondron isolation method. With the addition of FACS-sorting, based on type VI collagen staining, a cell yield of approximately 3-4*10^6 cells/gr cartilage tissue (Fig. 6.4E, Table 6.2) could be attained. Since this is a pure population of chondrons, it would be suitable for *in vitro* studies focusing on chondrons and ECM production. Moreover, the use of FACS is also highly recommended for single cell studies and more fundamental research. However, with clinical applications like ACI, only a small cartilage piece is available, and unfortunately, the yield of the combination of this isolation method and purification steps is too low for these purposes.[261] This low yield has been an issue from the introduction of the enzymatic procedure of isolating chondrons by Lee *et al*., back in 1997.[238] Nonetheless, the use of chondrons in cartilage tissue engineering do result in superior outcomes compared to only chondrocytes or MSCs.[252,254–256] Different methods to obtain chondrons which increase purity and yield should therefore be explored. Since the available digestive enzymes are not specific enough to digest only the cartilage ECM components, a tissue engineering approach could be a favorable alternative to the current methods. Chondrocytes are known to form a PCM during *in vitro* culture when embedded in agarose and hyaluronic acid hydrogels.[262,263] When this

process is optimized, tissue engineered chondrons could be a more homogeneous cell source compared to enzymatically isolated chondrons.

In this study, partial chondrons were defined as cells with a low-intensity type VI collagen staining. As can be seen after cell sorting, this population of cells have small remnants of PCM attached to the cell. It is however questionable whether these cells should be classified as chondrons or chondrocytes. In their study, Hing et al.[210] observed cells with similar punctuates of type VI collagen, which were indicated as chondrocytes. It remains unknown what the effect is of partial PCM digestion on biophysical stimuli in neocartilage formation. Full disruptions of the PCM could have significant effects on chondrocytes when presented with osmotic challenges during joint loading.[210] Since the PCM has a stress-shielding effect on chondrocytes[264], deformation of chondrocytes in partial chondrons could increase during compression. However, since PCM matrix components are still present in a partial chondron, its growth factor modulating role and cell-matrix interactions might still be functional.[209,212,265–267]

In conclusion, this study demonstrated the heterogeneity of cell populations obtained after enzymatic digestion of articular cartilage. It is suggested that an overnight chondron isolation protocol results in a superior yield of intact chondrons, compared to the gold standard 5-hour protocol. Cell sorting methods like FACS are suitable for obtaining a purified population of intact chondrons. This gives the most homogeneous chondrocyte populations. However, because partial chondrons and chondrocytes are filtered out, it also comes with a lower yield. Therefore, this method is less suitable for applications which demand large numbers of cells and have a limited tissue supply, like in vivo studies and clinical applications. For these purposes alternative isolation methods with higher yields may be more applicable. However, this comes at the expense of less homogeneity in the cell population, with larger numbers of partial chondrons and chondrocytes. Thus, care must be taken with interpretations of potential beneficial effects of chondrons. Increasing the homogeneity of chondron populations could have a positive impact on future in vitro studies investigating cell-PCM interactions and comparisons between chondrocytes and chondrons.

Acknowledgements
The authors thank Bart Tiemeijer for providing support during cell sorting.

Authorship contribution statement
MvM: Conceptualization; Formal analysis; Investigation; Methodology; Validation; Visualization; Writing – original draft; Writing – review & editing
GHS: Conceptualization; Formal analysis; Investigation; Methodology; Validation; Visualization; Writing – original draft; Writing – review & editing
LPVV: Resources; Methodology; Writing – review & editing
LAV: Methodology; Writing – review & editing
CCvD: Conceptualization; Supervision; Writing – review & editing
KI: Conceptualization; Funding acquisition; Supervision; Writing – review & editing
JF: Conceptualization; Funding acquisition; Supervision; Writing – review & editing

Funding statement
This research was financially supported by the Gravitation Program "Materials Driven Regeneration, funded by the Netherlands Organization for Scientific Research (024.003.013), the framework of Chemelot InSciTe (Project MimiCart), supported by the partners of Regenerative Medicine Crossing Borders (www.regmedxb.com) and powered by Health~Holland, Top Sector Life Sciences & Health.

7
General Discussion

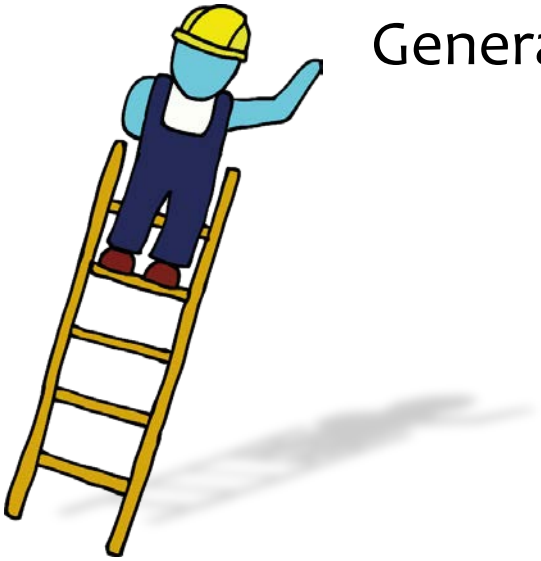

7.1 Main findings and applications

Focal cartilage defects occur frequently, due to trauma or diseased tissue, for example osteochondritis dissecans. If left untreated, focal cartilage defects can lead to osteoarthritis. With the aging population, an increased number of obese people, and evolutionary effect, OA will become one of the two diseases, besides dementia, which will cause the biggest increase in burden of society by 2040 in The Netherlands[52,268]. Treatment of focal defects should alleviate the progression into osteoarthritis. Currents methods used in the clinic to treat focal defects lead to the formation of fibrous cartilage in cell based methods or wear on opposing cartilage[61].

7.1.1 A biomimicking regenerative implant

Regenerative therapies for the treatment of osteochondral defects have been studied over the past decades, often including hydrogels, which shows promising outcomes combined with chondrocytes. However, such hydrogels are often too soft to resist loadbearing in the joint[68,70]. To develop a hydrogel with load bearing properties, inspiration was found in the structure and composition of native articular cartilage, where osmotic pressure is induced by the restricted swelling of the proteoglycan-rich ECM by the Benninghoff collagen architecture. A proof of principle of this concept is shown using a combination of a warp-knitted polyamide 6 (PA6) textile spacer fabric with a high swelling synthetic hydrogel (pHEMA - NaMA), mimicking the attraction of water due to fixed negative fixed charges, leading to restricted swelling. These constructs show promising results where biomechanical properties resemble that of native cartilage, including similar correlations between the FCD and stiffness, and time-dependent behavior (chapter 2).

However, both the synthetic hydrogel and spacer fabric cannot be translated to a regenerative therapy, as breakdown of the initial materials is needed to achieve full regeneration, in which native tissue can take over the function. Therefore, a first step was taken to develop a chondroitin sulfate (CS) and hyaluronic acid (HA) based hydrogel, which resulted in a biomimetic photopolymerizable hydrogel when these natural polymers were methacrylated. The ratio between CSMA and HAMA determined both the stability and the swelling ratio of the hydrogel (chapter 3). When restricted in a PA6 spacer fabric, peak- and equilibrium stiffnesses and time-dependent behavior were in the range of native cartilage.

The second step was to introduce the CSMA HAMA based hydrogel to a biodegradable 3D warp-knitted spacer fabric. Therefore, a PCL P4HB warp-knitted spacer-fabric was developed. When cell-free CSMA HAMA PCL P4HB constructs were implanted in an *ex vivo* osteochondral defect wear model, load sharing with the surrounding cartilage was observed. Recessed implant placement was crucial for the prevention of wear at the opposite cartilage (Chapter 4), which might be a good stepping stone for future research.

Chondrocytes embedded in a PEGDMA CSMA hydrogel, restricted from swelling by a PCL P4HB spacer fabric, synthesized collagen type II and VI, in a donor dependent manner over a culture period of 19 days. Mechanical stimulation did not show profound beneficial effects (chapter 5). In all restricted groups synthesis of a pericellular matrix (PCM) was observed, which might indicate the protective role of the PCM to the chondrocytes[251]. This raises the question whether seeding of chondrons could be beneficial in restricted swelling environments. To perform such study in the future, a protocol to obtain a homogenous population of chondrons was developed, using type VI collagen specific cell sorting. As this method resulted in a low cell yield, this method might be more suitable for single-cell technologies and studies (chapter 6). For large scale, synthetically produced chondrons might be an alternative solution[269].

This thesis revealed the promising features of a HydroSpacer to become a successful cartilage implant. However, the full long-term behavior, regenerative capacity and integration with the surrounding tissue will be a few of the multiple remaining challenges.

7.2 Remaining challenges and future perspectives

Creating functional cartilage

Regeneration is "the process in humans whereby lost specialized tissue is replaced by proliferation of undamaged specialized cells and restores the normal structure and function of the organ"[270]. Therefore, the aim of a regenerative cartilage implant should be to produce matrix, and to take over, overtime, the original structure and function of native cartilage. Articular cartilage specific matrix production has been showed in many publications using several types of hydrogels or scaffold materials, however creating

functional load bearing cartilage by tissue engineering is a major challenge. Moreover, recreating the original arch-like collagen structure is still the holy-grail, and might lead to the desired mechanical properties, which is previously shown in synthetic arch-like pile yarns presented in this thesis. Zonal formation is shown to be induced by for example cell-cell interactions, gradient hydrogels, depth dependent chondrocyte seeding densities, 3D bioprinting, scaffold design, ultrasound standing waves, cell pellet assembly or joint mimicking mechanical stimulation[207,229,271–277], but does often not lead to the original arch-like structure and mechanical function of native cartilage.

Cartilage regeneration and maturation after cell-therapy takes months to years[278,279]. Tensile strength of P4HB sutures declined in 12 weeks to 50% of its initial tensile strength, and is substantially hydrolytically and enzymatically degraded after one year[280,281]. The used CSMA HAMA hydrogels seem to be stable over a longer period, as shown in this thesis, but stability is dependent on the degree of methacrylation, and CSMA HAMA is susceptible for hydrolytical degradation[138]. Therefore, it of high importance that both the tensile strength of the P4HB pile yarns and the stability of the hydrogel match the regeneration and maturation period of cartilage.

7.2.1 Implant design and regenerative capacity

The ideal articular cartilage implant should be immediately load bearing, matching the mechanical properties and possess a low coefficient of friction to enable smooth articulation. The immediately load bearing properties can be developed by the introduction of a hydrogel with a FCD in a spacer fabric, inducing osmotic pressure. On the long-term, chondrocytes should be able to deposit ECM, and turn the synthetic construct into a living tissue. Proteoglycans will replace the leaking hydrogel, collagen will replace the spacer fabric, which is actively degraded. Because these processes have different time-constants, it is challenging to find a perfect balance and substitution. All these factors, among others spacer fabric, hydrogel and cells, play a role in the success of the development of a HydroSpacer ready for clinical translation. Below we will discuss these factors separately and propose potential options for optimization.

3D warp-knitted spacer fabric

Textiles have been used in tissue engineering in multiple fields, and in many forms from cardiovascular to cartilage[77,282]. One of the most well-know textile based constructs in the field of cartilage tissue engineering is the 3D woven scaffold developed by the group of Farshid Guilak[74,75,77,104]. In this construct, PCL fibers are woven in a tight architecture, creating small pore size, which have been filled with several types of hydrogels. The mass swelling ratio of an interpenetrating polymer network (IPN) hydrogel synthesized from agarose and poly(ethylene) glycol decreases from ten times in free swelling to two times in the woven scaffold. Moreover, a PEG hydrogel showed a mass swelling ratio of 35 for PEG hydrogels in free swelling, whereas introduced to the woven scaffold it resulted in a ratio of 4. These results suggest restricted swelling is induced by the introduction of the woven scaffold. However, due to the scaffold architecture, a large part of the weight is taking up by the PCL scaffold. This decreases the mass swelling ratio. Integrating both hydrogels to the woven scaffold leads to a tenfold increase in equilibrium moduli compared to free swelling hydrogels: from 0.05 MPa to 0.39 MPa and 0.03 MPa to 0.34 MPa for IPN and PEG hydrogels, respectively[104]. Tighter weaving of the scaffold shows to have a significantly higher stiffness compared to loose weaving[76], meaning that the structure and/or composition of the scaffold itself has a major influence on the stiffness. This is also observed with the woven scaffold infiltrated with single network hydrogels (agarose, alginate, fibrin and poly- acrylamide), where the PCL scaffold determines the stiffness. Only introduction of an IPN hydrogel shows a synergetic effect and improved stiffness[77]. This is different than the HydroSpacers introduced in this thesis, where the spacer fabric itself has a low influence on the stiffness[173]. The stiffness of PEGDMA CSMA hydrogels increases five times compared to free swelling, from 70 kPa to 360 kPa, with a 3 to 4 fold decrease in mass swelling ratio. Human adipose-derived stem cells (ASCs) were seeded to tightly woven scaffolds, resulting in large tissue engineered anatomically shaped cartilage constructs. After 36 days of *in vitro* culture, these constructs are mechanically functional[75]. Because of the large pores, and the dependency of a swelling hydrogel, HydroSpacers are not suitable for this technique. However, HydroSpacers could be more favorable for a regenerative approach, as the tight weave, and therefore small pore size does not promote tissue deposition throughout the construct and degradation of the material will be prolonged[75]. Promising is the reduced coefficient of friction when a hydrogel is introduced to a textile scaffold[76],

which also has been observed in the surface roughness of HydroSpacers[283], and might be beneficial for reducing wear.

As previously described, one of the most beautiful features of the spacer fabric material is the freedom of shape and dimensions[75], as it might be cut out from a larger piece. This makes the product easily available "from the shelf" with multiple standard sizes, but also versatile when a surgeon is able to intraoperative measure the exact dimensions of more complicated defects resulting in a perfect fit.

Stiffness and final thickness of the implant can be altered by the stiffness of the pile yarns in tension. Therefore, P4HB was chosen as pile yarn material in chapter 4, as PCL monofilaments were not able to withstand the high swelling pressure (data not shown). To enhance integration with neighboring bone tissue at the bottom, filaments might be adapted by using osteoconductive filaments[284]. For the surface articulating with the opposite cartilage, to reduced wear, a coating based on PRG4 could be applied on the PCL multifilament top layer to decrease the coefficient of friction[285]. Moreover, the apparent diameter of the monofilament used for the pile yarns could be decreased, as these monofilaments might "scratch" into the opposing cartilage[283]. Another proposed method without compromising on restricted swelling might be the use of softer pile yarns in a higher density, which will be more forgiving at the articulating surface. This might be optimized using computer models, enabling high through-put analysis.

The anisotropy of warp-knitted spacer fabrics is one of its major disadvantages for cartilage implant development. Due to swelling of hydrogels used in this thesis, the shape of spacer fabrics changed (Fig 1A-B) and start bulging (Fig 1C-D). To counteract these features, mechanically interlocking of the cartilage warp-knitted part with a stiffer bottom part, which can include the calcified cartilage layer and provide bone-anchoring, can be added to the spacer fabric design.

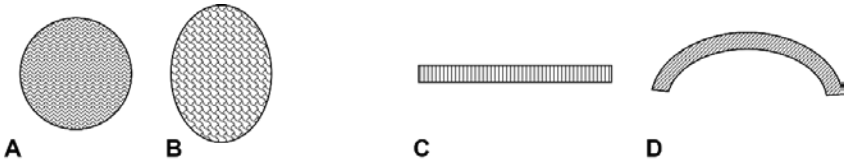

Figure 7.5 *Top view of shape change of anisotropic spacer fabrics, becoming more oval shape after introduction of a swelling hydrogel (A-B) and side view of a spacer fabric (C) and a bulging HydroSpacer(D). Effects are dependent on the swelling potential of the hydrogel.*

Hydrogel

As relative stiff elastic hydrogels were used in this thesis, ECM was produced in pericellular region, without further diffusion into the interterritorial regions. Using softer hydrogels initially, with the downside of a decreased load-bearing capacity, the synthesized ECM will be more distributed in the hydrogel, which will be beneficial in terms of stiffness on the long-term[233,286]. Combinations of short term load bearing properties and long-term ECM deposition and distribution, might be possible with double network hydrogels with different time scales of degradation[287]. Cells are able to sense the volume confinement, in which mechanotransduction is negatively affected, and thus stress-relaxation in a 3D environment is a key design factor for cartilage tissue engineering[288]. Moreover, enabling migration of cells leads to better integration with the surrounding cartilage after implantation[289]. Therefore, hydrogels should be developed which allow stress-relaxation, providing cell proliferation, migration, development of a collagen type VI-rich PCM and homogenous diffusion of the synthesized ECM (PG & collagen type II) into the interterritorial region to enhance maturation of the ECM and replace the initial function of the swelling hydrogel and the spacer fabric, respectively. This can be done by for example higher porosity, visco-elastic hydrogels, dynamic hydrogels based on click-chemistry or supramolecular polymers[122,162,290,291], without losing the ability to induce osmotic pressure when restricted. This might be chemically demanding, as already much research have been performed to optimize this, and a usable hydrogel have not been found yet.

In situ polymerization

As described in this thesis, Teflon molds and glass plates were used to contain the polymer (- cell) solution, to assure complete filling of the spacer fabric with the polymer solution and to prevent leakage. Prior to clinical

translation, injection *in situ* and the prevention of leakage simultaneously should be taken care of, which diminishes the chances of pushing the hydrogel out of the spacer fabric during fixation or press-fitting. Another advantage of *in situ* polymerization is the perfect fit of the HydroSpacer, including the *in situ* "press-fitting" by the swelling pressure of the hydrogel. This effect might not be so evident with pre-casted HydroSpacer prior to implantation. *In Situ* polymerization might also lead to an improved integration and adhesion of the hydrogel - cartilage interface[292]. In this thesis, UV-light was used for all hydrogel compositions. For *in situ* polymerization, alternative polymerization methods should be studied, to enhance *in situ* polymerization within the spacer fabric, using for example visible light or temperature regulated polymerization[162,293]. Moreover, long-term experiments, with for example cyclic loading should be performed to observe failure, (hydrogel) particles leakage and creep.

Fixation and integration

The main challenge for a HydroSpacer construct before it is suitable for clinical applications, is the fixation of the construct with the surrounding or underlying cartilage. The biomimetic properties of the HydroSpacer should enhance integration as it has shown that mimicking the mechanical properties of the native tissue causes less damage to the surrounding cartilage. It is load-bearing in all circumstances (peak, short, and long term loading), and show lower shear stresses at the interface[294]. The HydroSpacer must be press-fitted into a chondral defect, with the ideal situation of the spacer fabric enabling patient specific forms and shapes. By press-fitting a chondrocyte seeded implant, such as the HydroSpacer, migration of chondrocytes and direct attachment of collagen fibers from the surrounding tissue could enhance the integration[60,289]. To even further enhance the integration, a bioactive compound could be added to the spacer fabric, fusing the HydroSpacer with a bone part to create an osteochondral implant, or other internal fixation methods might be considered to ensure a stability[294–296]. To ensure primary (mechanical) and secondary (biological integration) stability, short and long-term studies should be performed, using for example *ex vivo* explants models[239].

Cartilage tissue engineering

After decades of articular tissue engineering, it is still not possible to create an exact copy of healthy cartilage. Tissue engineering is only possible when

cells produce articular cartilage specific extracellular matrix components, and mature in cartilage its specific architecture. In cartilage, *in vivo* migration of chondrocytes to an implant material is depending on the disruption of the collagen network[297,298]. To facilitate functional tissue engineering, cells embedded within the hydrogel/scaffold are needed to synthesize the ECM, and success is dependent on many factors, such as cell source, cell seeding density, internal/external cues such as chemical or physical factors and the composition of the scaffold (Fig. 1.6, General Introduction).

One aspect of creating high-quality tissue engineered articular cartilage is to recreate or grow the microenvironment / pericellular matrix of the chondrocyte[299]. This microenvironment, with distinct biomechanical properties, plays a crucial role in signal transduction of mechanical loading and osmotic challenge[300–302], and might play a pivotal role in articular cartilage tissue engineering. Current 1-step procedures using 10-20% recycled chondrons and allogenic MSCs as cell based therapy for cartilage defects show promising results[252]. However, when larger amounts of autologous chondrons are needed, intraoperative harvesting might not be realistic due to the cell number and donor site morbidity. Human induced pluripotent stem cells (iPSCs) are able to synthesize neo-cartilage similar to human primary articular chondrocytes[303–308]. Articular cartilage-derived progenitor cells (ASPCs) have as largest benefit, similar to iPSCs, an unlimited proliferation capacity. This enables the production of large amounts of cells, without losing its chondrogenic potential[309]. For these cell types, it would be interesting to study the behavior within a restricted swelling environment similar to that of native cartilage, and the development of a pericellular matrix. To create this original structure, fundamental research might be more focused on the (embryonic) development of cartilage, to fully understand the native growth of cartilage, in which degradation of collagen is needed for chondrocyte hypertrophy, tissue growth and proteoglycan synthesis[310,311].

7.2.2 Perspective

The development of a regenerative HydroSpacer might also beneficial for other patient groups. For example, older patients from 50-60 years onwards might benefit from synthetic cell-free HydroSpacer as developed in chapter 2. This patient group requires pain reduction to postpone total knee replacement. A synthetic HydroSpacer might achieve these needs providing

load bearing properties, without negatively affecting the surrounding and opposing cartilage as seen with metal implants[61]. Similar techniques using restricted pHEMA hydrogels have been explored in the field of artificial intervertebral discs, leading to comparable biomimetic results[312]. These results demonstrate the promising application of these types of synthetic biomimetic implants, which might also to applicable for menisci, or whole joints[75,313,314]. For the development of HydroSpacer-based osteochondral implants, electro writing or 3D bioprinting might be used for creating the bone part[315]. Polycaprolactone /hydroxyapatite bioinks already showed enhanced osteoconduction, osseoinduction and osseointegration[207,295,316,317]. On the contrary, the addition of a 3D printed bone part lengthens the production process, might limit the personalized shape and therefore intraoperative freedom, and might introduce sterilization issues[318]. To include all parameters of the implant design, it would be beneficial to develop a computational model to unravel the optimal HydroSpacer composition, stability and regenerative capacity, without the use of animal models[319,320]**.** After further development, the restricted swelling construct might be used as platform to study the regeneration and degeneration of cartilage.

7.3 conclusion

As osteoarthritis is rising to the most common disease in The Netherlands by 2040, it is of importance to develop a regenerative approach to treat focal defects for younger-aged patients and postpone more severe interventions, such as total knee replacements. In this thesis a proof-of-concept is presented of an implant based on a swelling hydrogel in a knitted spacer fabric. In this thesis, it is proven that this construct can induce a swelling pressure leading to biomimetic properties similar to that of native cartilage. Multiple combinations of hydrogel compositions and spacer fabric materials showed promising results in terms of mechanical properties and regenerative capacity. Further research to the combination of hydrogels, spacer fabric biomaterials and cell sources, can optimize the short- and long-term performance of such implants. Exploring the full potential of this regenerative approach, might ultimately facilitate clinical treatment of focal cartilage defects and decreasing the personal and societal burden of OA.

References

1. Masouros, S. D., Bull, A. M. J. & Amis, A. A. (i) Biomechanics of the knee joint. *Orthop. Trauma* **24**, 84–91 (2010).
2. Shepherd, D. E. T. & Seedhom, B. B. Thickness of human articular cartilage in joints of the lower limb. *Ann Rheum Dis* **58**, 27–34 (1999).
3. Fox, A. J. S., Bedi, A. & Rodeo, S. A. The Basic Science of Articular Cartilage: Structure, Composition, and Function. (2009). doi:10.1177/1941738109350438
4. Jahn, S., Seror, J. & Klein, J. Lubrication of Articular Cartilage. *Annu. Rev. Biomed. Eng.* **18**, 235–258 (2016).
5. Damen, A. H. A. *et al.* Proteoglycan 4 reduces friction more than other synovial fluid components for both cartilage-cartilage and cartilage-metal articulation. *Osteoarthr. Cartil.* **29**, 894–904 (2021).
6. Wong, B. L. *et al.* Biomechanics of cartilage articulation: Effects of lubrication and degeneration on shear deformation. *Arthritis Rheum.* **58**, 2065–2074 (2008).
7. de Boer, G. N., Raske, N., Soltanahmadi, S., Bryant, M. G. & Hewson, R. W. Compliant-poroelastic lubrication in cartilage-on-cartilage line contacts. *Tribol. - Mater. Surfaces Interfaces* **14**, 151–165 (2020).
8. Wright, V. & Dowson, D. Lubrication and cartilage. *J. Anat.* **121**, 107–18 (1976).
9. Poole, C. A., Ayad, S. & Gilbert, R. T. Chondrons from articular cartilage. V. Immunohistochemical evaluation of type VI collagen organisation in isolated chondrons by light, confocal and electron microscopy. *J. Cell Sci.* **103**, 1101–1110 (1992).
10. Wilusz, R. E., Sanchez-Adams, J. & Guilak, F. The structure and function of the pericellular matrix of articular cartilage. *Matrix Biology* **39**, 25–32 (2014).
11. Choi, J. B. *et al.* Zonal changes in the three-dimensional morphology of the chondron under compression: The relationship among cellular, pericellular, and extracellular deformation in articular cartilage. *J. Biomech.* **40**, 2596–2603 (2007).
12. Benninghoff, A. Form und Bau der Gelenkknorpel in ihren Beziehungen zur Funktion - Zweiter Teil: Der Aufbau des Gelenkknorpels in seinen Beziehungen zur Funktion. *Zeitschrift für Zellforsch. und Mikroskopische Anat.* **2**, 783–862 (1925).
13. Heinemeier, K. M. *et al.* Radiocarbon dating reveals minimal collagen turnover in both healthy and osteoarthritic human cartilage. *Sci. Transl. Med.* **8**, (2016).
14. Murray, I. R., Ray, T. E., Abrams, G. D. & Sherman, S. L. Functional Anatomy of Cartilage and Subchondral Bone in the Joint. in *Joint Function Preservation* 115–126 (Springer International Publishing, 2022). doi:10.1007/978-3-030-82958-2_10
15. Albro, M. B. *et al.* Raman spectroscopic imaging for quantification of depth-dependent and local heterogeneities in native and engineered cartilage. *npj Regen. Med.* **3**, 1–11 (2018).
16. Bloebaum, R. D., Wilson, A. S. & Martin, W. N. A Review of the Collagen Orientation in the Articular Cartilage. *Cartilage* **13**, 367S-374S (2021).
17. Youn, I., Choi, J. B., Cao, L., Setton, L. A. & Guilak, F. Zonal variations in the three-dimensional morphology of the chondron measured in situ using confocal microscopy. *Osteoarthr. Cartil.* **14**, 889–897 (2006).
18. Fan, X. *et al.* The deterioration of calcified cartilage integrity reflects the severity of osteoarthritis—A structural, molecular, and biochemical analysis. *FASEB J.* **36**, (2022).
19. Thorp, H. *et al.* Trends in articular cartilage tissue engineering: 3D mesenchymal stem cell sheets as candidates for engineered hyaline-like cartilage. *Cells* **10**, 1–22 (2021).
20. Maroudas, A. Balance between swelling pressure and collagen tension in normal and degenerate cartilage. *Nature* **260**, 808–809 (1976).
21. Mow, V. C. & Guo, X. E. Mechano-Electrochemical Properties Of Articular Cartilage: Their Inhomogeneities and Anisotropies. *Annu. Rev. Biomed. Eng.* **4**, 175–209 (2002).
22. Kempson, G. E., Muir, H., Swanson, S. A. V. & Freemas, M. A. R. Correlations between stiffness and the chemical constituents of cartilage on the human femoral head. *Biochim. Biophys. Acta - Mol. Cell Res.* **215**, 70–77 (1970).

23. Roughley, P. J. & Mort, J. S. The role of aggrecan in normal and osteoarthritic cartilage. *J. Exp. Orthop. 2014 11* **1**, 1–11 (2014).
24. Korhonen, R. K. *et al.* Fibril reinforced poroelastic model predicts specifically mechanical behavior of normal, proteoglycan depleted and collagen degraded articular cartilage. *J. Biomech.* **36**, 1373–1379 (2003).
25. Lu, X. L. & Mow, V. C. Biomechanics of articular cartilage and determination of material properties. *Med. Sci. Sports Exerc.* **40**, 193–199 (2008).
26. Mow, V. C., Ateshian, G. A., Lai, W. M. & Gu, W. Y. Effects of fixed charges on the stress-relaxation behavior of hydrated soft tissues in a confined compression problem. *Int. J. Solids Struct.* **35**, 4945–4962 (1998).
27. Räsänen, L. P. *et al.* The effect of fixed charge density and cartilage swelling on mechanics of knee joint cartilage during simulated gait. *J. Biomech.* **61**, 34–44 (2017).
28. Canal Guterl, C., Hung, C. T. & Ateshian, G. A. Electrostatic and non-electrostatic contributions of proteoglycans to the compressive equilibrium modulus of bovine articular cartilage. *J. Biomech.* **43**, 1343–1350 (2010).
29. Nickien, M., Thambyah, A. & Broom, N. D. How a decreased fibrillar interconnectivity influences stiffness and swelling properties during early cartilage degeneration. *J. Mech. Behav. Biomed. Mater.* **75**, 390–398 (2017).
30. Bachrach, N. M., Mow, V. C. & Guilak, F. Incompressibility of the solid matrix of articular cartilage under high hydrostatic pressures. *J. Biomech.* **31**, 445–451 (1998).
31. Soltz, M. A. & Ateshian, G. A. Interstitial Fluid Pressurization during Confined Compression Cyclical Loading of Articular Cartilage. *Ann. Biomed. Eng.* **28**, 150–159 (2000).
32. Mak, A. F. The apparent viscoelastic behavior of articular cartilage–the contributions from the intrinsic matrix viscoelasticity and interstitial fluid flows. *J. Biomech. Eng.* **108**, 123–130 (1986).
33. Mow, V. C., Holmes, M. H. & Lai, W. M. Fluid transport and mechnical properties of articular cartilage: a review. *biomechnics* **17**, 377–394 (1980).
34. Li, L. P., Herzog, W., Korhonen, R. K. & Jurvelin, J. S. The role of viscoelasticity of collagen fibers in articular cartilage: Axial tension versus compression. *Med. Eng. Phys.* **27**, 51–57 (2005).
35. Lai, W. M., Hou, J. S. & Mow, V. C. A Triphasic Theory for the Swelling Properties of Hydrated Charged Soft Biological Tissues. in *Biomechanics of Diarthrodial Joints* (1990). doi:10.1007/978-1-4612-3448-7_10
36. Lai, W. M., Hou, J. S. & Mow, V. C. A Triphasic Theory for the Swelling and Deformation Behaviors of Articular Cartilage. *J. Biomech. Eng.* (1991). doi:10.1115/1.2894880
37. Mow, V. C., Holmes, M. H. & Michael Lai, W. Fluid transport and mechanical properties of articular cartilage: A review. *Journal of Biomechanics* **17**, 377–394 (1984).
38. Wilson, W., van Donkelaar, C. C., van Rietbergen, B. & Huiskes, R. A fibril-reinforced poroviscoelastic swelling model for articular cartilage. *J. Biomech.* **38**, 1195–1204 (2005).
39. Han, G., Hess, C., Eriten, M. & Henak, C. R. Uncoupled poroelastic and intrinsic viscoelastic dissipation in cartilage. *J. Mech. Behav. Biomed. Mater.* **84**, 28–34 (2018).
40. Korhonen., R. & Saarakkala, S. Biomechanics and Modeling of Skeletal Soft Tissues. in *Theoretical Biomechanics* (InTech, 2011). doi:10.5772/19975
41. Han, E., Chen, S. S., Klisch, S. M. & Sah, R. L. Contribution of Proteoglycan Osmotic Swelling Pressure to the Compressive Properties of Articular Cartilage. *Biophys. J.* **101**, 916–924 (2011).
42. Athanasiou, K. A., Rosenwasser, M. P., Buckwalter, J. A., Malinin, T. I. & Mow, V. C. Interspecies comparisons of in situ intrinsic mechanical properties of distal femoral cartilage. *J. Orthop. Res.* **9**, 330–340 (1991).
43. Thambyah, A., Nather, A. & Goh, J. Mechanical properties of articular cartilage covered by the meniscus. *Osteoarthr. Cartil.* **14**, 580–588 (2006).
44. Froimson, M. I., Ratcliffe, A., Gardner, T. R. & Mow, V. C. Differences in patellofemoral joint cartilage material properties and their significance to the etiology of cartilage surface fibrillation. *Osteoarthr. Cartil.* **5**, 377–386 (1997).
45. Jurvelin, J. S., Buschmann, M. D. & Hunziker, E. B. Mechanical anisotropy of the human

knee articular cartilage in compression. *Proc. Inst. Mech. Eng. H.* **217**, 215–219 (2003).
46. Démarteau, O., Pillet, L., Inaebnit, A. M. & Borens, O. Biomechanical characterization and in vitro mechanical injury of elderly human femoral head cartilage : comparison to adult bovine humeral head cartilage. *Osteoarthr. Cartil.* **14**, 589–596 (2006).
47. Jurvelin, J. S., Buschmann, M. D. & Hunziker, E. B. Optical and mechanical determination of Poisson's ratio of adult bovine humeral articular cartilage. *J. Biomech.* **30**, 235–241 (1997).
48. Paschos, N. K., Makris, E. A., Hu, J. C. & Athanasiou, K. A. Topographic Variations in Biomechanical and Biochemical Evaluating Native and Engineered Cartilage. *Arthrosc. J. Arthrosc. Relat. Surg.* **30**, 1317–1326 (2014).
49. Korhonen, R. K. *et al.* comparison of the equilibrium reponse fo AC in unconfined compression and Indentation. *J. Biomech.* **35**, 903=909 (2002).
50. Freed, L. E., Langer, R., Martin, I., Pellis, N. R. & Vunjak-Novakovic, G. Tissue engineering of cartilage in space. *Proc. Natl. Acad. Sci. U. S. A.* **94**, 13885–90 (1997).
51. Lin, W. & Klein, J. Recent Progress in Cartilage Lubrication. *Adv. Mater.* **33**, 2005513 (2021).
52. National Institute for Public Health and the Environment. Public Health Foresight Study 2018 (VTV-2018): diseases. *ttps://www.vtv2018.nl/en/* h (2018).
53. Jackson, D. W., Lalor, P. A., Aberman, H. M. & Simon, T. M. Spontaneous repair of full-thickness defects of articular cartilage in a goat model: A preliminary study. *J. Bone Jt. Surg.* **83**, 53–64 (2001).
54. Prakash, D. & Learmonth, D. Natural progression of osteo-chondral defect in the femoral condyle. *Knee* **9**, 7–10 (2002).
55. Leja, L. & Minas, T. MACI (autologous cultured chondrocytes on porcine collagen membrane) in patients 40 years and older: short-term clinical outcomes and patient satisfaction. *J. Cartil. Jt. Preserv.* **0**, (2023).
56. Bayliss, L. E. *et al.* The effect of patient age at intervention on risk of implant revision after total replacement of the hip or knee: a population-based cohort study. *Lancet (London, England)* **389**, 1424–1430 (2017).
57. Pareek, A. *et al.* Long-Term Outcomes after Autologous Chondrocyte Implantation: A Systematic Review at Mean Follow-Up of 11.4 Years. *Cartilage* **7**, 298–308 (2016).
58. Kraeutler, M. J., Aliberti, G. M., Scillia, A. J., McCarty, E. C. & Mulcahey, M. K. Microfracture Versus Drilling of Articular Cartilage Defects: A Systematic Review of the Basic Science Evidence. *Orthopaedic Journal of Sports Medicine* **8**, (2020).
59. LaPrade, R. F., Bursch, L. S., Olson, E. J., Havlas, V. & Carlson, C. S. Histologic and immunohistochemical characteristics of failed articular cartilage resurfacing procedures for osteochondritis of the knee: A case series. *Am. J. Sports Med.* **36**, 360–368 (2008).
60. Khan, I., Gilbert, S., Singhrao, S., Duance, V. & Archer, C. Cartilage integration: Evaluation of the reasons for failure of integration during cartilage repair. A review. *Eur. Cells Mater.* **16**, 26–39 (2008).
61. Diermeier, T. *et al.* Effects of focal metallic implants on opposing cartilage - An in-vitro study with an abrasion test machine. *BMC Musculoskelet. Disord.* **21**, 261 (2020).
62. Custers, R. J. H. *et al.* Articular cartilage degeneration following the treatment of focal cartilage defects with ceramic metal implants and compared with microfracture. *J. Bone Jt. Surg. - Ser. A* **91**, 900–910 (2009).
63. Catoira, M. C., Fusaro, L., Di Francesco, D., Ramella, M. & Boccafoschi, F. Overview of natural hydrogels for regenerative medicine applications. *J. Mater. Sci. Mater. Med.* **30**, 1–10 (2019).
64. Beddoes, C. M., Whitehouse, M. R., Briscoe, W. H. & Su, B. Hydrogels as a replacement material for damaged articular hyaline cartilage. *Materials (Basel).* **9**, (2016).
65. Xiao, Y., Friis, E. A., Gehrke, S. H. & Detamore, M. S. Mechanical Testing of Hydrogels in Cartilage Tissue Engineering: Beyond the Compressive Modulus. *Tissue Eng. Part B Rev.* **19**, 403–412 (2013).
66. Yang, J., Zhang, Y. S., Yue, K. & Khademhosseini, A. Cell-laden hydrogels for osteochondral and cartilage tissue engineering. *Acta Biomaterialia* **57**, 1–25 (2017).
67. Wei, W. & Dai, H. Articular cartilage and osteochondral tissue engineering techniques: Recent advances and challenges. *Bioactive Materials* **6**, 4830–4855 (2021).

68. Cook, R. F. & Oyen, M. L. On the failure and fracture of hydrogels for cartilage replacement. *J. Phys. Mater* **4**, 21001 (2021).
69. Tsou, Y. H., Khoneisser, J., Huang, P. C. & Xu, X. Hydrogel as a bioactive material to regulate stem cell fate. *Bioact. Mater.* **1**, 39–55 (2016).
70. Neves, S. C., Moroni, L., Barrias, C. C. & Granja, P. L. Leveling Up Hydrogels: Hybrid Systems in Tissue Engineering. *Trends Biotechnol.* **38**, 292–315 (2020).
71. Visser, J. *et al.* Reinforcement of hydrogels using three-dimensionally printed microfibres. *Nat. Commun.* **6**, 6933 (2015).
72. Wasyłeczko, M., Sikorska, W. & Chwojnowski, A. Review of synthetic and hybrid scaffolds in cartilage tissue engineering. *Membranes* **10**, 1–28 (2020).
73. Arjmandi, M. *et al.* Mechanical and tribological properties of a novel hydrogel composite reinforced by three-dimensional woven textiles as a functional synthetic cartilage. *Compos. Part A Appl. Sci. Manuf.* **115**, 123–133 (2018).
74. Moutos, F. T., Freed, L. E. & Guilak, F. A biomimetic three-dimensional woven composite scaffold for functional tissue engineering of cartilage. *Nat. Mater.* **6**, 162–167 (2007).
75. Moutos, F. T. *et al.* Anatomically shaped tissue-engineered cartilage with tunable and inducible anticytokine delivery for biological joint resurfacing. *Proc. Natl. Acad. Sci.* **113**, E4513–E4522 (2016).
76. Valonen, P. K. *et al.* In vitro generation of mechanically functional cartilage grafts based on adult human stem cells and 3D-woven poly(ε-caprolactone) scaffolds. *Biomaterials* **31**, 2193–2200 (2010).
77. Liao, I. C., Moutos, F. T., Estes, B. T., Zhao, X. & Guilak, F. Composite three-dimensional woven scaffolds with interpenetrating network hydrogels to create functional synthetic articular cartilage. *Adv. Funct. Mater.* **23**, 5833–5839 (2013).
78. Römgens, A. M., Van Donkelaar, C. C. & Ito, K. Contribution of collagen fibers to the compressive stiffness of cartilaginous tissues. *Biomech. Model. Mechanobiol.* **12**, 1221–1231 (2013).
79. Schäfer, B. *et al.* Warp-Knitted Spacer Fabrics: A Versatile Platform to Generate Fiber-Reinforced Hydrogels for 3D Tissue Engineering. *Materials (Basel).* **13**, 3518 (2020).
80. Cooke, M. E., Lawless, B. M., Jones, S. W. & Grover, L. M. Matrix degradation in osteoarthritis primes the superficial region of cartilage for mechanical damage. *Acta Biomater.* **78**, 320–328 (2018).
81. Lu, X. L. *et al.* Indentation Determined Mechanoelectrochemical Properties and Fixed Charge Density of Articular Cartilage. *Ann. Biomed. Eng.* **32**, 370–379 (2004).
82. Lux Lu, X., Miller, C., Chen, F. H., Edward Guo, X. & Mow, V. C. The generalized triphasic correspondence principle for simultaneous determination of the mechanical properties and proteoglycan content of articular cartilage by indentation. *J. Biomech.* **40**, 2434–2441 (2007).
83. Murakami, T., Sakai, N., Sawae, Y., Tanaka, K. & Ihari, M. Influence of Proteoglycan on Time-Dependent Mechanical Behaviors of Articular Cartilage under Constant Total Compressive Deformation. *JSME Int. J. Ser. C* **47**, 1049–1055 (2004).
84. Maroudas, A. & Bannon, C. Measurement of swelling pressure in cartilage and comparison with the osmotic pressure of constituent proteoglycans. *Biorheology* **18**, 619–632 (1981).
85. Grodzinsky, A. J., Roth, V., Myers, E., Grossman, W. D. & Mow, V. C. The Significance of Electromechanical and Osmotic Forces in the Nonequilibrium Swelling Behavior of Articular Cartilage in Tension. *J. Biomech. Eng.* **103**, 221–231 (1981).
86. Kiviranta, P. *et al.* Collagen network primarily controls Poisson's ratio of bovine articular cartilage in compression. *J. Orthop. Res.* **24**, 690–699 (2006).
87. Korhonen, R. K. & Jurvelin, J. S. Compressive and tensile properties of articular cartilage in axial loading are modulated differently by osmotic environment. *Med. Eng. Phys.* **32**, 155–160 (2010).
88. Maroudas, A. Physicochemical Properties of Cartilage in the Light of Ion Exchange Theory. *Biophys. J.* **8**, 575–595 (1968).
89. Eisenberg, S. R. & Grodzinsky, A. J. Swelling of articular cartilage and other connective tissues: Electromechanochemical forces. *J. Orthop. Res.* **3**, 148–159 (1985).

90. Canal Guterl, C., Hung, C. T. & Ateshian, G. A. Electrostatic and non-electrostatic contributions of proteoglycans to the compressive equilibrium modulus of bovine articular cartilage. *J. Biomech.* (2010). doi:10.1016/j.jbiomech.2010.01.021
91. Brown, E. T. T., Damen, A. H. A. & Thambyah, A. The mechanical significance of the zonally differentiated collagen network of articular cartilage in relation to tissue swelling. *Clin. Biomech.* **79**, 104926 (2020).
92. Wilson, W., Van Donkelaar, C. C., Van Rietbergen, B., Ito, K. & Huiskes, R. Stresses in the local collagen network of articular cartilage: A poroviscoelastic fibril-reinforced finite element study. *J. Biomech.* **37**, 357–366 (2004).
93. Quiroga, J. M. P., Wilson, W., Ito, K. & van Donkelaar, C. C. Relative contribution of articular cartilage's constitutive components to load support depending on strain rate. *Biomech. Model. Mechanobiol.* **16**, 151–158 (2017).
94. Armiento, A. R., Alini, M. & Stoddart, M. J. Articular fibrocartilage - Why does hyaline cartilage fail to repair? *Adv. Drug Deliv. Rev.* **146**, 289–305 (2019).
95. Magnussen, R. A., Dunn, W. R., Carey, J. L. & Spindler, K. P. Treatment of focal articular cartilage defects in the knee: A systematic review. *Clin. Orthop. Relat. Res.* **466**, 952–962 (2008).
96. Moutos, F. T., Freed, L. E. & Guilak, F. A biomimetic three-dimensional woven composite scaffold for functional tissue engineering of cartilage. *Nat. Mater.* **6**, 162–167 (2007).
97. Schäfer, B. *et al.* Warp-Knitted Spacer Fabrics: A Versatile Platform to Generate Fiber-Reinforced Hydrogels for 3D Tissue Engineering. *Materials (Basel).* **13**, 3518 (2020).
98. Cutcliffe, H. C. & Defrate, L. E. comparison of cartilage Mechanical properties Measured During creep and Recovery. (2020). doi:10.1038/s41598-020-58220-2
99. Chahine, N. O., Chen, F. H., Hung, C. T. & Ateshian, G. A. Direct measurement of osmotic pressure of glycosaminoglycan solutions by membrane osmometry at room temperature. *Biophys. J.* (2005). doi:10.1529/biophysj.104.057315
100. Chen, S. S., Falcovitz, Y. H., Schneiderman, R., Maroudas, A. & Sah, R. L. Depth-dependent compressive properties of normal aged human femoral head articular cartilage: relationship to fixed charge density. *Osteoarthr. Cartil.* **9**, 561–569 (2001).
101. Gu, W. Y., Lai, W. M. & Mow, V. C. Transport of fluid and ions through a porous-permeable charged-hydrated tissue, and streaming potential data on normal bovine articular cartilage. *J. Biomech.* **26**, 709–723 (1993).
102. Zhou, C. & Wu, Q. A novel polyacrylamide nanocomposite hydrogel reinforced with natural chitosan nanofibers. *Colloids Surfaces B Biointerfaces* (2011). doi:10.1016/j.colsurfb.2010.12.030
103. Sanchez-Adams, J., Leddy, H. A., McNulty, A. L., O'Conor, C. J. & Guilak, F. The Mechanobiology of Articular Cartilage: Bearing the Burden of Osteoarthritis. *Current Rheumatology Reports* **16**, 1–9 (2014).
104. Moffat, K. L. *et al.* Composite Cellularized Structures Created from an Interpenetrating Polymer Network Hydrogel Reinforced by a 3D Woven Scaffold. *Macromol. Biosci.* **18**, 1800140 (2018).
105. Bank, R. A., Soudry, M., Maroudas, A., Mizrahi, J. & Tekoppele, J. M. The increased swelling and instantaneous deformation of osteoarthritic cartilage is highly correlated with collagen degradation. *Arthritis Rheum.* **43**, 2202–2210 (2000).
106. Schinagl, R. M., Gurskis, D., Chen, A. C. & Sah, R. L. Depth-dependent confined compression modulus of full-thickness bovine articular cartilage. *J. Orthop. Res.* **15**, 499–506 (1997).
107. Little, C. J., Bawolin, N. K. & Chen, X. Mechanical Properties of Natural Cartilage and Tissue-Engineered Constructs. *Tissue Eng. Part B Rev.* **17**, 213–227 (2011).
108. Edwards, P. K., Ackland, T. & Ebert, J. R. Clinical Rehabilitation Guidelines for Matrix-Induced Autologous Chondrocyte Implantation on the Tibiofemoral Joint. | *J. Orthop. Sport. Phys. Ther.* **102**, 102–119 (2014).
109. Heuijerjans, A., Wilson, W., Ito, K. & van Donkelaar, C. C. Osteochondral resurfacing implantation angle is more important than implant material stiffness. *J. Orthop. Res.* **36**, 2911–2922 (2018).

110. Schuurmans, C. C. L. *et al.* Hyaluronic acid and chondroitin sulfate (meth)acrylate-based hydrogels for tissue engineering: Synthesis, characteristics and pre-clinical evaluation. *Biomaterials* **268**, 120602 (2021).
111. Levett, P. A. *et al.* A biomimetic extracellular matrix for cartilage tissue engineering centered on photocurable gelatin, hyaluronic acid and chondroitin sulfate. *Acta Biomater.* **10**, 214–223 (2014).
112. Van Vlierberghe, S., Dubruel, P. & Schacht, E. Biopolymer-based hydrogels as scaffolds for tissue engineering applications: A review. *Biomacromolecules* **12**, 1387–1408 (2011).
113. Peppas, N. A., Hilt, J. Z., Khademhosseini, A. & Langer, R. Hydrogels in Biology and Medicine: From Molecular Principles to Bionanotechnology. *Adv. Mater.* **18**, 1345–1360 (2006).
114. Li, J. & Mooney, D. J. Designing hydrogels for controlled drug delivery. *Nat. Rev. Mater.* **1**, 16071 (2016).
115. Tavakoli, S. & Klar, A. S. Advanced Hydrogels as Wound Dressings. *Biomolecules* **10**, 1169 (2020).
116. Chandel, A. K. S., Kumar, C. U. & Jewrajka, S. K. Effect of polyethylene glycol on properties and drug encapsulation-release performance of biodegradable/cytocompatible agarose-polyethylene glycol-polycaprolactone amphiphilic Co-network gels. *ACS Appl. Mater. Interfaces* **8**, 3182–3192 (2016).
117. Singh Chandel, A. K., Kannan, D., Nutan, B., Singh, S. & Jewrajka, S. K. Dually crosslinked injectable hydrogels of poly(ethylene glycol) and poly[(2-dimethylamino)ethyl methacrylate]-: B -poly(N -isopropyl acrylamide) as a wound healing promoter. *J. Mater. Chem. B* **5**, 4955–4965 (2017).
118. Lee, K. Y. & Mooney, D. J. Hydrogels for tissue engineering. *Chem. Rev.* **101**, 1869–1879 (2001).
119. Slaughter, B. V., Khurshid, S. S., Fisher, O. Z., Khademhosseini, A. & Peppas, N. A. Hydrogels in Regenerative Medicine. *Adv. Mater.* **21**, 3307–3329 (2009).
120. Hoffman, A. S. Hydrogels for biomedical applications. *Adv. Drug Deliv. Rev.* **54**, 3–12 (2002).
121. Mantha, S. *et al.* Smart Hydrogels in Tissue Engineering and Regenerative Medicine. *Materials (Basel).* **12**, 3323 (2019).
122. Mihajlovic, M., Fermin, L., Ito, K., Van Nostrum, C. F. & Vermonden, T. Hyaluronic acid-based supramolecular hydrogels for biomedical applications. *Multifunct. Mater.* **4**, 032001 (2021).
123. Igarashi, N. *et al.* Effect of Molecular Sizes of Chondroitin Sulfate on Interaction with L-Selectin. *Int. J. Carbohydr. Chem.* **2013**, 1–9 (2013).
124. Kogan, G., Šoltés, L., Stern, R. & Gemeiner, P. Hyaluronic acid: A natural biopolymer with a broad range of biomedical and industrial applications. *Biotechnol. Lett.* **29**, 17–25 (2007).
125. Chung, C., Beecham, M., Mauck, R. L. & Burdick, J. A. The influence of degradation characteristics of hyaluronic acid hydrogels on in vitro neocartilage formation by mesenchymal stem cells. *Biomaterials* **30**, 4287–4296 (2009).
126. Hu, X., Li, D., Zhou, F. & Gao, C. Biological hydrogel synthesized from hyaluronic acid, gelatin and chondroitin sulfate by click chemistry. *Acta Biomater.* **7**, 1618–1626 (2011).
127. Ko, C. S., Huang, J. P., Huang, C. W. & Chu, I. M. Type II collagen-chondroitin sulfate-hyaluronan scaffold cross-linked by genipin for cartilage tissue engineering. *J. Biosci. Bioeng.* **107**, 177–182 (2009).
128. Levett, P. A. *et al.* A biomimetic extracellular matrix for cartilage tissue engineering centered on photocurable gelatin, hyaluronic acid and chondroitin sulfate. *Acta Biomater.* **10**, 214–223 (2014).
129. Guo, Y., Yuan, T. & Xiao, Z. Hydrogels of collagen / chondroitin sulfate / hyaluronan interpenetrating polymer network for cartilage tissue engineering. 2267–2279 (2012). doi:10.1007/s10856-012-4684-5
130. Zhu, M., Feng, Q., Sun, Y., Li, G. & Bian, L. Effect of cartilaginous matrix components on the chondrogenesis and hypertrophy of mesenchymal stem cells in hyaluronic acid hydrogels. *J. Biomed. Mater. Res. - Part B Appl. Biomater.* **105**, 2292–2300 (2017).
131. Levett, P. A., Hutmacher, D. W., Malda, J. & Klein, T. J. Hyaluronic Acid Enhances the

Mechanical Properties of Tissue-Engineered Cartilage Constructs. *PLoS One* **9**, e113216 (2014).
132. Costantini, M. *et al.* 3D bioprinting of BM-MSCs-loaded ECM biomimetic hydrogels for in vitro neocartilage formation. *Biofabrication* **8**, 035002 (2016).
133. Visser, J. *et al.* Reinforcement of hydrogels using three-dimensionally printed microfibres. *Nat. Commun.* **6**, 6933 (2015).
134. Schuiringa, G. H., Ito, K. & Van Donkelaar, C. C. The osmotic swelling in HydroSpacers can be used to create load-bearing cartilage implants. *26th Congress of the European Society of Biomechanics, July 11-14, 2021, Milan, Italy*
135. Abbadessa, A. *et al.* A Synthetic Thermosensitive Hydrogel for Cartilage Bioprinting and Its Biofunctionalization with Polysaccharides. *Biomacromolecules* **17**, 2137–2147 (2016).
136. Abbadessa, A. *et al.* A thermo-responsive and photo-polymerizable chondroitin sulfate-based hydrogel for 3D printing applications. *Carbohydr. Polym.* **149**, 163–174 (2016).
137. Stenekes, R. J. H. & Hennink, W. E. Polymerization kinetics of dextran-bound methacrylate in an aqueous two phase system. *Polymer (Guildf).* **41**, 5563–5569 (2000).
138. Schuurmans, C. C. L. *et al.* Hydrolytic (In)stability of Methacrylate Esters in Covalently Cross-Linked Hydrogels Based on Chondroitin Sulfate and Hyaluronic Acid Methacrylate. *ACS Omega* **6**, 26302–26310 (2021).
139. De Groot, C. J. *et al.* In vitro biocompatibility of biodegradable dextran-based hydrogels tested with human fibroblasts. *Biomaterials* **22**, 1197–1203 (2001).
140. Esterbauer, H., Zollner, H. & Scholz, N. Reaction of Glutathione with Conjugated Carbonyls. *Zeitschrift fur Naturforsch. - Sect. C J. Biosci.* **30**, 466–473 (1975).
141. Osman, R., Weinstein, H., Namboodiri, K. & Rabinowitz, J. R. Reactivities of Acrylic and Methacrylic Acids in a Nucleophilic Addition Model of Their Biological Activity. *J. Am. Chem. Soc.* **110**, 1701–1707 (1988).
142. Kurata, S., Morishita, K., Kawase, T. & Umemoto, K. Cytotoxic effects of acrylic acid, methacrylic acid, their corresponding saturated carboxylic acids, HEMA, and hydroquinone on fibroblasts derived from human pulp. *Dent. Mater. J.* **31**, 219–225 (2012).
143. Van De Wetering, P. *et al.* A mechanistic study of the hydrolytic stability of poly(2-(dimethylamino)ethyl methacrylate). *Macromolecules* **31**, 8063–8068 (1998).
144. Van Dijk-Wolthuis, W. N. E., Van Steenbergen, M. J., Underberg, W. J. M. & Hennink, W. E. Degradation kinetics of methacrylated dextrans in aqueous solution. *J. Pharm. Sci.* **86**, 413–417 (1997).
145. Van Dijk-Wolthuis, W. N. E., Hoogeboom, J. A. M., Van Steenbergen, M. J., Tsang, S. K. Y. & Hennink, W. E. Degradation and Release Behavior of Dextran-Based Hydrogels. *Macromolecules* **30**, 4639–4645 (1997).
146. Pichert, A. *et al.* Characterization of the interaction of interleukin-8 with hyaluronan, chondroitin sulfate, dermatan sulfate and their sulfated derivatives by spectroscopy and molecular modeling. *Glycobiology* **22**, 134–145 (2012).
147. Varghese, S. *et al.* Chondroitin sulfate based niches for chondrogenic differentiation of mesenchymal stem cells. *Matrix Biol.* **27**, 12–21 (2008).
148. Lee, C. T., Kung, P. H. & Lee, Y. Der. Preparation of poly(vinyl alcohol)-chondroitin sulfate hydrogel as matrices in tissue engineering. *Carbohydr. Polym.* **61**, 348–354 (2005).
149. Martens, P., Metters, A. T., Anseth, K. S. & Bowman, C. N. A generalized bulk-degradation model for hydrogel networks formed from multivinyl cross-linking molecules. *J. Phys. Chem. B* **105**, 5131–5138 (2001).
150. Burdick, J. A., Chung, C., Jia, X., Randolph, M. A. & Langer, R. Controlled degradation and mechanical behavior of photopolymerized hyaluronic acid networks. *Biomacromolecules* **6**, 386–391 (2005).
151. Poldervaart, M. T. *et al.* 3D bioprinting of methacrylated hyaluronic acid (MeHA) hydrogel with intrinsic osteogenicity. *PLoS One* **12**, e0177628 (2017).
152. Leach, J. B., Bivens, K. A., Patrick, C. W. & Schmidt, C. E. Photocrosslinked hyaluronic acid hydrogels: Natural, biodegradable tissue engineering scaffolds. *Biotechnol. Bioeng.* **82**, 578–589 (2003).
153. Hachet, E., Van Den Berghe, H., Bayma, E., Block, M. R. & Auzély-Velty, R. Design of

biomimetic cell-interactive substrates using hyaluronic acid hydrogels with tunable mechanical properties. *Biomacromolecules* **13**, 1818–1827 (2012).
154. Lin, C. C. & Anseth, K. S. PEG hydrogels for the controlled release of biomolecules in regenerative medicine. *Pharm. Res.* **26**, 631–643 (2009).
155. Arjmandi, M. *et al.* Mechanical and tribological properties of a novel hydrogel composite reinforced by three-dimensional woven textiles as a functional synthetic cartilage. *Compos. Part A Appl. Sci. Manuf.* **115**, 123–133 (2018).
156. Shinzawa, H. & Mizukado, J. Water absorption by polyamide (PA) 6 studied with two-trace two-dimensional (2T2D) near-infrared (NIR) correlation spectroscopy. *J. Mol. Struct.* **1217**, 128389 (2020).
157. Valonen, P. K. *et al.* In vitro generation of mechanically functional cartilage grafts based on adult human stem cells and 3D-woven poly(ε-caprolactone) scaffolds. *Biomaterials* **31**, 2193–2200 (2010).
158. Bachmann, B. *et al.* Stiffness Matters: Fine-Tuned Hydrogel Elasticity Alters Chondrogenic Redifferentiation. *Front. Bioeng. Biotechnol.* **8**, 373 (2020).
159. Castilho, M., Mouser, V., Chen, M., Malda, J. & Ito, K. Bi-layered micro-fibre reinforced hydrogels for articular cartilage regeneration. *Acta Biomater.* **95**, 297–306 (2019).
160. Schuurman, W. *et al.* Gelatin-Methacrylamide Hydrogels as Potential Biomaterials for Fabrication of Tissue-Engineered Cartilage Constructs. *Macromol. Biosci.* **13**, 551–561 (2013).
161. Hayami, J. W. S., Waldman, S. D. & Amsden, B. G. Photo-cross-linked methacrylated polysaccharide solution blends with high chondrocyte viability, minimal swelling, and moduli similar to load bearing soft tissues. *Eur. Polym. J.* **72**, 687–697 (2015).
162. Mihajlovic, M. *et al.* Viscoelastic Chondroitin Sulfate and Hyaluronic Acid Double-Network Hydrogels with Reversible Cross-Links. *Biomacromolecules* **23**, 1350–1365 (2022).
163. Hjelle, K., Solheim, E., Strand, T., Muri, R. & Brittberg, M. Articular cartilage defects in 1,000 knee arthroscopies. *Arthroscopy* **18**, 730–4 (2002).
164. Widuchowski, W., Widuchowski, J. & Trzaska, T. Articular cartilage defects: Study of 25,124 knee arthroscopies. *Knee* **14**, 177–182 (2007).
165. Curl, W. W. *et al.* Cartilage injuries: a review of 31,516 knee arthroscopies. *Arthroscopy* **13**, 456–60 (1997).
166. Damen, A. H. A., Nickien, M., Ito, K. & van Donkelaar, C. C. The performance of resurfacing implants for focal cartilage defects depends on the degenerative condition of the opposing cartilage. *Clin. Biomech. (Bristol, Avon)* **79**, (2020).
167. Custers, R. J. H. *et al.* Cartilage degeneration in the goat knee caused by treating localized cartilage defects with metal implants. *Osteoarthr. Cartil.* **18**, 377–388 (2010).
168. Pastrama, M. *et al.* Ultrasound-Based Quantification of Cartilage Damage After InVivo Articulation With Metal Implants. *Cartilage* **13**, 1540S (2021).
169. Oungoulian, S. R. *et al.* Wear and damage of articular cartilage with friction against orthopedic implant materials. *J. Biomech.* **48**, 1957–1964 (2015).
170. Martinez-Carranza, N. *et al.* Focal knee resurfacing and effects of surgical precision on opposing cartilage. A pilot study on 12 sheep. *Osteoarthr. Cartil.* **21**, 739–745 (2013).
171. Roth, K. E. *et al.* Biological responses to individualized small titanium implants for the treatment of focal full-thickness knee cartilage defects in a sheep model. *Knee* **27**, 1078–1092 (2020).
172. Custers, R. J. H. *et al.* Articular damage caused by metal plugs in a rabbit model for treatment of localized cartilage defects. *Osteoarthr. Cartil.* **15**, 937–945 (2007).
173. Mihajlovic, M. *et al.* Viscoelastic Chondroitin Sulfate and Hyaluronic AcidDouble-Network Hydrogels with Reversible Cross-Links. *Biomacromolecules* **23**, 1350 (2022).
174. Schuiringa, G. H., Pastrama, M., Ito, K. & van Donkelaar, C. C. Towards a load bearing hydrogel: A proof of principle in the use of osmotic pressure for biomimetic cartilage constructs. *J. Mech. Behav. Biomed. Mater.* 137, 105552 (2023).
175. Manda, K., Ryd, L. & Eriksson, A. Finite element simulations of a focal knee resurfacing implant applied to localized cartilage defects in a sheep model. *J. Biomech.* **44**, 794–801 (2011).
176. Becher, C., Huber, R., Thermann, H., Paessler, H. H. & Skrbensky, G. Effects of a contoured

articular prosthetic device on tibiofemoral peak contact pressure: a biomechanical study. *Knee Surg. Sports Traumatol. Arthrosc.* **16**, 56–63 (2008).
177. Kirker-Head, C. A., Van Sickle, D. C., Ek, S. W. & McCool, J. C. Safety of, and biological and functional response to, a novel metallic implant for the management of focal full-thickness cartilage defects: Preliminary assessment in an animal model out to 1 year. *J. Orthop. Res.* **24**, 1095–1108 (2006).
178. Schuiringa, G. H., Mihajlovic, M., van Donkelaar, C. C., Vermonden, T. & Ito, K. Creating a Functional Biomimetic Cartilage Implant Using Hydrogels Based on Methacrylated Chondroitin Sulfate and Hyaluronic Acid. *Gels* **8**, 457 (2022).
179. Schmidt, T. A., Gastelum, N. S., Nguyen, Q. T., Schumacher, B. L. & Sah, R. L. Boundary lubrication of articular cartilage: Role of synovial fluid constituents. *Arthritis Rheum.* **56**, 882–891 (2007).
180. Aşık, E. E. *et al.* Surface texture analysis of different focal knee resurfacing implants after 6 and 12 months in vivo in a goat model. *J. Orthop. Res.* (2022). doi:10.1002/JOR.25274
181. Fukubayashi, T. & Kurosawa, H. The Contact Area and Pressure Distribution Pattern of the Knee: *A Study of Normal and Osteoarthrotic Knee Joints. Acta Orthop. Scand.* **51**, 871–879 (1980).
182. Marlovits, S., Zeller, P., Singer, P., Resinger, C. & Vécsei, V. Cartilage repair: Generations of autologous chondrocyte transplantation. *Eur. J. Radiol.* **57**, 24–31 (2006).
183. Urban, J. P. G. The chondrocyte: a cell under pressure. *Rheumatology* **33**, 901–908 (1994).
184. Wilson, W., Driessen, N. J. B., van Donkelaar, C. C. & Ito, K. Prediction of collagen orientation in articular cartilage by a collagen remodeling algorithm. *Osteoarthr. Cartil.* **14**, 1196–1202 (2006).
185. Genes, N. G., Rowley, J. A., Mooney, D. J. & Bonassar, L. J. Effect of substrate mechanics on chondrocyte adhesion to modified alginate surfaces. *Arch. Biochem. Biophys.* **422**, 161–167 (2004).
186. Zhang, Q., Yu, Y. & Zhao, H. The effect of matrix stiffness on biomechanical properties of chondrocytes. *Acta Biochim. Biophys. Sin. (Shanghai).* **48**, 958–965 (2016).
187. Li, X. *et al.* 3D culture of chondrocytes in gelatin hydrogels with different stiffness. *Polymers (Basel).* **8**, 269 (2016).
188. V Thomas, L., VG, R. & D Nair, P. Effect of stiffness of chitosan-hyaluronic acid dialdehyde hydrogels on the viability and growth of encapsulated chondrocytes. *Int. J. Biol. Macromol.* **104**, 1925–1935 (2017).
189. Kock, L. M., Geraedts, J., Ito, K. & Donkelaar, C. C. van. Low Agarose Concentration and TGF-β3 Distribute Extracellular Matrix in Tissue-Engineered Cartilage. *https://home.liebertpub.com/tea* (2013). doi:10.1089/TEN.TEA.2012.0541
190. Schuh, E. *et al.* The influence of matrix elasticity on chondrocyte behavior in 3D. *J. Tissue Eng. Regen. Med.* **6**, e31–e42 (2012).
191. Schuh, E. *et al.* Chondrocyte redifferentiation in 3D: The effect of adhesion site density and substrate elasticity. *J. Biomed. Mater. Res. Part A* **100A**, 38–47 (2012).
192. Toh, W. S., Lim, T. C., Kurisawa, M. & Spector, M. Modulation of mesenchymal stem cell chondrogenesis in a tunable hyaluronic acid hydrogel microenvironment. *Biomaterials* **33**, 3835–3845 (2012).
193. Steward Zimmer Biomet, A. J. & Wagner, D. The pericellular environment regulates cytoskeletal development and the differentiation of mesenchymal stem cells and determines their response to hydrostatic pressure. (2014). doi:10.22203/eCM.v025a12
194. Takahashi, K. *et al.* Hydrostatic pressur influences mRNA exprssion of trnsforming growth factor-?1 and heat shock protein 70 in chondrocyte-like cell line. *J. Orthop. Res.* **15**, 150–158 (1997).
195. Smith, R. L. *et al.* In vitro stimulation of articular chondrocyte mRNA and extracellular matrix synthesis by hydrostatic pressure. *J. Orthop. Res.* **14**, 53–60 (1996).
196. Yi, B., Xu, Q. & Liu, W. An overview of substrate stiffness guided cellular response and its applications in tissue regeneration. *Bioactive Materials* **15**, 82–102 (2022).
197. Offeddu, G. S., Tanase, C. E., Toumpaniari, S., Oyen, M. L. & Cameron, R. E. Stiffening by Osmotic Swelling Constraint in Cartilage-Like Cell Culture Scaffolds. *Macromol. Biosci.* **18**,

1800247 (2018).
198. Grodzinsky, A. J., Levenston, M. E., Jin, M. & Frank, E. H. Cartilage tissue remodeling in response to mechanical forces. *Annu. Rev. Biomed. Eng.* **2**, 691–713 (2000).
199. Sah, R. L.-Y. *et al.* Biosynthetic response of cartilage explants to dynamic compression. *J. Orthop. Res.* **7**, 619–636 (1989).
200. Kock, L. M., Ito, K. & Van Donkelaar, C. C. Sliding indentation enhances collagen content and depth-dependent matrix distribution in tissue-engineered cartilage constructs. *Tissue Eng. - Part A* **19**, 1949–1959 (2013).
201. Bian, L., Zhai, D. Y., Zhang, E. C., Mauck, R. L. & Burdick, J. A. Dynamic compressive loading enhances cartilage matrix synthesis and distribution and suppresses hypertrophy in hMSC-laden hyaluronic acid hydrogels. *Tissue Eng. - Part A* **18**, 715–724 (2012).
202. Aisenbrey, E. A. & Bryant, S. J. The role of chondroitin sulfate in regulating hypertrophy during MSC chondrogenesis in a cartilage mimetic hydrogel under dynamic loading. *Biomaterials* **190–191**, 51–62 (2019).
203. Kim, H. D., Lee, Y., Kim, Y., Hwang, Y. & Hwang, N. S. Biomimetically reinforced polyvinyl alcohol-based hybrid scaffolds for cartilage tissue engineering. *Polymers (Basel).* **9**, (2017).
204. Bryant, S. J., Arthur, J. A. & Anseth, K. S. Incorporation of tissue-specific molecules alters chondrocyte metabolism and gene expression in photocrosslinked hydrogels. *Acta Biomater.* **1**, 243–252 (2005).
205. Villanueva, I., Gladem, S. K., Kessler, J. & Bryant, S. J. Dynamic loading stimulates chondrocyte biosynthesis when encapsulated in charged hydrogels prepared from poly(ethylene glycol) and chondroitin sulfate. *Matrix Biol.* **29**, 51–62 (2010).
206. Damen, A. H. A., Schuiringa, G. H., Ito, K. & van Donkelaar, C. C. The effect of HydroSpacer implant placement on the wear of opposing and adjacent cartilage. *J. Orthop. Res.* (2022). doi:10.1002/jor.25487
207. Castilho, M., Mouser, V., Chen, M., Malda, J. & Ito, K. Bi-layered micro-fibre reinforced hydrogels for articular cartilage regeneration. *Acta Biomater.* **95**, 297–306 (2019).
208. Nims, R. J. *et al.* Constrained Cage Culture Improves Engineered Cartilage Functional Properties by Enhancing Collagen Network Stability. *Tissue Eng. - Part A* **23**, 847–858 (2017).
209. Vincent, T. L., McLean, C. J., Full, L. E., Peston, D. & Saklatvala, J. FGF-2 is bound to perlecan in the pericellular matrix of articular cartilage, where it acts as a chondrocyte mechanotransducer. *Osteoarthr. Cartil.* **15**, 752–763 (2007).
210. Hing, W. A., Sherwin, A. F., Ross, J. M. & Poole, C. A. The influence of the pericellular microenvironment on the chondrocyte response to osmotic challenge. *Osteoarthr. Cartil.* **10**, 297–307 (2002).
211. Guilak, F. The Pericellular Matrix as a Transducer of Biomechanical and Biochemical Signals in Articular Cartilage. *Ann. N. Y. Acad. Sci.* **1068**, 498–512 (2006).
212. Vincent, T. L., McClurg, O. & Troeberg, L. The Extracellular Matrix of Articular Cartilage Controls the Bioavailability of Pericellular Matrix-Bound Growth Factors to Drive Tissue Homeostasis and Repair. *International Journal of Molecular Sciences* **23**, 6003 (2022).
213. Van Osch, G. J. V. M., Van Der Veen, S. W., Bumat, P. & Verwoerd-Verhoef, H. L. Effect of transforming growth factor-β on proteoglycan synthesis by chondrocytes in relation to differentiation stage and the presence of pericellular matrix. *Matrix Biol.* **17**, 413–424 (1998).
214. Wang, Q. G. *et al.* Molecular profiling of single cells in response to mechanical force: Comparison of chondrocytes, chondrons and encapsulated chondrocytes. *Biomaterials* **31**, 1619–1625 (2010).
215. Wang, Q. G. *et al.* Gene expression profiles of dynamically compressed single chondrocytes and chondrons. *Biochem. Biophys. Res. Commun.* **379**, 738–742 (2009).
216. Liu, C. *et al.* Protective effects of the pericellular matrix of chondrocyte on articular cartilage against the development of osteoarthritis. *Histol. Histopathol.* **33**, 757–764 (2018).
217. Nicodemus, G. D. & Bryant, S. J. The role of hydrogel structure and dynamic loading on chondrocyte gene expression and matrix formation. *J. Biomech.* **41**, 1528–1536 (2008).
218. Zhen, G. *et al.* Mechanical stress determines the configuration of TGFβ activation in articular cartilage. *Nat. Commun.* **12**, 1–16 (2021).

219. Neu, C. P., Khalafi, A., Komvopoulos, K., Schmid, T. M. & Reddi, A. H. Mechanotransduction of bovine articular cartilage superficial zone protein by transforming growth factor β signaling. *Arthritis Rheum.* **56**, 3706–3714 (2007).
220. Blunk, T. *et al.* Differential effects of growth factors on tissue-engineered cartilage. *Tissue Eng.* **8**, 73–84 (2002).
221. Kock, L., Van Donkelaar, C. C. & Ito, K. Tissue engineering of functional articular cartilage: The current status. *Cell and Tissue Research* **347**, 613–627 (2012).
222. Imler, S. M., Doshi, A. N. & Levenston, M. E. Combined effects of growth factors and static mechanical compression on meniscus explant biosynthesis. *Osteoarthr. Cartil.* **12**, 736–744 (2004).
223. Byers, B. A., Mauck, R. L., Chiang, I. E. & Tuan, R. S. Transient exposure to transforming growth factor beta 3 under serum-free conditions enhances the biomechanical and biochemical maturation of tissue-engineered cartilage. *Tissue Eng. - Part A.* **14**, 1821–1834 (2008).
224. Lima, E. G. *et al.* The beneficial effect of delayed compressive loading on tissue-engineered cartilage constructs cultured with TGF-β3. *Osteoarthr. Cartil.* **15**, 1025–1033 (2007).
225. Aprile, P. & Kelly, D. J. Hydrostatic Pressure Regulates the Volume, Aggregation and Chondrogenic Differentiation of Bone Marrow Derived Stromal Cells. *Front. Bioeng. Biotechnol.* **8**, 1526 (2021).
226. Zhao, Z. *et al.* Mechanotransduction pathways in the regulation of cartilage chondrocyte homoeostasis. *Journal of Cellular and Molecular Medicine* **24**, 5408–5419 (2020).
227. Jung, Y. K. *et al.* Degrading products of chondroitin sulfate can induce hypertrophy-like changes and MMP-13/ADAMTS5 production in chondrocytes. *Sci. Rep.* **9**, (2019).
228. Schwartz, N. B. & Domowicz, M. S. Roles of Chondroitin Sulfate Proteoglycans as Regulators of Skeletal Development. *Frontiers in Cell and Developmental Biology* **10**, (2022).
229. Zhu, D., Trinh, P., Liu, E. & Yang, F. Cell-Cell Interactions Enhance Cartilage Zonal Development in 3D Gradient Hydrogels. *ACS Biomater. Sci. Eng.* **9**, 831–843 (2023).
230. Mauck, R. L., Wang, C. C. B., Oswald, E. S., Ateshian, G. A. & Hung, C. T. The role of cell seeding density and nutrient supply for articular cartilage tissue engineering with deformational loading. *Osteoarthr. Cartil.* **11**, 879–890 (2003).
231. Gao, Y. *et al.* The ECM-cell interaction of cartilage extracellular matrix on chondrocytes. *BioMed Research International* **2014**, (2014).
232. Asanbaeva, A., Masuda, K., Thonar, E. J.-M. A., Klisch, S. M. & Sah, R. L. Mechanisms of cartilage growth: Modulation of balance between proteoglycan and collagen in vitro using chondroitinase ABC. *Arthritis Rheum.* **56**, 188–198 (2007).
233. Sengers, B. G., Van Donkelaar, C. C., Oomens, C. W. J. & Baaijens, F. P. T. The local matrix distribution and the functional development of tissue engineered cartilage, a finite element study. *Ann. Biomed. Eng.* **32**, 1718–1727 (2004).
234. van Donkelaar, C. C., Chao, G., Bader, D. L. & Oomens, C. W. J. A reaction–diffusion model to predict the influence of neo-matrix on the subsequent development of tissue-engineered cartilage. *Comput. Methods Biomech. Biomed. Engin.* **14**, 425–432 (2011).
235. Bryant, S. J., Anseth, K. S., Lee, D. A. & Bader, D. L. Crosslinking density influences the morphology of chondrocytes photoencapsulated in PEG hydrogels during the application of compressive strain. *J. Orthop. Res.* **22**, 1143–1149 (2004).
236. Nicodemus, G. D., Skaalure, S. C. & Bryant, S. J. Gel structure has an impact on pericellular and extracellular matrix deposition, which subsequently alters metabolic activities in chondrocyte-laden PEG hydrogels. *Acta Biomater.* **7**, 492–504 (2011).
237. Van Mourik, M. *et al.* Enzymatic Isolation of Articular Chondrons: Is It Much Different Than That of Chondrocytes? *Tissue Eng. - Part C Methods* **29**, 30–40 (2023).
238. Lee, G. M., Poole, C. A., Kelley, S. S., Chang, J. & Caterson, B. Isolated chondrons: A viable alternative for studies of chondrocyte metabolism in vitro. *Osteoarthr. Cartil.* **5**, 261–274 (1997).
239. Kleuskens & M.W.A. *A human ex vivo model for evaluation of osteochondral regeneration and integration*. (2022).
240. Chung, C. & Burdick, J. A. Engineering cartilage tissue. *Advanced Drug Delivery Reviews* **60**,

243–262 (2008).
241. Gu, W. Y., Yao, H., Huang, C. Y. & Cheung, H. S. New insight into deformation-dependent hydraulic permeability of gels and cartilage, and dynamic behavior of agarose gels in confined compression. *J. Biomech.* **36**, 593–598 (2003).
242. Song, L., Baksh, D. & Tuan, R. S. Mesenchymal stem cell-based cartilage tissue engineering: Cells, scaffold and biology. *Cytotherapy* **6**, 596–601 (2004).
243. Zhu, W. *et al.* Highly Porous Type II Collagen-Containing Scaffolds for Enhanced Cartilage Repair with Reduced Hypertrophic Cartilage Formation. *Bioeng. 2022, Vol. 9, Page 232* **9**, 232 (2022).
244. Niethammer, T. R. *et al.* Graft Hypertrophy After Third-Generation Autologous Chondrocyte Implantation Has No Correlation With Reduced Cartilage Quality: Matched-Pair Analysis Using T2-Weighted Mapping. *Am. J. Sports Med.* **46**, 2414–2421 (2018).
245. Bartlett, W. *et al.* Autologous chondrocyte implantation versus matrix-induced autologous chondrocyte implantation for osteochondral defects of the knee. A prospective, randomised study. *J. Bone Jt. Surg. - Ser. B* **87**, 640–645 (2005).
246. Davies, R. L. & Kuiper, N. J. Regenerative Medicine: A Review of the Evolution of Autologous Chondrocyte Implantation (ACI) Therapy. (2019). doi:10.3390/bioengineering6010022
247. Larson, C. M., Kelley, S. S., Blackwood, A. D., Banes, A. J. & Lee, G. M. Retention of the native chondrocyte pericellular matrix results in significantly improved matrix production. *Matrix Biol.* **21**, 349–359 (2002).
248. Vonk, L. A. *et al.* Preservation of the chondrocyte's pericellular matrix improves cell-induced cartilage formation. *J. Cell. Biochem.* **110**, 260–271 (2010).
249. Graff, R. D., Kelley, S. S. & Lee, G. M. Role of pericellular matrix in development of a mechanically functional neocartilage. *Biotechnol. Bioeng.* **82**, 457–464 (2003).
250. Rothdiener, M. *et al.* Human osteoarthritic chondrons outnumber patient- and joint-matched chondrocytes in hydrogel culture—Future application in autologous cell-based OA cartilage repair? *J. Tissue Eng. Regen. Med.* **12**, e1206–e1220 (2018).
251. Peters, H. C. *et al.* The protective role of the pericellular matrix in chondrocyte apoptosis. *Tissue Eng. - Part A* **17**, 2017–2024 (2011).
252. de Windt, T. S. *et al.* Allogeneic MSCs and Recycled Autologous Chondrons Mixed in a One-Stage Cartilage Cell Transplantion: A First-in-Man Trial in 35 Patients. *Stem Cells* **35**, 1984–1993 (2017).
253. Saris, T. F. F. *et al.* Five-Year Outcome of 1-Stage Cell-Based Cartilage Repair Using Recycled Autologous Chondrons and Allogenic Mesenchymal Stromal Cells: A First-in-Human Clinical Trial. *Am. J. Sports Med.* **49**, 941–947 (2021).
254. Bekkers, J. E. J. *et al.* Single-stage cell-based cartilage regeneration using a combination of chondrons and mesenchymal stromal cells: Comparison with microfracture. *Am. J. Sports Med.* **41**, 2158–2166 (2013).
255. Owida, H. A., De Las Heras Ruiz, T., Dhillon, A., Yang, Y. & Kuiper, N. J. Co-culture of chondrons and mesenchymal stromal cells reduces the loss of collagen VI and improves extracellular matrix production. *Histochem. Cell Biol.* **148**, 625–638 (2017).
256. Duan, W. *et al.* Combination of chondrocytes and chondrons improves extracellular matrix production to promote the repairs of defective knee cartilage in rabbits. *J. Orthop. Transl.* **28**, 47–54 (2021).
257. Aydelotte, M. B. & Kuettner, K. E. Differences between sub-populations of cultured bovine articular chondrocytes. I. Morphology and cartilage matrix production. *Connect. Tissue Res.* **18**, 205–222 (1988).
258. Talukdar, S., Nguyen, Q. T., Chen, A. C., Sah, R. L. & Kundu, S. C. Effect of initial cell seeding density on 3D-engineered silk fibroin scaffolds for articular cartilage tissue engineering. *Biomaterials* **32**, 8927–8937 (2011).
259. Mouser, V. H. M. *et al.* Ex vivo model unravelling cell distribution effect in hydrogels for cartilage repair. *ALTEX - Altern. to Anim. Exp.* **35**, 65–76 (2018).
260. Dimaraki, A. *et al.* Bioprinting of a Zonal-Specific Cell Density Scaffold: A Biomimetic Approach for Cartilage Tissue Engineering. *Appl. Sci.* **11**, 7821 (2021).

261. Brittberg, M. *et al.* Treatment of Deep Cartilage Defects in the Knee with Autologous Chondrocyte Transplantation. *N. Engl. J. Med.* **331**, 889–895 (1994).
262. Chang, J. & Poole, C. A. Confocal analysis of the molecular heterogeneity in the pericellular microenvironment produced by adult canine chondrocytes cultured in agarose gel. *Histochem. J.* **29**, 515–528 (1997).
263. Owida, H. A., Kuiper, N. L. & Yang, Y. Maintenance and Acceleration of Pericellular Matrix Formation within 3D Cartilage Cell Culture Models. *Cartilage* **13**, 847S-861S (2021).
264. Alexopoulos, L. G., Setton, L. A. & Guilak, F. The biomechanical role of the chondrocyte pericellular matrix in articular cartilage. *Acta Biomater.* **1**, 317–325 (2005).
265. Keppie, S. J. *et al.* Matrix-Bound Growth Factors are Released upon Cartilage Compression by an Aggrecan-Dependent Sodium Flux that is Lost in Osteoarthritis. *Function* **2**, zqab037 (2021).
266. Hayes, A. J., Farrugia, B. L., Biose, I. J., Bix, G. J. & Melrose, J. Perlecan, A Multi-Functional, Cell-Instructive, Matrix-Stabilizing Proteoglycan With Roles in Tissue Development Has Relevance to Connective Tissue Repair and Regeneration. *Frontiers in Cell and Developmental Biology* **10**, 575 (2022).
267. Gao, G., Chen, S., Pei, Y. A. & Pei, M. Impact of perlecan, a core component of basement membrane, on regeneration of cartilaginous tissues. *Acta Biomaterialia* **135**, 13–26 (2021).
268. Richard, D. *et al.* Evolutionary Selection and Constraint on Human Knee Chondrocyte Regulation Impacts Osteoarthritis Risk. *Cell* **181**, 362-381.e28 (2020).
269. Kahle, E. R. *et al.* Molecular Engineering of Pericellular Microniche via Biomimetic Proteoglycans Modulates Cell Mechanobiology. *ACS Nano* **16**, 1220–1230 (2022).
270. Mason, C. & Dunnill, P. A brief definition of regenerative medicine. *Regenerative Medicine* **3**, 1–5 (2008).
271. Sharma, B. *et al.* Designing zonal organization into tissue-engineered cartilage. *Tissue Eng.* **13**, 405–414 (2007).
272. Schuurman, W. *et al.* Three-dimensional assembly of tissue-engineered cartilage constructs results in cartilaginous tissue formation without retainment of zonal characteristics. *J. Tissue Eng. Regen. Med.* **10**, 315–324 (2016).
273. Ren, X. *et al.* Engineering zonal cartilage through bioprinting collagen type II hydrogel constructs with biomimetic chondrocyte density gradient. *BMC Musculoskelet. Disord.* **17**, 301 (2016).
274. Owida, H. A., Yang, R., Cen, L., Kuiper, N. J. & Yang, Y. Induction of zonal-specific cellular morphology and matrix synthesis for biomimetic cartilage regeneration using hybrid scaffolds. *J. R. Soc. Interface* **15**, (2018).
275. Armstrong, J. P. K. *et al.* Tissue Engineering Cartilage with Deep Zone Cytoarchitecture by High-Resolution Acoustic Cell Patterning. *Adv. Healthc. Mater.* **11**, 2200481 (2022).
276. Zhu, D., Tong, X., Trinh, P. & Yang, F. Mimicking Cartilage Tissue Zonal Organization by Engineering Tissue-Scale Gradient Hydrogels as 3D Cell Niche. *Tissue Eng. - Part A* **24**, 1–10 (2018).
277. Park, I.-S. *et al.* Effect of joint mimicking loading system on zonal organization into tissue-engineered cartilage. *PLoS One* **13**, e0202834 (2018).
278. Lutianov, M., Naire, S., Roberts, S. & Kuiper, J. H. A mathematical model of cartilage regeneration after cell therapy. *J. Theor. Biol.* **289**, 136–150 (2011).
279. Hollander, A. P. *et al.* Maturation of tissue engineered cartilage implanted in injured and osteoarthritic human knees. *Tissue Eng.* **12**, 1787–1798 (2006).
280. Odermatt, E. K. *et al.* MonoMax suture: A new long-term absorbable monofilament suture made from poly-4-hydroxybutyrate. *Int. J. Polym. Sci.* **2012**, (2012).
281. Keridou, I. *et al.* Microstructural changes during degradation of biobased poly(4-hydroxybutyrate) sutures. *Polymers (Basel).* **12**, (2020).
282. Akbari, M. *et al.* Textile Technologies and Tissue Engineering: A Path Toward Organ Weaving. *Adv. Healthc. Mater.* (2016). doi:10.1002/adhm.201500517
283. Damen, A. *Biotribology of cartilage resurfacing implants*. (2022).
284. Alcala-Orozco, C. R. *et al.* Hybrid biofabrication of 3D osteoconductive constructs comprising Mg-based nanocomposites and cell-laden bioinks for bone repair. *Bone* **154**,

116198 (2022).
285. Damen, A. H. A. *et al.* Friction reducing ability of a poly-l-lysine and dopamine modified hyaluronan coating for polycaprolactone cartilage resurfacing implants. *J. Biomed. Mater. Res. Part B Appl. Biomater.* (2023). doi:10.1002/jbm.b.35251
286. Kock, L. M., Geraedts, J., Ito, K. & van Donkelaar, C. C. Low Agarose Concentration and TGF-β3 Distribute Extracellular Matrix in Tissue-Engineered Cartilage. *Tissue Eng. Part A* **19**, 1621–1631 (2013).
287. Vega, S. L., Kwon, M. Y. & Burdick, J. A. Recent advances in hydrogels for cartilage tissue engineering. *Eur. Cells Mater.* **33**, 59–75 (2017).
288. Lee, H. P., Gu, L., Mooney, D. J., Levenston, M. E. & Chaudhuri, O. Mechanical confinement regulates cartilage matrix formation by chondrocytes. *Nat. Mater.* **16**, 1243–1251 (2017).
289. Bentley, G. *et al.* A prospective, randomised comparison of autologous chondrocyte implantation versus mosaicplasty for osteochondral defects in the knee. *J. Bone Jt. Surg. - Ser. B* **85**, 223–230 (2003).
290. Chaudhuri, O. *et al.* Hydrogels with tunable stress relaxation regulate stem cell fate and activity. *Nat. Mater.* **15**, 326–334 (2016).
291. Crispim, J. F. & Ito, K. De novo neo-hyaline-cartilage from bovine organoids in viscoelastic hydrogels. *Acta Biomater.* **128**, 236–249 (2021).
292. Hua, Y. *et al.* Ultrafast, tough, and adhesive hydrogel based on hybrid photocrosslinking for articular cartilage repair in water-filled arthroscopy. *Sci. Adv.* **7**, (2021).
293. Benedikt, S. *et al.* Highly efficient water-soluble visible light photoinitiators. *J. Polym. Sci. Part A Polym. Chem.* **54**, 473–479 (2016).
294. Vahdati, A. & Wagner, D. R. Implant size and mechanical properties influence the failure of the adhesive bond between cartilage implants and native tissue in a finite element analysis. *J. Biomech.* **46**, 1554–1560 (2013).
295. Grzeskowiak, R. M. *et al.* Bone and Cartilage Interfaces With Orthopedic Implants: A Literature Review. *Frontiers in Surgery* **7**, 144 (2020).
296. Ishibashi, Y., Kimura, Y., Sasaki, S., Sasaki, E. & Takahashi, A. Internal Fixation of Osteochondritis Dissecans Using PushLock Suture Anchors. *Arthrosc. Tech.* **10**, e705–e709 (2021).
297. Shiromoto, Y. *et al.* Increased migratory activity and cartilage regeneration by superficial-zone chondrocytes in enzymatically treated cartilage explants. *BMC Musculoskelet. Disord.* **23**, 256 (2022).
298. Morales, T. I. Chondrocyte moves: clever strategies? *Osteoarthritis and Cartilage* **15**, 861–871 (2007).
299. Xu, W., Zhu, J., Hu, J. & Xiao, L. Engineering the biomechanical microenvironment of chondrocytes towards articular cartilage tissue engineering. *Life Sciences* **309**, 121043 (2022).
300. Korhonen, R. K. & Herzog, W. Depth-dependent analysis of the role of collagen fibrils, fixed charges and fluid in the pericellular matrix of articular cartilage on chondrocyte mechanics. *J. Biomech.* **41**, 480–485 (2008).
301. Hing, W. A., Sherwin, A. F., Ross, J. M. & Poole, C. A. The influence of the pericellular microenvironment on the chondrocyte response to osmotic challenge. *Osteoarthr. Cartil.* **10**, 297–307 (2002).
302. Gilbert, S. J., Bonnet, C. S. & Blain, E. J. Mechanical cues: Bidirectional reciprocity in the extracellular matrix drives mechano-signalling in articular cartilage. *International Journal of Molecular Sciences* **22**, 13595 (2021).
303. Lach, M. S. *et al.* The Induced Pluripotent Stem Cells in Articular Cartilage Regeneration and Disease Modelling: Are We Ready for Their Clinical Use? *Cells* **11**, (2022).
304. Satake, T. *et al.* Induction of iPSC-derived Prg4-positive cells with characteristics of superficial zone chondrocytes and fibroblast-like synovial cells. *BMC Mol. Cell Biol.* **23**, 30 (2022).
305. Takao, T. *et al.* A novel chondrocyte sheet fabrication using human-induced pluripotent stem cell-derived expandable limb-bud mesenchymal cells. *Stem Cell Res. Ther.* **14**, 34 (2023).

306. Nguyen, D. *et al.* Cartilage Tissue Engineering by the 3D Bioprinting of iPS Cells in a Nanocellulose/Alginate Bioink. *Sci. Rep.* **7**, (2017).
307. Rodríguez Ruiz, A. *et al.* Cartilage from human-induced pluripotent stem cells: comparison with neo-cartilage from chondrocytes and bone marrow mesenchymal stromal cells. *Cell Tissue Res.* **386**, 309–320 (2021).
308. Ruiz, A. R. *et al.* A comparison of chondrogenesis oriented differentiating protocols for induced pluripotent stem cells. *Osteoarthr. Cartil.* **28**, S517–S518 (2020).
309. Rikkers, M., Korpershoek, J. V., Levato, R., Malda, J. & Vonk, L. A. Progenitor Cells in Healthy and Osteoarthritic Human Cartilage Have Extensive Culture Expansion Capacity while Retaining Chondrogenic Properties. *Cartilage* **13**, 129S-142S (2021).
310. PATRA, D., XING, X., BRYAN, J. & SANDELL, L. Abnormal matrix in S1Pcko mice leads to lack of bone formation. *Matrix Biol.* **25**, S71–S71 (2006).
311. Van Donkelaar, C. C. & Wilson, W. Mechanics of chondrocyte hypertrophy. *Biomech. Model. Mechanobiol.* **11**, 655–664 (2012).
312. Jacobs, C. A. M. *et al.* Biomechanical evaluation of a novel biomimetic artificial intervertebral disc in canine cervical cadaveric spines. *JOR SPINE* e1251 (2023). doi:10.1002/jsp2.1251
313. Vrancken, A. C. T., Buma, P. & Van Tienen, T. G. Synthetic meniscus replacement: A review. *International Orthopaedics* **37**, 291–299 (2013).
314. Peng, Y. *et al.* Natural biopolymer scaffold for meniscus tissue engineering. *Frontiers in Bioengineering and Biotechnology* **10**, 1003484 (2022).
315. Peiffer, Q. C. *et al.* Melt electrowriting onto anatomically relevant biodegradable substrates: Resurfacing a diarthrodial joint. *Mater. Des.* **195**, 109025 (2020).
316. Biscaia, S. *et al.* 3D Printed Poly(ε-caprolactone)/Hydroxyapatite Scaffolds for Bone Tissue Engineering: A Comparative Study on a Composite Preparation by Melt Blending or Solvent Casting Techniques and the Influence of Bioceramic Content on Scaffold Properties. *Int. J. Mol. Sci.* **23**, 2318 (2022).
317. Duarte Campos, D. F., Drescher, W., Rath, B., Tingart, M. & Fischer, H. Supporting Biomaterials for Articular Cartilage Repair. *Cartilage* **3**, 205–221 (2012).
318. Gu, Y., Forget, A. & Shastri, V. P. Biobridge: An Outlook on Translational Bioinks for 3D Bioprinting. *Adv. Sci.* **9**, 2103469 (2022).
319. Márquez-Flórez, K., Garzón-Alvarado, D. A., Carda, C. & Sancho-Tello, M. Computational model of articular cartilage regeneration induced by scaffold implantation in vivo. *J. Theor. Biol.* **561**, 111393 (2023).
320. Lacroix, D. & Prendergast, P. J. A mechano-regulation model for tissue differentiation during fracture healing: Analysis of gap size and loading. *J. Biomech.* **35**, 1163–1171 (2002).

Summary

Cartilage defects are themselves debilitating but also may lead to progressive osteoarthritis. For regeneratively treating such defects, hydrogels are promising cell carriers using their ability of maintaining the chondrocyte's phenotype and in some cases mimicking the native extracellular matrix. However, the strong load bearing function of articular cartilage tissue contrasts with the poor load bearing capacity of most soft hydrogels used for chondrocyte culturing / cartilage tissue engineering. If the load bearing capacity of such chondrocyte-seeded hydrogels would be sufficient to carry the severe loading conditions in the joint, they may be used in cartilage repair strategies. It is known that the internal osmotic pressure generated in native cartilage is one of the major sources for its strong load-bearing characteristics. This osmotic pressure exists because in native cartilage, the swelling potential of the proteoglycans is balanced by the strong, swelling-restricting collagen network. This thesis postulates that this mechanically favourable situation can be mimicked by a hydrogel constructed of a negatively charged polymer that would naturally swell due to osmotic swelling, and restricting this swelling by placing it inside a textile spacer fabric. This would then recreate the natural load-bearing mechanism of cartilage as well as the native environment of chondrocytes.

First, a proof of principle of the load-bearing capacity of such a construct is demonstrated using synthetic poly 2-hydroxyethyl methacrylate (pHEMA) sodium methacrylate (NaMA) hydrogels, where swelling of the hydrogel is restricted by the tension developing in the warp-knitted polyamide 6 (PA6) spacer fabric, referred to as a HydroSpacer. Free swelling hydrogels increased up to 9-fold the initial weight, whereas HydroSpacer swelling was restricted to 1.2-fold. This restricted swelling of pHEMA-NaMA hydrogels in warp knitted PA6 spacer fabrics lead to an internal osmotic pressure. Regression analysis revealed a positive linear relationship between peak and equilibrium stress and osmotic pressure, showing that the mechanical properties of a HydroSpacer can be tuned by adjusting the swelling capacity of the hydrogel via the FCD.

Although synthetic pHEMA hydrogels show promising results in terms of load bearing, these types of hydrogels are not suitable for regenerative purposes and cell encapsulation due to cytotoxicity and long UV exposure for polymerization. For this reason, biocompatible hydrogel formulations inducing a swelling pressure in a restricted environment were studied. Examples of such hydrogels

are extracellular matrix (ECM)-like biopolymer-based hydrogels, which use methacrylated natural polymers chondroitin sulfate (CSMA) and hyaluronic acid (HAMA). It was found that free swelling 10 wt% CSMA HAMA hydrogels swell 230% and are stable for more than 120 days. When they are confined by a PA6 spacer fabric, after 28 days their volumetric swelling was 53% less, the apparent peak and the equilibrium modulus were significantly larger, and these moduli and the time constant were similar to native bovine cartilage. Moreover, the cell viability in the CSMA/HAMA PA6 constructs was comparable to that in gelatin–methacrylamide (GelMA) PA6 constructs at one day after polymerization. These results suggested that using a HydroSpacer construct with an ECM-like biopolymer-based hydrogel is a promising approach for mimicking the load-bearing properties of native cartilage and the encapsulation of cells. Unfortunately, decreased stability due to batch-to-batch variations led to discontinuation of the CSMA/HAMA hydrogel for long term cell-based experiments.

To create a functional regenerative implant with long-term clinical success, in addition to initial load bearing, the implant should also possess low frictional properties to prevent wear of opposing cartilage. This was tested using a biodegradable spacer-fabric made from polycaprolactone (PCL) and poly-4-hydroxybutyrate (P4HB), which was injected with the previously developed CSMA HAMA hydrogel. These HydroSpacer were then implanted in osteochondral defects made in healthy bovine cartilage. Using a custom-made device, the implanted HydroSpacer could be moved against healthy cartilage similar to the gait cycle, mimicking the native movements and forces. From this research, results showed that placement of the HydroSpacer was essential for the prevention of wear of the opposing cartilage. Moreover, the surrounding cartilage did not show any damage, suggesting load sharing of the HydroSpacer with the surrounding cartilage and therefore the load bearing properties as previously observed in mechanical tests.

ECM production by chondrocytes should be sufficiently fast to keep up with biomaterial degradation. Composite synthetic / ECM-like biopolymer-based polyethylene glycol dimethacrylate (PEGDMA) CSMA hydrogels have shown promising effect on ECM production. However, this was never studied in a restricted swelling environment. It is interesting to explore how chondrocytes would respond, as it may be hypothesized that in a cartilage-mimicking mechanical environment, they might not be stimulated to produce ECM proteins. If so, then the question is whether this might be counteracted with dynamic

mechanical stimulation. A biodegradable polycaprolactone (PCL) and poly-4-hydroxybutyrate (P4HB) spacer fabric filled with PEGDMA CSMA hydrogel is used to study both the effect of hydrostatic pressure by restricted swelling and the addition of dynamic mechanical stimulation on bovine chondrocytes. Collagen synthesis was observed in both free and restricted swelling hydrogels. One out of three donors showed a more extensive collagen deposition in a HydroSpacer compared to a free swelling hydrogel, meaning that collagen deposition might not be impeded by the restricted swelling. Dynamic loading showed variable outcomes, in which both an increase and decrease in collagen deposition was observed. With these outcomes, no conclusions can be drawn, other than that donor variability might influence the outcomes. Primary bovine chondrocytes form PCM and deposited collagen type II in both free swelling and HydroSpacer system, which was donor dependent and independent on mechanical loading. The presence of PCM appeared essential for the synthesis of type II collagen in a restricted swelling environment.

The outcomes of chapter 4 showed that a pericellular matrix might influence the synthesis of type II collagen in a restricted swelling environment. In native cartilage mechanotransduction is mainly regulated by the (PCM) surrounding chondrocytes. Recent studies showed that the use of chondrons (chondrocytes encapsulated by PCM) increased ECM production and cell survival, which might be beneficial for the regenerative capacity in a restricted swelling tissue engineered construct. To reveal the effect of the presence of a PCM, it is best to compare groups of samples with only chondrocytes vs samples with only chondrons. Unfortunately, the current gold standard chondron isolation protocol, dating from 1997, results in low cell yield and heterogeneous isolated populations. A new isolation protocol was developed using a Type VI collagen staining, fluorescence-activated cell sorting (FACS) analysis and specific cell sorting, resulting in higher cell yield and a homogenic chondron population. These may be used in future studies to explore the effects of biomimetic environments on chondrocyte stimulation.

In conclusion, the combination of warp-knitted spacer fabrics and swelling hydrogels results in HydroSpacers which mimic the load bearing properties of native cartilage. Using biocompatible and biodegradable swelling polymers, a promising regenerative cartilage implant material is developed, in which the FCD, restricted swelling and mechanical loading are closer to the native environment than in commonly used hydrogels. These HydroSpacers are initially load-bearing

and may therefore allow for earlier activity of patients after treatment, thus enhancing and shortening post-surgical recovery. The interaction between osmotic pressure, (dynamic) loading, matrix synthesis, and the effect of a mechanotransduction-modulating PCM are the next steps to bring the current HydroSpacers closer to clinical application.

Samenvatting

Kraakbeen defecten kunnen ontstaan vanwege trauma of ziektes, bijvoorbeeld osteochondritis dissecans. Als deze defecten niet worden behandeld, kan dit uiteindelijk leiden tot osteoartritis. Deze degeneratieve ziekte is progressief, en zal uiteindelijk leiden naar bot op bot contact, wat zeer pijnlijk is en waardoor bewegen moeilijk steeds moeilijker zal gaan. Om dit te voorkomen, kunnen kraakbeendefecten worden behandelend door bijvoorbeeld regeneratieve methodes te gebruiken waar kraakbeen weer opnieuw wordt gevormd op de plek van het defect. Het grootste nadeel van deze regeneratieve behandelingen is dat het weefsel dat gevormd wordt, nog erg afwijkt van het oorspronkelijke weefsel, waardoor het niet dezelfde eigenschappen heeft. Andere methodes zijn het gebruik van metalen of kunststof implantaten. Dit heeft helaas vaak tot gevolg dat het kraakbeen wat tegenover het implantaat beweegt, beschadigd raakt. Daarom zijn er nieuwe methodes nodig voor een regeneratieve aanpak, zodat "jonge" patienten, tot 50/60 jaar, en daardoor een totale knie vervanging kunnen uitstellen. Voor een regeneratieve aanpak worden vaak hydrogelen gebruikt. Dit zijn polymeren die veel water aantrekken, wat waardoor het oorspronkelijke kraakbeen wordt nagebootst. Met nieuw weefselvorming zal tegelijkertijd ook de hydrogel afbreken, zodat er uiteindelijk een geheel nieuw eigen weefsel is gevormd. Helaas heeft het gebruik van hydrogelen ook nadelen. Het grootste nadeel is dat deze gelen erg zacht zijn, hierdoor kan na implantatie het gewricht niet belast worden. En omdat het dragen van het lichaam een van de belangrijkste functies van kraakbeen is, is dit essentieel.
In kraakbeen komt het vermogen om het lichaam te dragen door de structuur en compostitie van de extracellulaire matrix van kraakbeen. Deze extracellulaire matrix bestaat uit enerzijds glycosaminoglycanen, wat polysacharides zijn met een negatieve lading, waardoor veel water wordt aangetrokken en anderzijds collageen vezels die deze zwelling tegengaan. Hierdoor ontstaat er een osmotische druk, waardoor het kraakbeen hoge krachten kan opvangen.
Dit proefschrift heeft als hoofdvraag of dit mechanisme kan worden nagebootst door een hydrogel die is gemaakt van een negatief geladen polymeer, waardoor en een 3D gebreid matje, een zogenaamde "spacer-fabric", die deze zwelling tegen kan gaan. Deze 3D gebreide structuur bestaat uit een gebreide boven- en onderkant met daar tussenin vezels die loodrecht op deze twee lagen staan, waardoor deze van elkaar staan en er ruimte ontstaat om een hydrogel in te injecteren. Samen met de hydrogel noemen we dit een HydroSpacer.

Dit principe zal eerst worden getest met behulp van synthetische materialen die niet geschikt zullen zijn voor regeneratieve doeleinden, maar vooral als doel heeft om te onderzoeken of deze methode leidt tot het tegengaan van zwelling en daardoor het creëren stijfheden vergelijkbaar met kraakbeen. HydroSpacers zijn gemaakt van synthetische poly-2-hydroxyethylmethacrylaat (pHEMA) natriummethacrylaat (NaMA) hydrogelen en een 3D gebreid polyamide 6 (PA6) materiaal. Vrij zwellende hydrogelen zwelden tot 9 keer het oorspronkelijke gewicht, terwijl de zwelling van HydroSpacer beperkt was tot 1,2 keer. Deze beperkte zwelling van pHEMA-NaMA hydrogels in de spacer fabrics leidde tot een interne osmotische druk. Regressieanalyse liet een positieve lineaire relatie zien tussen piek- en evenwichtsspanning en osmotische druk, wat aantoont dat de mechanische eigenschappen van een HydroSpacer afhankelijk zijn van het zwelvermogen van de hydrogel en de negatieve ladingen die in de hydrogel aanwezig zijn. Hoewel synthetische pHEMA hydrogelen veelbelovende resultaten laten zien in termen van draagkracht, zijn dit soort hydrogelen niet geschikt voor regeneratieve doeleinden en cel inkapseling vanwege cytotoxiciteit en lange UV-blootstelling voor polymerisatie.

Om deze redenen werden biocompatibele hydrogelcomposities ontwikkeld die zijn gebaseerd op extracellulaire matrix (ECM)-achtige biologische polymeren chondroïtinesulfaat (CS) en hyaluronzuur (HA). Om crosslinking mogelijk te maken, werden deze polymeren voorzien van een methacrylaat groep (MA). Het bleek dat vrij zwellende CSMA HAMA hydrogelen 230% zwellen en stabiel blijven voor meer dan 120 dagen. Wanneer ze worden geïnjecteerd in een PA6 spacer-fabric nam de zwelling af tot 53%. Dit leidde tot significant hogere piek en equilibrium stijfheden. Van nog groter belang was dat deze moduli en de tijdconstante vergelijkbaar waren met natuurlijk kraakbeen. Bovendien waren chondrocyten die gezaaid waren in de CSMA/HAMA PA6-constructen levensvatbaar en waren het aantal levende cellen één dag na polymerisatie vergelijkbaar met de veel gebruikte gelatine-methacrylamide (GelMA) hydrogel die ook was geïnjecteerd in PA6 spacer-fabrics. Deze resultaten suggereerden dat het gebruik van een HydroSpacer met een ECM gebaseerde hydrogel een veelbelovende benadering is voor het nabootsen van het draagvermogen van natuurlijk kraakbeen en voor het inbedden van cellen. Helaas leidde verminderde stabiliteit als gevolg van batch variaties tot stopzetting van de CSMA/HAMA-hydrogel voor langdurige cel experimenten.

Naast het draagvermogen, is de lage frictie in een gewricht ook zeer belangrijk

voor het pijnloos en soepel functioneren van een gewricht. Daarnaast is het van belang dat implantaten geen beschadigingen toebrengt aan het overstaande kraakbeen. Dit is getest door middel van de HydroSpacer, gemaakt van een biologisch afbreekbare spacer fabric (polycaprolacton (PCL) en poly-4-hydroxybutyraat (P4HB)) en de eerder gebruikte CSMA HAMA hydrogel. Deze HydroSpacers werden geïmplanteerd in osteochondrale defecten gemaakt in gezond kraakbeen van runderen. Met behulp van een machine kon het geïmplanteerde materiaal over gezond kraakbeen worden bewogen, waarbij de natuurlijke beweging en krachten tijdens lopen werden nagebootst. Uit dit onderzoek bleek dat de plaatsing van de HydroSpacer essentieel is voor het voorkomen van het beschadigen van het tegenoverliggende weefsel. Daarnaast bleek uit het niet beschadigde omringende kraakbeen, het implantaat draagvermogen toonde zoals eerder in mechanische testen was aangetoond.

Om een functioneel regeneratief implantaat te creëren met langdurig klinisch succes, moet naast initiële belasting, ook de ECM-productie door chondrocyten voldoende moeten zijn om de afbraak van het biomateriaal bij te houden. Dit werd getest door midddel van chondrocyten te implanteren in een samengestelde synthetische/ ECM-achtige polyethyleenglycol dimethacrylaat (PEGDMA) CSMA-hydrogel. Deze hydrogel werd geïnjecteerd in PCL P4HB spacer fabrics. Het doel van deze studie was om te onderzoeken hoe chondrocyten reageren als ze zijn ingebed in een omgeving die kraakbeen nabootst, en waardoor mogelijk chondrocyten niet worden gestimuleerd om ECM-eiwitten te produceren. Daarnaast was het de vraag als dit dan kon worden tegengegaan met het dynamische mechanisch stimuleren van deze HydroSpacers. Collageensynthese werd waargenomen in zowel vrij zwellende hydrogelen als in HydroSpacers. Een van de drie donoren vertoonde een meer aanwezig collageen depositie in een HydroSpacer in vergelijking met een vrij zwellende hydrogel, wat betekent dat de collageen synthese mogelijk niet geheel wordt belemmerd door de hydrostatische druk. Daarnaast liet de dynamische stimulatie variabele uitkomsten zien, waar zowel een toename als een afname van collageen synthese werd waargenomen. Uit deze uitkomsten kunnen geen conclusies worden getrokken, behalve dat donor variabiliteit de uitkomsten eventueel zou kunnen beïnvloeden. Naast collagen type 2 synthese, werd ook collageen type VI waargenomen rondom de chondrocyten. Dit wijst erop dat chondrocyten in staat waren om een pericellulaire matrix (PCM) te vormen, wat bekend staat vanwege het beschermende vermogen voor de cellen. Daarnaast leek de aanwezigheid van PCM essentieel te zijn voor de synthese van type II collageen in een

HydroSpacer omgeving.

Recente studies toonden aan dat het gebruik van chondrons (chondrocyten ingekapseld door PCM) de ECM-productie en overleving van cellen verhoogde, wat gunstig zou kunnen zijn voor het regeneratieve vermogen in een HydroSpacer implantaat. Om het effect van de aanwezigheid van een PCM te onderzoeken, is een homogene chondron populatie essentieel. De huidige gouden standaard protocol voor chondron-isolatie, daterend uit 1997, resulteerde in een lage cel opbrengst en een heterogene populatie bestaande uit chondrons en chondrocyten. Daarom werd er in deze thesis een nieuw isolatieprotocol ontwikkeld met behulp van specifieke type VI collageen kleuring en fluorescentie-geactiveerde cel sortering (FACS) analyse en specifieke cel sortering op type VI collageen, wat resulteerde in een hogere cel opbrengst en een homogene chondron populatie.

Concluderend, de combinatie van 3D gebreide spacer-fabrics en zwellende hydrogelen resulteert in HydroSpacers die het dragend vermogen van natuurlijk kraakbeen kan nabootsen. Met behulp van biocompatibele en biologisch afbreekbare polymeren wordt een veelbelovend regeneratief kraakbeenimplantaat materiaal ontwikkeld, waarin de negatieve lading, beperkte zwelling en mechanische belasting dichter bij de oorspronkelijke kraakbeen omgeving liggen dan bij veelgebruikte hydrogelen. Deze HydroSpacers zijn instantaan belastbaar en kunnen daarom zorgen voor eerdere activiteit van patiënten na de behandeling, waardoor het postoperatieve herstel wordt verbeterd en verkort. Het onderzoeken van de interactie tussen osmotische druk, (dynamische) belasting, matrix synthese en het effect van een PCM die mechanische signalen kan omvormen, zijn de volgende stappen om de huidige HydroSpacers dichter bij klinische toepassing te brengen.

List of Publications

Publications related to this thesis

G. H. Schuiringa, M. Pastrama, C. C. van Donkelaar, K. Ito (2023). Towards a load bearing hydrogel: A proof of principle in the use of osmotic pressure for biomimetic cartilage constructs. Journal of the Mechanical Behavior of Biomedical Materials, 137, 105552.

G. H. Schuiringa*, M. Mihajlovic*, C. C. van Donkelaar, T. Vermonden, K. Ito (2022). Creating a Functional Biomimetic Cartilage Implant Using Hydrogels Based on Methacrylated Chondroitin Sulfate and Hyaluronic Acid. Gels, 8(7), 457.
***** These authors contributed equally to this work

M. van Mourik*, **G. H. Schuiringa***, L. P. Verhagen, L. A. Vonk, C. C. van Donkelaar, K. Ito, J. Foolen (2023). Enzymatic isolation of articular chondrons: is it much different than that of chondrocytes? Tissue Engineering. Part C: Methods, Volume 29, Issue 1, Pages 30-40
***** These authors contributed equally to this work

A.H.A. Damen, **G. H. Schuiringa,** K. Ito, C. C. van Donkelaar (2023), The effect of HydroSpacer implant placement on the wear of opposing and adjacent cartilage, Journal of Orthopaedic Research, Volume 41, Issue 7, Pages 1397-1406

Other publications

Mihajlovic, M., Rikkers, M., Mihajlovic, M., Viola, M., **Schuiringa, G.H.**, Ilochonwu, B. C., Masereeuw, R., Vonk, L., Malda, J., Ito, K., & Vermonden, T. (2022). Viscoelastic Chondroitin Sulfate and Hyaluronic Acid Double-Network Hydrogels with Reversible Cross-Links. Biomacromolecules, 23(3), 1350-1365.

Van Gestel, N., **Schuiringa, G.H.**, Hennissen, J. H. P. H., Delsing, A., Ito, K., van Rietbergen, B., Hofmann, S., & Arts, C. (2019). Resorption of the calcium phosphate layer on S53P4 bioactive glass by osteoclasts. Journal of Materials Science: Materials in Medicine, 30(8), [94]

Curriculum Vitae

Gerke Hendrik (Rienk) Schuiringa werd op 11 november 1992 geboren in Marum. Nadat hij zijn vwo-diploma behaalde op de Lindenborg te Leek in 2011, startte hij de Bachelor Bouwkunde aan Technische Universiteit Eindhoven. Na het behalen van zijn propedeuse, wisselde hij in 2012 naar de Bachelor Medische Wetenschappen en Technologie, die hij in 2015 afrondde. Zijn Master Biomedical Engineering in de Orthopaedic Biomechanics groep van prof. dr. Keita Ito rondde hij af met zijn afstudeerproject onder begeleiding van dr. Sandra Hoffman, met de focus op het vermogen van osteoclasten om bioactief glas te resorberen. Onder begeleiding van prof. Bill Walsh bij de Surgical & Orthopaedic Research Laboratory aan de University of New South Wales, Sydney, Australië onderzocht hij tijdens zijn afstudeerstage de antibacteriële eigenschappen van gecoat allograft bot. Nadat hij in 2018 zijn Masterdiploma ontving, begon hij als PhD kandidaat in de Orthopaedic Biomechanics groep. Onder supervisie van dr. René van Donkelaar en prof. dr. Keita Ito maakte hij deel uit van het Chemelot InSciTe MimiCart en RegMed XB consortium. De resultaten van dit onderzoek zijn beschreven in dit proefschrift. In 2023 is Rienk gestart als projectmanager bij RegMed XB.

Gerke Hendrik (Rienk) Schuiringa was born on the 11th of November in Marum, The Netherlands. After obtaining his VWO diploma from the Lindenborg in Leek, he started the Bachelor Architecture, Urbanism and Building Sciences at the Eindhoven University of Technology. After obtaining his Propedeuse, he switched to the Bachelor Medical Engineering and Science. After obtaining his bachelor degree, he continued with a masters in Biomedical Engineering in the Orthopaedic Biomechanics group of prof. Keita Ito. During his graduation project, he studied the degradation of bioactive glass granules by osteoclastic activity under supervision of Sandra Hoffman, PhD and was followed by an internship at the Surgical & Orthopaedic Research Laboratory of the University of New South Wales, Sydney, Australia, supervised by prof. Bill Walsh, focusing on the anti-bacterial properties coated rabbit bone allograft in comparison to bioactive glass. After graduating in 2028, he started as PhD candidate in the Chemelot InSciTe MimiCart and RegMed XB consortium under supervision of René van Donkelaar, PhD and prof. Keita Ito. Results of this research are presented in this dissertation. Rienk started in 2023 as project manager at RegMed XB.

Dankwoord

This is the end… Het moment is eindelijk daar, en wat een fijn gevoel om de laatste pagina's van dit proefschrift te mogen schrijven. Dat heb ik gelukkig niet alleen hoeven doen, letterlijk en figuurlijk. Ik heb genoten van mijn PhD tijd en een bedankje voor alle collega's, vrienden en familie, is wel het minste wat ik kan doen.

Dear **Keita**, thank you for the opportunity to do a PhD in the Orthopaedic Biomechanics group. It was an honor to work with and to learn from you and I really enjoyed the discussions we had throughout these years. I appreciate your calmness in (from time to time) stressful periods, your almost seemingly infinite knowledge, and the way you keep the research group such an open and welcome place.

Beste **René**, bedankt voor je vertrouwen en het warme welkom in de kraakbeen groep. Jouw toegankelijkheid, fijne creatieve en positieve manier van denken en open gesprekken hebben grotendeels geleid naar het afronden van deze thesis. Naast de fijne samenwerking, moet ik je ook bedanken voor alle gezelligheid, tijdens (late avonden op) OPB retreats, dakterras-borrels, BBQ's en conferenties, en dat je me al geo-cachend tot grote hoogtes hebt weten te brengen.

Naast mijn promotor en co-promotor wil ik ook graag mijn commissie bedanken. Dear **Sandra,** I cannot imagine a better ending of my TU/e career with you part of my committee. As supervisor of my BSc and MSc thesis, you taught me the skills and formed me as researcher. **Tina Vermonden**, dank voor de samenwerking met de CSMA HAMA hydrogel, en alle input tijdens meetings en het schrijven van het artikel. **Jos Malda,** dank voor de input tijdens RegMed XB meetings, en conferenties. Het werk dat je in Utrecht doet is nog steeds erg inspirerend. Ik zou ook graag de andere leden van de commissie, **Gerjo van Osch** en **Marcel Karperien** willen bedanken voor jullie tijd en energie om mijn thesis te lezen en te bediscussiëren tijdens mijn verdediging.

Toen ik de vraag van René kreeg of ik bij hem een PhD wilde doen, was de nauwe samenwerking met jullie, **Alicia en Meike,** een doorslaggevende factor waarom ik ja zei tegen dit PhD avontuur. Ik ben dan ook trots en dankbaar dat jullie vandaag naast mij staan als paranimfen, zonder jullie had ik de eindstreep niet gehaald. Het laatste jaar was dan ook veel te lang zonder jullie. Ik ben super trots

op jullie, met de manier waarop jullie beiden je PhD hebben behaald, en dat ik, aan jullie zijde, daar deel van heb mogen uitmaken.
Lieve Alicia, we zaten met onze voetjes in het zand in Sydney toen je de mail van René kreeg met de vraag of je een PhD wilde gaan doen, nog geen flauw idee dat ik een half jaar later je directe collega zou gaan worden. En wat heb ik daarvan genoten. Dank voor je humor, je nuchterheid, je planning tips and tricks (of mij daar juist op afkeurde), de motivatie om toch maar onszelf weer naar het SSC te slepen, en op de valreep toch nog een paper samen! Ik hoop dat we ooit nog eens onze continenten bingo kunnen voortzetten.
Lieve Meike, wie kon bedenken met een biertje tijdens Borrel XL, misschien net iets te aangeschoten, en net iets te veel details delend, we samen onze PhD zouden gaan doen als directe collega's. Het kende vele hoogtepunten maar ook dieptepunten, maar het is gelukt! Dank dat je altijd klaar stond met een luisterend oor, parate lab kennis of met de dansschoenen aan. En ik zal natuurlijk nooit ons USA roadtripje vergeten, en ben ook erg dankbaar om dat als collega's/ vrienden te hebben gedaan. Lieve paranimfen, lieve drie Musketiers, voor de laatste keer: Eén voor allen en allen voor één!

Ik ben ook blij dat ik veel onderzoek samen heb mogen uitvoeren met collega's van andere onderzoekgroepen en binnen de **MimiCart** en **RegMed XB** consortia. Special thanks to the team of ITA RWTH-Aachen, **Nikola, Kai, Charlotte**, without you there was no spacer fabric and no thesis. Dear **Marko,** thanks for all your efforts on the CSMA HAMA hydrogel, which resulted in our paper together. I really enjoyed working with you, and I wish you all the best with your academic career. Team Utrecht, **Margot** en **Iris**, jullie ook bedankt voor het sharing is caring van de CSMA DRAMA, maar ook voor de gezelligheid tijdens conferenties! Daarnaast ook dank aan de office collega's van RegMed XB voor het warme welkom in jullie team.

Dank ook aan het **Tech Team** van het Cellab. **Mascha**, dank voor je opbeurende woorden en het buurten in het Biolab en **Liesbeth** bedankt voor je hulp met het chondronen paper. Er is 1 man in Gemini die een standbeeld verdient, en dat is **Jurgen.** Dank voor je eindeloze oplossingen en je gouden handen. Zonder jou was onderzoek doen onmogelijk.

Onderzoek doen was ook onmogelijk zonder alle lieve collega's in het **Cellab** en **Biolab**. **Bart** en **Laura vE** bedankt voor jullie FACS-hulp. **Pim,** één keer gewogen is niet geleefd! **Cas,** dank voor je goede kamergenootschap. En wat was ik zonder

de immunogirls: **Dewy, Hannah, Suzanne, en Tamar** jullie maakten mijn lab dagen stukken dragelijker.

Ik wil ook graag de OPB-groep bedanken voor de goede sfeer, teambuilding en collegialiteit! **Marloes,** we hebben elkaar door het chondronen paper gesleept en het heeft wat bloed, zweet en tranen gekost (niet in die volgorde per se). Maar we mogen trots zijn op het resultaat. **Bregje,** Queen of the Cellab en de taartenkoningin (voor onze verjaardagen), wat heb ik van jouw enthousiasme, in en buiten het lab genoten. Ik heb ook genoten van alle retreats en meerkampen (en vooral de BBQ na die tijd). Voor de sportiviteit een extra bedankje voor **Celien** en **Esther,** die net als Alicia en Bente mij naar het SSC sleepten (also thanks to the lovely lessons of Greta, Iker en Sem). **Floor,** jouw enthousiasme zorgde voor een niet te evenaren handmade escape-room box. **Maria,** thanks for the mentoring during the first years and your input with the first paper, and of course for the best cartilage group dinners and drinks ever (also huge thanks to **Chris**!).

Evelien en **Yvon,** dank voor al het regelwerk, maar ook voor het gezellige kletsen zo af en toe, het was nooit een straf om even bij jullie binnen te vallen. Evelien, ook veel dank voor het regelen van mijn verdediging.

I would also like to thank the MSc students I supervised during my PhD. **Sarah**, thanks for setting up the silk constructs method. **Jet** voor dit verder zetten, maar ook zeker voor het lachen. Onderzoek met een bakje spuug zal ik nooit vergeten. **Zaina** en **Amber** jullie ook erg bedankt om het verder te optimaliseren en toe te passen.

Of course a huge thanks to all my colleagues of Hok 4,14. **Ahmad, Daniek, Elmer, Evianne, Fleur, Jeroen, Kaja, Luca, Mathieu, Moeen, Nicky, Niels, Tara, Tijmen and Tim** thanks for all the nice Hok-uitjes, coffee/tea/cake moments and the foosball tournaments**. Arjan**, een betere buurman op kantoor had ik niet kunnen wensen (want er was vaak veel plek...), maar ook zeker vanwege alle gezellige borrels en dinertjes, laten we dat vooral voortzetten!

Aan **Kantoor 4.12** heb ik ook veel te danken. Ten eerste heel veel kilo's pepernoten en paaseitjes uit de KOEktrommel (Thanks **Laura**). **Elias** en **Jordy**, dank voor alle lab en niet lab-gerelateerde praatjes, maar ook voor het meehelpen slopen en het padellen, ik wens iedereen zulke fijne collega's toe. **Nicole,** zonder jouw aanbeveling was ik waarschijnlijk nooit een PhD begonnen, maar ook zeker dank voor het goede voorbeeld geven hoe studenten te

begeleiden tijdens een MSc project. Eén persoon uit 4.12 kan en mag ik niet vergeten te bedanken: **Willeke,** zonder jouw koppeldrang zat ik nu niet in Zuid-Limburg.

Door die koppeldrang wil ik ook graag de Paaspop en Ponykamp vriendengroepen bedanken voor alle festivals, tent-, tuin- en huisfeestjes, wat voor veel welkome afleiding heeft gezorgd. **Karlijn,** we zullen zorgen dat we snel nieuwe gordijnen hebben hangen, en ik hoop nog veel potjes padel te mogen spelen met **Ruben.** Daarnaast dank **Michel** en **Kelly**, het is fijn om vrienden te hebben die veel van je struggles begrijpen, maar ook van een goede BBQ houden ;)

Mylene, samen zijn we gestart met bouwkunde, als intro broertje en zusje, en als mama en papa doorgegaan bij BMT. Dank voor je altijd luisterend oor en me te wijzen op het gebruik van te veel '…' in appjes… En onthoudt, alles komt goed!

Ik schrijf dit dankwoord tussen de Berlijn pride, Milkshake en Amsterdam pride in, dus een stukje diversity en regenboog kleuren mag zeker niet ontbreken. **Tomas,** ondanks tijd en afstand ben ik dankbaar dat we elkaar nog geregeld zien en ik hoop dat we samen met **Mark** nog heel wat gluhwijntjes mogen drinken. **Bram** en **Dave,** mede door jullie voelde ik meteen thuis in de Hulsberg groep, en ik hoop op nog heel wat spelletjesavonden en Berlijn tripjes samen met jullie. **Djordee** en **Levi,** dank voor alle fijne afleiding de afgelopen tijd, en dat dat nog lang zo door mag blijven gaan! **Toussaint**, dank voor het ontwerpen van mijn cover!

Lieve **Bente** en **Janine**, 10+ jaren lief en leed en ik kan jullie dan ook niet meer dan genoeg bedanken. Jullie zijn naast m'n beste vriendinnen, m'n tweede 3 musketiers en mijn tweede team paranimfen, de girls who run the world. Het is about damn time dat we met z'n drieën dr. mogen zijn, want de afgelopen 4/5 jaar was hysteria, maar niks was impossible en we did it our way. Please go easy on me tijdens het feestje, want al het unholy mag binnen onze 3 muren blijven… En ja, ik wilde supermassive black hole gebruiken, maar doe dat toch maar niet… Lieve **Daniëlle, Rob, Thomas en Job,** van al het bovenstaande maakten jullie ook deel uit, en ik had het nooit zonder jullie willen doen, dank daarvoor! Dat we nog heel vaak in ons tentenkamp op Pinkpop mogen zitten, en 's ochtends mogen aanschuiven bij **Oma** (die nooit genoeg boeketjes kan ontvangen als dank).

Lieve schoonfamilie, bij jullie voelt het als thuiskomen, letterlijk en figuurlijk. **Jos** en **Mariëlle**, dank voor jullie gastvrijheid, alle gezelligheid en ook zeker voor mijn privé kantoortje waar ik veel woorden van deze thesis op papier heb gezet. We mogen heel trots zijn op hoe we het afgelopen jaar met elkaar hebben samengewoond, en die dankbaarheid is niet uit te drukken in woorden. **Janou,** ik kwam helaas niet uit Hulsberg en sprak ook geen woord Limburgs, maar ik kan me geen leukere schoonzus wensen, dankjewel!

Lieve familie, ook al woon je in het Limburgse heuvelland, Marum blijft de basis. Lieve **Alied**, dank voor je nuchterheid, nait soez'n en broez'n mentaliteit, die ik af en toe nodig had. Ik wens je samen met **Rory** (prima kerel) en lieve **Milou** alle goeds. Lieve **Tante Manny**, ik heb enorme waardering voor hoe u tegen het leven aankijkt en ben dankbaar voor de mooie band die wij, ook met Janny, hebben. De mooie levenslessen, "*kiek noar die zulf",* zal ik niet snel vergeten. Lieve **Papa** en **Mama,** dank voor al jullie steun en toeverlaat de afgelopen jaren. Ook al ga ik steeds verder bij jullie weg wonen, het heeft geen enkele invloed op onze band. En met alle vrije tijd die nu voor jullie ligt, en een standplaats bij ons in de straat, zal die vast alleen nog maar beter worden.

Lieve **Ruben**, het leven samen met jou en Seppe is een groot avontuur, en daar kan ik je niet genoeg voor bedanken. Met twee nieuwe banen, een iets onderschatte verbouwing, een Philips debacle, en ohja een vriend die een PhD moest afronden, was het misschien niet het meest relaxte jaar, maar er is geen Limburgse heuvel te hoog, of een Wissengracht te diep. Bedankt (ook al leek dat af en toe niet zo) voor alle gratis PhD tips and tricks die jij me gaf als ervaringsdeskundige, dit heeft ervoor gezorgd dat ik hier nu sta. Lieve Ruben, kôm laot ôs nao 't zuuje gaon, dao bin ik neet gebaore, mor bin veer gelökkig gewaore. De leefde dies dich oetstraols, reup un hiemels gevuil op bie mich. Met jou, en alle lieve vrienden en familie om ons heen, heb ik heel veel zin in de toekomst!

Liefs,
Rienk